



Search for dark matter produced in association with a single top quark and an energetic W boson in $\sqrt{s} = 13$ TeV pp collisions with the ATLAS detector

The ATLAS Collaboration

This paper presents a search for dark matter, χ , using events with a single top quark and an energetic W boson. The analysis is based on proton–proton collision data collected with the ATLAS experiment at $\sqrt{s} = 13$ TeV during LHC Run 2 (2015–2018), corresponding to an integrated luminosity of 139 fb^{-1} . The search considers final states with zero or one charged lepton (electron or muon), at least one b -jet and large missing transverse momentum. In addition, a result from a previous search considering two-charged-lepton final states is included in the interpretation of the results. The data are found to be in good agreement with the Standard Model predictions and the results are interpreted in terms of 95% confidence-level exclusion limits in the context of a class of dark matter models involving an extended two-Higgs-doublet sector together with a pseudoscalar mediator particle. The search is particularly sensitive to on-shell production of the charged Higgs boson state, H^\pm , arising from the two-Higgs-doublet mixing, and its semi-invisible decays via the mediator particle, a : $H^\pm \rightarrow W^\pm a (\rightarrow \chi\chi)$. Signal models with H^\pm masses up to 1.5 TeV and a masses up to 350 GeV are excluded assuming a $\tan\beta$ value of 1. For masses of a of 150 (250) GeV, $\tan\beta$ values up to 2 are excluded for H^\pm masses between 200 (400) GeV and 1.5 TeV. Signals with $\tan\beta$ values between 20 and 30 are excluded for H^\pm masses between 500 and 800 GeV.

1 Introduction

The existence of non-luminous matter, referred to as dark matter (DM), is strongly suggested by a wide variety of astrophysical and cosmological measurements [1, 2]. Despite the strong evidence supporting the presence of DM, which accounts for 26% of the energy content of the universe [3, 4], its nature and properties remain largely unknown and constitute one of the most important unanswered questions in modern physics. Assuming that its main component is a weakly interacting massive particle (WIMP or χ) [5], DM produced in proton–proton collisions does not interact with the ATLAS detector and it can be detected only if produced in association with Standard Model (SM) particles. This leads to signatures with missing transverse momentum (\vec{p}_T^{miss} , its modulus denoted by E_T^{miss}).

The signal model considered in this search belongs to a class of simplified models for DM searches at the Large Hadron Collider (LHC). It involves an extended two-Higgs-doublet sector (2HDM) [6–14], together with an additional pseudoscalar mediator (a) that couples to a fermionic DM candidate. This 2HDM+ a model [10, 15] represents the simplest ultraviolet-complete and renormalisable framework for investigating the broad phenomenology predicted by spin-0 mediator-based DM models [15–27].

The 2HDM+ a model offers a rich phenomenology [28–33], with a variety of final states that might arise depending on the production and decay modes of the various bosons composing the Higgs sector, as investigated in Refs. [15, 34–38]. A recent analysis performed by the ATLAS Collaboration [39] has considered topologies characterised by the presence of E_T^{miss} and a single top quark in the context of 2HDM+ a models. That search allowed masses of the additional charged Higgs bosons, H^\pm , from 400 GeV to 1.1 TeV to be excluded at a 95% confidence level (CL) for different values of the a -boson mass and for low values (< 2) of $\tan\beta$ (the ratio of the vacuum expectation values of the two Higgs doublets), which significantly affects the phenomenology of the 2HDM+ a model. Values of the a -boson mass up to 330 GeV are also excluded at 95% CL for $\tan\beta = 1$ and an H^\pm mass of 800 GeV. CMS has also performed a search for these topologies [40], where the results are interpreted in the context of a different set of simplified models.

As in the case of the SM single top-quark production, the associated production of DM with a single top quark has three production modes at leading order (LO): t -channel production, s -channel production and associated production with a W boson (tW). In the 2HDM+ a model, the dominant production mode for

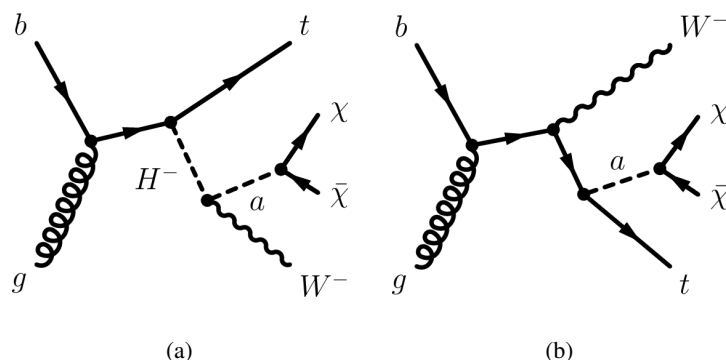


Figure 1: Representative diagrams of tW +DM production from the 2HDM+ a model considered in this analysis. Charge-conjugate diagrams are considered as well.

single-top-quark final states is the tW +DM channel, through the diagrams depicted in Figure 1. On-shell production of charged Higgs bosons dominates the tW +DM production mode when $H^\pm \rightarrow W^\pm a$ decays are kinematically allowed and the H^\pm mass is a few hundred GeV. Furthermore, the cross-section for this inclusive tW +DM production mode has a local minimum at $\tan\beta \approx 5$ and two local maxima at low $\tan\beta$ (< 2) and $\tan\beta \in [20, 30]$ [28]. The aim of the search presented in this paper is to extend the current results obtained by ATLAS for the 2HDM+ a model by improving the sensitivity to single top-quark production in association with dark matter in the tW +DM process. The focus is to improve upon the current ATLAS limits at low $\tan\beta$ and to provide, for the first time, sensitivity to signal benchmarks probing the tW +DM cross-section maximum at high $\tan\beta$ values.

This paper presents a dedicated search for associated production of a single top quark, a W boson and DM particles, based on 139 fb^{-1} of proton–proton (pp) collisions at a centre-of-mass energy $\sqrt{s} = 13 \text{ TeV}$ produced at the LHC and collected by the ATLAS detector (see Section 2) between 2015 and 2018. Due to the similarity of the experimental signature to $t\bar{t}$ production, the analysis is also sensitive to DM produced in association with two top quarks ($t\bar{t}$ +DM). This final state is not considered in the optimization of the analysis, but its contribution is added to the tW +DM signal, according to the prediction of the 2HDM+ a model, when interpreting the final result. The analysis relies on Monte Carlo (MC) simulations, described in Section 3, which aid in the estimation of the SM background and DM signals. This search improves upon previous results [39] by targeting final states with an energetic W boson decaying hadronically or leptonically and characterised by the presence of exactly zero or one lepton ($\ell = e, \mu$). The hadronic decays of the W boson are identified by requiring the presence of at least one high- p_T large-radius jet consistent with originating from the hadronization of a resonant di-quark pair. In addition, at least one jet arising from the fragmentation of b -hadrons (b -jet) is required as a signature of the additional presence of a top quark, while large E_T^{miss} is required as a sign of the production of DM particles. The identification of these objects, as well as the event reconstruction, is described in Section 4. Section 5 presents the selection of events in the one- or zero-lepton analysis channels, and also the method used to combine these two channels with the dilepton analysis described in Ref. [39]. Their combination maximises the sensitivity to tW +DM processes and further tightens previous constraints for 2HDM+ a models using the tW +DM channel. Systematic uncertainties are described in Section 6, followed by the experimental results and their interpretation in the context of the 2HDM+ a model in Section 7. Finally, Section 8 is devoted to the conclusions.

2 The ATLAS detector

The ATLAS detector [41] is a multipurpose particle detector with a forward–backward symmetric cylindrical geometry and nearly 4π coverage in solid angle.¹ The inner tracking detector (ID) consists of pixel and microstrip silicon detectors covering the pseudorapidity region $|\eta| < 2.5$, surrounded by a transition radiation tracker which enhances electron identification in the region $|\eta| < 2.0$. An inner pixel layer, the insertable B-layer [42, 43], was added at a mean radius of 3.3 cm during the period between Run 1 and Run 2 of the LHC. The inner detector is surrounded by a thin superconducting solenoid providing an axial 2 T magnetic field and by a fine-granularity lead/liquid-argon (LAr) electromagnetic calorimeter covering

¹ ATLAS uses a right-handed coordinate system with its origin at the nominal interaction point in the centre of the detector. The positive x -axis is defined by the direction from the interaction point to the centre of the LHC ring, with the positive y -axis pointing upwards, while the beam direction defines the z -axis. Cylindrical coordinates (r, ϕ) are used in the transverse plane, ϕ being the azimuthal angle around the z -axis. The pseudorapidity η is defined in terms of the polar angle θ by $\eta = -\ln \tan(\theta/2)$. Rapidity is defined as $y = 0.5 \ln[(E + p_z)/(E - p_z)]$ where E denotes the energy and p_z is the component of the momentum along the beam direction. The angular distance ΔR is defined as $\sqrt{(\Delta\eta)^2 + (\Delta\phi)^2}$.

$|\eta| < 3.2$. A steel/scintillator-tile calorimeter provides hadronic coverage in the central pseudorapidity range ($|\eta| < 1.7$). The endcap ($1.5 < |\eta| < 3.2$) and forward ($3.1 < |\eta| < 4.9$) regions of the hadron calorimeter are made of LAr active layers with either copper or tungsten as the absorber material. A muon spectrometer with an air-core toroid magnet system surrounds the calorimeters. Three layers of high-precision tracking chambers provide coverage in the range $|\eta| < 2.7$, while dedicated fast chambers allow triggering in the region $|\eta| < 2.4$. The ATLAS trigger system consists of a hardware-based level-1 trigger followed by a software-based high-level trigger [44]. An extensive software suite [45] is used in the reconstruction and analysis of real and simulated data, in detector operations, and in the trigger and data acquisition systems of the experiment.

3 Data and simulated events

The dataset used in the analysis corresponds to an integrated luminosity of 139 fb^{-1} of pp collisions at a centre-of-mass energy of 13 TeV recorded by the ATLAS detector with stable beam conditions. The uncertainty in the integrated luminosity is 1.7% [46], obtained using the LUCID-2 detector [47] for the primary luminosity measurements. The number of interactions in the same and temporally adjacent bunch crossings (pile-up) is 33.7 on average across all data-taking years. All detector subsystems are required to be operational for this dataset [48]. Candidate events were recorded using a combined set of triggers based on the presence of $E_{\text{T}}^{\text{miss}}$ or charged leptons ($\ell = e, \mu$). The $E_{\text{T}}^{\text{miss}}$ trigger [49] is fully efficient for events with reconstructed $E_{\text{T}}^{\text{miss}} > 250 \text{ GeV}$ and is used for the zero-lepton and one-lepton analysis channels. Triggers based on single leptons [50, 51] are used to define auxiliary selections that aid in the estimation of the SM background processes. These selections require the presence of a muon or electron with transverse momentum, p_{T} (or transverse energy E_{T} for electrons), above certain thresholds, and impose data quality and lepton identification and isolation requirements.

Dedicated MC simulated samples are used to model the SM and signal processes and to estimate their expected yields. The 2HDM+ a model considered in this paper assumes a type-II [52, 53] coupling structure of the Higgs sector, and has a CP-conserving potential and a softly broken Z_2 symmetry [52]. The additional pseudoscalar mediator of the model couples to DM particles and to the SM, and mixes with the pseudoscalar partner of the SM Higgs boson. The most important parameters that determine the phenomenology of the model are the masses of the CP-even (h and H), CP-odd (a and A) and charged (H^\pm) bosons; the mass of the DM particle (χ); the three quartic couplings between the scalar doublets and the a boson ($\lambda_{P_1}, \lambda_{P_2}$ and λ_3) and the coupling between the a boson and the DM particle (g_χ); the ratio of the vacuum expectation values (VEVs) of the two Higgs doublets ($\tan \beta$); and the mixing angles of the CP-even and CP-odd weak eigenstates, denoted by α and θ , respectively. The alignment limit ($\cos(\beta - \alpha) = 0$) and the decoupling limit are assumed. Thus the lightest CP-even mass eigenstate, h , can be identified as the SM Higgs boson with couplings predicted by the SM. The electroweak vacuum expectation value is set to 246 GeV. The mixing angle θ is fixed at $\sin \theta = 1/\sqrt{2}$, yielding full mixing between the a and A bosons and the largest cross-section for the processes of interest. To further reduce the parameter space, unitary couplings between the a -boson mediator and the DM particle χ ($g_\chi = 1$) are considered, with the DM particle mass set to $m_\chi = 10 \text{ GeV}$. This has a negligible effect on the kinematic properties in the final states of interest, as long as $a \rightarrow \chi\chi$ is kinematically allowed. Following the prescriptions in Ref. [15], the masses of the heavy CP-even Higgs boson, H , and charged bosons, H^\pm , are set equal to the mass of the heavy CP-odd partner, A , and the three quartic couplings are set to a value of 3 for compatibility with

constraints from electroweak precision measurements [10] and to ensure the stability of the Higgs potential for most of the parameter space of interest.²

The signal MC samples include tW production in association with DM particles. They were generated using LO matrix elements calculated by the MADGRAPH5_AMC@NLO 2.7.3 [54] generator interfaced to PYTHIA 8.244 [55], which used parameter values set to the A14 tune [56] to model parton showering (PS), hadronization and the underlying event. The five-flavour scheme NNPDF3.0NLO [57] set of parton distribution functions (PDFs) was used. Signal cross-sections are calculated at LO accuracy in QCD. Additional simulated samples are used for $t\bar{t}$ +DM processes. They were generated using LO matrix elements with up to one extra parton calculated by MADGRAPH5_AMC@NLO 2.6.7 interfaced to PYTHIA 8.244, with the same PDF set and tune as used for the tW processes. In this case, signal cross-sections are calculated at next-to-leading-order (NLO) accuracy using the same version of MADGRAPH5_AMC@NLO as suggested in Ref. [23]. The top-quark decays in all signal samples were simulated using MADSPIN [58]. The final results are presented as a function of the (m_a, m_{H^\pm}) parameters while setting $\tan\beta$ to unity, or varying the $(m_{H^\pm}, \tan\beta)$ parameters while setting m_a to 250 GeV or 150 GeV.

The SM background processes were simulated using various MC event generators, accurate to NLO in perturbation theory, depending on the process. All background processes are normalised to the best available theoretical calculation of their respective cross-sections. The event generators, the accuracy of theoretical cross-sections, the underlying-event set of tuned parameters, and the PDF sets used in simulating the SM background processes most relevant for this analysis are summarised in Table 1. Note that the NNPDF2.3LO PDF sets [59] were used for the parton-shower and hadronization steps in samples using PYTHIA 8.

For all samples, except those generated using SHERPA [60–65], the EVTGEN 1.2.0 [66] program was used to simulate the properties of the b - and c -hadron decays. All generated events were then processed using the ATLAS simulation infrastructure [67] and GEANT4 [68], which models the response of the various ATLAS subdetectors with high precision. In some cases, a faster simulation based on a parameterization of the calorimeter response, and on GEANT4 for the other detector subsystems [67], was used. Subsequently, simulated events are reconstructed after including a realistic modelling of pile-up interactions, with pile-up profiles matching the ones in data. These profiles were obtained by overlaying each hard-scatter event with minimum-bias events simulated using the soft QCD processes of PYTHIA 8.186 [69] with the NNPDF2.3LO set of PDFs [59] and the A3 tune [70].

4 Object identification and event reconstruction

All collision events considered in this paper are required to have at least one reconstructed interaction vertex with a minimum of two associated tracks each having $p_T > 500$ MeV. In events with multiple vertices, the one with the highest sum of squared transverse momenta of associated tracks is chosen as the primary vertex [83]. Minimal quality criteria are applied to reject events with detector noise [48], non-collision backgrounds or events with jets failing basic cleaning requirements [84].

² As pointed out in Ref. [15], for the parameter space considered in this paper, only values $m_{H^\pm} < 600$ GeV provide a bounded-from-below scalar potential [52] for the 2HDM+ a model. This constraint can be relaxed by up to a factor of 2 if the quartic coupling λ_3 assumes a value closer to the perturbativity limit, and it can be relaxed further in more general 2HDMs containing additional quartic couplings [11], as discussed in Ref. [31].

Table 1: List of MC generators and the PDF sets used to simulate the different SM background processes. Diboson includes WW , WZ and ZZ production. Information is also given on the generator used to simulate the parton-shower and hadronization step and the underlying-event set of tuned parameters. The last column presents the perturbative QCD highest-order accuracy (NLO, next-to-next-to-leading order (NNLO), and next-to-next-to-leading logarithm (NNLL)) achieved in the calculation of the cross-section later used to normalize of the different samples. Samples using PYTHIA 8 used NNPDF2.3LO set of PDFs [59] for the parton-shower and hadronization step. Diboson cross-sections are directly taken from SHERPA.

Process	Generator	PDF set	PS and frag./hadr.	UE tune	Cross-section accuracy	
Top pair ($t\bar{t}$)	POWHEG BOX v2 [71–74]	NNPDF3.0NLO	PYTHIA 8	A14	NNLO+NNLL [75]	
Single top	t -channel	POWHEG BOX v2 [76]	NNPDF3.0NLO	PYTHIA 8	A14	NNLO+NNLL [77]
	s - and tW -channel	POWHEG BOX v2 [78]	NNPDF3.0NLO	PYTHIA 8	A14	NNLO+NNLL [79, 80]
V +jets ($V = W/Z$)	SHERPA 2.2.1 [60–65]	NNPDF3.0NNLO	SHERPA	Default	NNLO [81]	
Diboson	SHERPA 2.2.1 or 2.2.2 [65]	NNPDF3.0NNLO	SHERPA	Default	NLO	
tZ ; $tWZ(\rightarrow \ell\bar{\ell})$; $t\bar{t} + V$, $V = W, Z, h$	MADGRAPH5_AMC@NLO 2.3.3 [54]	NNPDF3.0NLO	PYTHIA 8	A14	NLO [54, 82]	
$t\bar{t}$; $t\bar{t}\bar{t}$	MADGRAPH5_AMC@NLO 2.3.3 [54]	NNPDF3.1NLO	PYTHIA 8	A14	NLO [54, 82]	
$tWZ(\rightarrow \nu\nu)$	MADGRAPH5_AMC@NLO 2.6.7 [54]	NNPDF3.0NLO	PYTHIA 8	A14	NLO [54]	

Electrons (e), muons (μ) and jets are considered with two levels of quality requirements: baseline and signal. The baseline requirements have looser identification criteria. For each event, the missing transverse momentum [85] \vec{p}_T^{miss} , with magnitude E_T^{miss} , is calculated as the negative vector sum of the transverse momenta of all baseline reconstructed objects and the ‘soft term’. The soft term includes all tracks associated with the primary vertex but not matched to any reconstructed lepton or jet. Tracks not associated with the primary vertex are not considered in the \vec{p}_T^{miss} calculation, improving the \vec{p}_T^{miss} resolution by reducing the effect of pile-up. A quality criterion for the matching of topological cell clusters [86] in the electromagnetic calorimeter to electrons is also imposed in events containing electrons with $|\eta| \in [1.37, 1.52]$ in data recorded during 2015 and 2016. Baseline reconstructed physics objects are also used when resolving possible reconstruction ambiguities (overlap removal). The details of the object prioritization and requirements in this procedure can be found in Ref. [87].

Electron candidates are reconstructed from energy deposits in the electromagnetic calorimeter that are matched to charged-particle tracks in the inner detector [88]. Baseline quality criteria include $p_T > 4.5$ GeV, $|\eta| < 2.47$ and satisfying the ‘LooseAndBLayer’ likelihood identification³ operating point [88]. The longitudinal impact parameter, z_0 , relative to the primary vertex is required to satisfy $|z_0 \sin \theta| < 0.5$ mm. Signal-quality electrons are required to also satisfy $p_T > 20$ GeV and the ‘Medium’ likelihood identification criterion. The significance of the transverse impact parameter, d_0 , must satisfy $|d_0/\sigma(d_0)| < 5$ for these electrons. Signal electrons with $p_T < 200$ GeV are also required to be isolated⁴ from other activity in the detector by satisfying the ‘Loose’ isolation working point, while those with larger p_T are required to pass the ‘HighPtCaloOnly’ isolation working point, as described in Ref. [89].

Muon candidates are reconstructed from matching tracks in the inner detector and muon spectrometer [90]. Requirements for baseline-quality muons include $p_T > 4$ GeV, $|\eta| < 2.7$ and satisfying the ‘Medium’

³ The electron identification criteria are based on a likelihood built by combining information from the electron track and shower shapes of the electron energy deposit in the calorimeter. Four operating are defined - VeryLoose, Loose, Medium and Tight - corresponding to increasing cuts on the likelihood discriminant. Track quality criteria are required on top of this selection. The ‘LooseAndBLayer’ uses the Loose working point likelihood requirement, but requires in addition that the electron track has a hit in the innermost pixel layer.

⁴ Isolation quality cuts are assessed by studying the energy deposits within a cone in ΔR around the physics object. Energy deposits in the calorimeter and the tracker are considered to define the ‘Loose’ working points while only energy deposits in the calorimeter are used to define the ‘HighPtCaloOnly’.

identification criterion⁵ [90]. Like the electrons, their longitudinal impact parameter relative to the primary vertex is required to satisfy $|z_0 \sin \theta| < 0.5$ mm. Signal-quality muons must satisfy $p_T > 20$ GeV and a requirement on their transverse impact parameter significance of $|d_0/\sigma(d_0)| < 3$. Furthermore, they are required to be isolated based on the ‘Loose’ isolation criterion [90], which relies on variables calculated from energy deposits within a cone around the muon. The angular width of this cone depends on the p_T of the muon, decreasing at higher p_T .

Jets are reconstructed using the anti- k_t algorithm [91, 92] with a radius parameter $R = 0.4$ and particle-flow objects (PFO) as inputs. PFOs combine information from the inner detector and calorimeter to reconstruct the energy and path of charged particles and neutral particles as described in Ref. [93]. Jet energy scale corrections, derived from MC simulation and data, are used to calibrate the average energies of jet candidates to the scale of their constituent particles [94]. To further reduce the effect of pile-up interactions, a jet-vertex-tagger (JVT) algorithm is used to identify jets originating from the primary vertex using track information [95]. Jets with $|\eta| < 2.4$ and $p_T < 60$ GeV are required to satisfy the ‘Tight’ working point of this tagger, which corresponds to a JVT score of at least 0.5. In addition, jets with $|\eta| > 2.5$ and $p_T < 50$ GeV are required to pass a ‘Tight’ forward-JVT requirement [96], which corresponds to a forward-JVT score of less than 0.4 and a jet-timing requirement of less than 10 ns. Baseline-quality jets are selected in the region $|\eta| < 4.5$ and must have a $p_T > 20$ GeV. Signal-quality jets are required to fulfil $|\eta| < 2.5$ and $p_T > 30$ GeV.

Jets containing b -hadrons are identified as arising from b -quarks (‘ b -tagged’ jets or b -jets) using a multivariate algorithm (DL1r) [97]. These b -tagged jets are reconstructed in the region $|\eta| < 2.5$ and require $p_T > 30$ GeV. The b -tagging working point used in this analysis provides an efficiency of 77% for b -jets in simulated $t\bar{t}$ events.

A second category of jets is reconstructed by applying the anti- k_t algorithm with radius parameter $R = 1.0$ to a collection of noise-suppressed topological calorimeter-cell clusters calibrated using ‘local hadronic cell weighting’ [86] to correct for the non-compensating response of the ATLAS calorimeter. These jets are referred to as large- R jets to distinguish them from the $R = 0.4$ version, also called small- R jets or simply ‘jets’. Large- R jets [98] are trimmed to remove pile-up and underlying-event effects. This trimming, extensively described in Ref. [99], is a grooming technique in which the original constituents of the jets are reclustered using the k_t algorithm [100] with a radius parameter, R_{sub} , to produce a collection of subjets. These subjets are then discarded if they have less than a specific fraction, f_{cut} , of the p_T of the original jet. The trimming parameters used are $R_{\text{sub}} = 0.2$ and $f_{\text{cut}} = 0.05$. The jet energy scale and resolution and the mass scale and resolution of these large- R jets are then corrected via a calibration procedure described in Refs. [101, 102]. Large- R jets are required to have a $p_T > 200$ GeV and $|\eta| < 2.0$. To avoid reconstruction ambiguities between large- R jets and leptons, those large- R jets overlapping with signal leptons are removed. Ambiguities between large- R and baseline jets are not removed, as large- R jets are only used to construct higher-level quantities in order to identify hadronically decaying W bosons in the event. A set of W -tagging identification criteria [103] are applied to these large- R jets to identify those with topologies consistent with the decay of energetic hadronically decaying W bosons. These identification criteria are only used for jets with a mass between 40 GeV and 600 GeV and a $p_T < 2.5$ TeV and are based on the mass of the large R -jet, the number of inner-detector tracks associated with the jet and the D_2 variable [104]. This latter variable uses jet substructure energy correlations to identify deposits consistent with 2-prong particle decays against QCD quark and gluon initiated jets.

⁵ The ‘Medium’ muon identification criteria requires well-reconstructed muon tracks the inner detector and muon spectrometer (only muon spectrometer tracks in the region $2.5 < |\eta| < 2.7$) and a good q/p compatibility between both.

To compensate for remaining differences between data and simulation in trigger, particle identification and reconstruction efficiencies, correction factors are derived and applied to the samples of simulated events [89, 90, 105, 106].

5 Analysis strategy

This analysis complements and extends a previous search performed by the ATLAS Collaboration [39], by targeting final states with an energetic W boson and characterised by the presence of exactly zero or one lepton, referred to as the tW_{0L} and tW_{1L} channels, respectively.

Top-quark decays contain a W boson, and hence tW +DM signals contain two W bosons in the decay chain. The tW_{0L} channel selects tW +DM events where both bosons in the event decay hadronically, while the tW_{1L} channel selects events where one of them decays hadronically and the other decays leptonically. Both selections require high jet multiplicity and significant E_T^{miss} from two DM particles escaping detection. In both channels, the W boson arising from the decay of the massive H^\pm boson is often produced with relatively high p_T , thus being significantly boosted. When this W boson decays hadronically, it is reconstructed as a single large- R jet and W -tagged using the procedure described in Section 4. The one-lepton channel described in Ref. [39] is extended to include such boosted W -boson events. It is constructed to be statistically independent of the tW_{0L} channel so that all signal regions (SRs) in this paper can be statistically combined. The tW_{2L} analysis channel in Ref. [39] targets tW +DM events with two opposite-sign leptons and is statistically independent of the SRs presented in this paper. As a consequence, this channel can be combined with tW_{0L} and tW_{1L} to derive the final results.

The relative importance of SM background processes varies across the different SRs. However, the most important can be broadly classified by the presence of genuine E_T^{miss} produced by non-interacting particles, e.g. neutrinos, or E_T^{miss} associated with the presence of particles that are either misidentified, mismeasured or outside the kinematic acceptance of the detector. Examples of backgrounds containing genuine E_T^{miss} , which constitute a significant part of the SM background yields in their respective channels, are the Z +jets background in the tW_{0L} channel, where the Z boson decays into two neutrinos; and W +jets production in the tW_{1L} channel, where a lepton and neutrino are present in the decay. Other backgrounds such as $t\bar{t}$ or W +jets (in the tW_{0L} channel) are examples of backgrounds that have high E_T^{miss} due to leptons in the event which either escape detection or are misidentified as jets. Due to this, both make a large contribution in the tW_{0L} and tW_{1L} channels. Contributions from $t\bar{t}Z$ and single top-quark production, in particular the associated production of a top quark with a W boson, are also significant. The estimation of these five dominant SM backgrounds (Z +jets, W +jets, $t\bar{t}$, $t\bar{t}Z$ and single top quark) is aided by the use of six dedicated control regions (CRs), which are designed to be orthogonal to the SRs and are used to constrain six background normalization parameters in a phase space as close as possible to that of the SRs. The background normalizations are derived in common regions for the two analysis channels, with the exception of the $t\bar{t}$ background. Because $t\bar{t}$ has different compositions in the two channels, separate control regions and normalization parameters are used for tW_{0L} and tW_{1L} channels. The validity of the background estimation strategy is confirmed in specific validation regions (VRs) adapted for each defined SR. The potential signal contamination in the CRs and VRs is found to be small: $< 2.5\%$ and $< 10\%$ of the total SM expectation for all analysis channels, respectively.

The strategy for the statistical analysis and combinations performed in this paper closely follows the one used in Ref. [39], and relies on a profile likelihood fit [107], with the systematic uncertainties, described in Section 6, introduced as nuisance parameters constrained by a Gaussian distribution. Following the

definition of Ref. [39], the fit is performed using two configurations: background-only and exclusion fit set-ups. In the background-only configuration the fit is used to estimate the reliability of the background prediction in the VRs. It is performed using all tW_{0L} and tW_{1L} CRs in a simultaneous fit and assuming no contribution from ‘beyond-the-SM’ (BSM) physics processes. The six normalization factors of the SM backgrounds are hence determined in all the control regions simultaneously. The normalization factors determined in this set-up are applied to the VRs in order to verify that the background predictions agree with the data. The background-only fit configuration is also used to estimate the model-independent limits in Section 7, by extrapolating the background prediction of this fit to the SRs and estimating upper limits on the event yields of a general BSM signal in inclusive (i.e. single-bin) SRs. In this way, exact knowledge of BSM signal correlations across bins is not needed to estimate the result. Additionally, this configuration is also used to quantify the significance of possible data deviations from SM predictions. In the exclusion fit set-up, all CRs and SRs are fit simultaneously in order to test a BSM signal plus SM background hypothesis against a SM-only hypothesis. Unlike the model-independent configuration, these SRs are multi-bin regions that profit of the shape of benchmark signals to enhance the sensitivity to the 2HDM+ a model in different areas of the parameter space. All correlations between CRs and SRs are taken into account by the common background normalization parameters and systematic uncertainty nuisance parameters. This configuration is used to place limits on the production cross-section at a given point in the parameter space of the 2HDM+ a model.

5.1 Signal regions

An optimization procedure is followed to derive the event selection criteria for the tW_{0L} and tW_{1L} channels. It follows a two-step process, using a varying set of kinematic variables. First, a manual, coarse optimization is carried out, seeking to maximise the sensitivity of the event selection to a set of benchmark signal models. Then a random grid search algorithm [108] is used to fine-tune the coarse selection criteria.

The tW_{0L} channel selection criteria are summarised in Table 2. Following the signal topology, this channel selects events with exactly zero leptons, at least four jets and at least one large- R jet which is consistent with the hadronic decay of a W boson (W -tagged). Exactly one jet with $p_T > 50$ GeV is required to be b -tagged. Further requirements are placed on the W -boson candidate and the b -jet to suppress events where they both originate from the decay of the same top quark, as it is assumed that the boosted W boson in the signal topology arises from the decay of the charged Higgs boson. These requirements involve a large angular separation between the W -tagged large- R jet and the leading (highest- p_T) b -tagged jet ($\Delta R_{W\text{-tagged}, b_1}$) and an invariant mass of their combined four-vector ($m_{W\text{-tagged}, b_1}$) larger than the top-quark mass.

Requirements on E_T^{miss} and its object-based significance, $S_{E_T^{\text{miss}}}$ [109], are used to enhance the selection of events with invisible particles in the final state. As the momentum of the DM particles in the signal strongly depends on the mass difference between the a -boson mediator and the H^\pm boson, the signal region is further split into five bins in E_T^{miss} to maximise the sensitivity of this analysis throughout the full considered parameter space. These five bins are defined with E_T^{miss} intervals [250, 330] GeV, [330, 400] GeV, [400, 500] GeV, [500, 600] GeV and ≥ 600 GeV, referred to, respectively, as $\text{SR}_{tW_{0L}}^{\text{bin1}} - \text{SR}_{tW_{0L}}^{\text{bin5}}$. Inclusive signal regions, defined with $E_T^{\text{miss}} \geq 250, 330, 400, 500$ and 600 GeV, are also defined in this analysis as ‘discovery regions’. These single-bin overlapping SRs can be used to estimate either the significance of an excess or an upper limit on the signal yield with less stringent assumptions about the kinematic properties of the signal. The minimum azimuthal angle between E_T^{miss} and the leading four jets, $\min[\Delta\phi(\text{jet}_{1-4}, E_T^{\text{miss}})]$, is used to suppress fake E_T^{miss} arising from mismeasured jets. The transverse mass variable constructed from the

Table 2: Summary of the tW_{0L} and tW_{1L} signal region selections. The tW_{0L} signal region and the tW_{1L} region searching for hadronic top decays ($SR_{tW_{1L}}^{\text{had.top}}$) are further split into bins of E_T^{miss} to increase the sensitivity for different signal model parameters as described in the text. The signal region seeking leptonic top decays ($SR_{tW_{1L}}^{\text{lep.top}}$) is used inclusively.

Variable	$SR_{tW_{0L}}$	$SR_{tW_{1L}}^{\text{lep.top}}$	$SR_{tW_{1L}}^{\text{had.top}}$
Trigger	E_T^{miss}	E_T^{miss}	E_T^{miss}
E_T^{miss} [GeV]	≥ 250	≥ 250	≥ 250
$\mathcal{S}_{E_T^{\text{miss}}}$	≥ 14	≥ 15	-
$\min[\Delta\phi(\text{jet}_{1-4}, E_T^{\text{miss}})]$	≥ 0.9	≥ 0.5	≥ 0.5
Number of baseline leptons	0	1	1
Number of signal leptons	0	1	1
$p_T^{\ell_1}$ [GeV]	-	≥ 30	≥ 30
Number of signal jets	≥ 4	≥ 2	≥ 3
$p_T^{j_1}$ [GeV]	≥ 100	≥ 50	≥ 50
$p_T^{j_2}$ [GeV]	≥ 60	≥ 30	≥ 30
$p_T^{j_3}$ [GeV]	≥ 60	-	≥ 30
$p_T^{j_4}$ [GeV]	≥ 40	-	-
Number of b -tagged jets	≥ 1	≥ 1	≥ 1
$p_T^{b_1}$ [GeV]	≥ 50	≥ 50	≥ 50
$p_T^{b_2}$ [GeV]	≤ 50	≤ 50	≤ 50
Number of W -tagged jets ($N_{W\text{-tagged}}^{J;R=1.0}$)	≥ 1	≥ 1	-
$p_T^{J;R=1.0}$ [GeV]	≥ 200	≥ 200	-
$\Delta R_{W\text{-tagged}, b_1}$	≥ 1.0	-	-
$m_{W\text{-tagged}, b_1}$ [GeV]	≥ 220	-	-
$m_T(b_1, E_T^{\text{miss}})$ [GeV]	≥ 180	-	-
m_{b_1, \cancel{b}_1} [GeV]	-	≥ 200	≤ 200
$m_T(\ell, E_T^{\text{miss}})$ [GeV]	-	≥ 130	≥ 200
am_{T2} [GeV]	-	≥ 180	≥ 180
m_W^{had} [GeV]	-	-	≥ 60

leading b -jet of the event and the \vec{p}_T^{miss} , $m_T(b_1, E_T^{\text{miss}})$, [110] is used to suppress events from semileptonic $t\bar{t}$ decays, which exhibit an endpoint in $m_T(b_1, E_T^{\text{miss}})$ when the E_T^{miss} in the event arises entirely from a missed W boson.

The tW_{1L} channel, also summarised in Table 2, selects events with exactly one lepton and exactly one b -tagged jet with $p_T > 50$ GeV. As in the tW_{0L} channel, requirements in E_T^{miss} , $\mathcal{S}_{E_T^{\text{miss}}}$ and $\min[\Delta\phi(\text{jet}_{1-4}, E_T^{\text{miss}})]$ are used to enhance the selection of events with invisible particles and suppress events with fake E_T^{miss} . The one-lepton channel was explored previously in Ref. [39] and strategies used in the previous paper are now extended with ideas presented in Refs. [28, 111] and further enhanced by the use of W -tagging techniques.

In the tW_{1L} channel, events are selected with a boosted hadronically decaying W boson from the H^\pm boson decays and a leptonically decaying W -boson from the top quark decays. These events are selected for the $\text{SR}_{tW_{1L}}^{\text{lep.top}}$ region. The complementary set of events, where the W boson from the H^\pm boson decays leptonically and the W boson from the top quark decays hadronically, are selected for the $\text{SR}_{tW_{1L}}^{\text{had.top}}$ region. A new variable, called m_{b_1, \cancel{b}_1} , is used to guarantee that $\text{SR}_{tW_{1L}}^{\text{lep.top}}$ and $\text{SR}_{tW_{1L}}^{\text{had.top}}$ are statistically independent. It is constructed as the invariant mass of the leading b -jet (b_1) and the highest- p_T jet that is not b -tagged (\cancel{b}_1). Signal events with the top quark decaying hadronically exhibit an endpoint in m_{b_1, \cancel{b}_1} slightly below the top-quark mass, while events with a leptonically decaying top quark extend beyond this endpoint [28].

Following the previous analysis [39], the $\text{SR}_{tW_{1L}}^{\text{lep.top}}$ and $\text{SR}_{tW_{1L}}^{\text{had.top}}$ regions exploit both the transverse mass of the lepton and the E_T^{miss} , $m_T(\ell, E_T^{\text{miss}})$, and the asymmetric transverse mass [112–116], am_{T2} , to suppress the background from semileptonic and dileptonic $t\bar{t}$ decays, respectively. The latter is constructed to have an endpoint at the top-quark mass for dileptonic $t\bar{t}$ events where one of the leptons is outside the acceptance or misidentified. In addition, the $\text{SR}_{tW_{1L}}^{\text{lep.top}}$ region requires at least one W -tagged large- R jet, while $\text{SR}_{tW_{1L}}^{\text{had.top}}$ uses the variable m_W^{had} [39, 116]. Here, m_W^{had} uses a variable-radius jet reconstruction algorithm with standard jet inputs to identify the hadronically decaying W bosons in the event even when their momentum is not high enough to be reconstructed within a large- R jet. As in the tW_{0L} channel, binning the SRs in E_T^{miss} is the optimal strategy to maximise the sensitivity throughout the full model parameter space. However, due to the low event yield in $\text{SR}_{tW_{1L}}^{\text{lep.top}}$, this strategy is implemented only in the $\text{SR}_{tW_{1L}}^{\text{had.top}}$ region. Five different bins are then defined with E_T^{miss} intervals [250, 300] GeV, [300, 350] GeV, [350, 400] GeV, [400, 450] GeV and ≥ 450 GeV, referred to as $\text{SR}_{tW_{1L}}^{\text{had.top bin1}}$ – $\text{SR}_{tW_{1L}}^{\text{had.top bin5}}$. Similarly, inclusive ‘discovery’ SRs are defined with $E_T^{\text{miss}} \geq 250, 300, 350, 400$ and 450 GeV.

5.2 Background estimation and validation

Control regions are designed to support the estimation of the dominant backgrounds. In the tW_{0L} channel, the three most important backgrounds are Z + jets, $t\bar{t}$ and W + jets. In the tW_{1L} channel, the most important backgrounds are $t\bar{t}$ and $t\bar{t}Z$ in $\text{SR}_{tW_{1L}}^{\text{lep.top}}$ and $t\bar{t}$ and W + jets in $\text{SR}_{tW_{1L}}^{\text{had.top}}$. All background processes, with the exception of $t\bar{t}$, are estimated in common CRs and with common normalization parameters for the tW_{0L} and tW_{1L} channels. Figure 2 schematically depicts the requirements imposed on the main analysis observables in the CRs (and VRs) in order to ensure orthogonality to the SRs and low signal contamination, as well as high purity in the targeted background, in each region.

The composition of the $t\bar{t}$ background in the tW_{0L} and tW_{1L} channels is very different. In the former, the background is dominated by semileptonic $t\bar{t}$ decays, while in the latter, dileptonic $t\bar{t}$ decays dominate. In

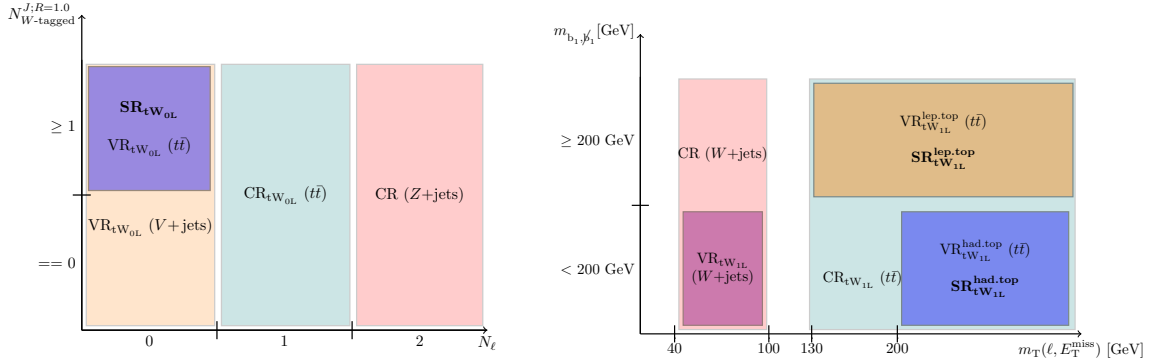


Figure 2: Schema of the definitions of the different regions corresponding to (left) the tW_{0L} channel in $N_{W\text{-tagged}}^{J;R=1.0}$ and the number of leptons (N_ℓ) and (right) the tW_{1L} channel in $m_T(\ell, E_T^{\text{miss}})$ and m_{b_1, \bar{b}_1} . Orthogonality between the different regions observed to overlap is ensured by the inversion of some selection cuts in variables that aren't depicted in this figure. $m_{W\text{-tagged}, b_1}$ and $\Delta R_{W\text{-tagged}, b_1}$ are inverted to ensure the orthogonality of the tW_{0L} signal and validation regions. The $t\bar{t}$ validation regions and the tW_{1L} regions are independent thanks to the inversion of the selection cuts on am_{T2} . Finally, m_W^{had} ensures the orthogonality of the W +jets control and validation regions.

both cases, these backgrounds satisfy the selection criteria because one lepton is misidentified as a jet or falls outside of the detector fiducial area. Due to the difference in composition, two control regions are defined in order to normalise the $t\bar{t}$ background for the tW_{0L} and tW_{1L} channels. The tW_{0L} $t\bar{t}$ CR is enriched in semileptonic $t\bar{t}$ events by requiring exactly one lepton, low $m_T(\ell, E_T^{\text{miss}})$, low am_{T2} and dropping the $\mathcal{S}_{E_T^{\text{miss}}}$ requirement. Requirements similar to those in the tW_{0L} SRs are also imposed on the presence of a W -tagged large- R jet and on $\Delta R_{W\text{-tagged}, b_1}$ and $m_{W\text{-tagged}, b_1}$ to ensure that this control region scans a topology similar to that in the SRs. The tW_{1L} $t\bar{t}$ CR is enriched in dileptonic $t\bar{t}$ events by inverting the constraints on am_{T2} and $p_T^{b_2}$. Since this region is used to estimate the $t\bar{t}$ background in both tW_{1L} SRs, if a variable has different requirements in the two SRs, the requirement is either dropped in the CR or chosen to be the looser one.

The Z +jets background, dominated in the tW_{0L} signal region by $Z(\rightarrow \nu\nu)$ +jets, is estimated by selecting a large high-purity sample of events with two same-flavour opposite-sign (SF-OS) leptons, as presented in Figure 2. The leptons from the Z -boson decay are treated as invisible particles and added to the E_T^{miss} of the event, now denoted by $E_{T, \ell\ell}^{\text{miss}}$, to mimic the behaviour of the Z +jets background in the tW_{0L} SR, where this background is dominant. The CR is defined by following the selection criteria of the tW_{0L} SR, but variables built with E_T^{miss} in the SR are built with $E_{T, \ell\ell}^{\text{miss}}$ instead. The W +jets background is estimated in a CR selecting events with exactly one lepton and $m_T(\ell, E_T^{\text{miss}})$ in the W -boson mass range [40, 100] GeV (as presented in Figure 2), high $\mathcal{S}_{E_T^{\text{miss}}}$ and low m_W^{had} to ensure high acceptance for W +jets events.

The estimation of the $t\bar{t}Z$ background is performed in a selection requiring exactly three leptons as described in Ref. [87]. A Z -boson candidate is reconstructed from the SF-OS lepton pair with invariant mass closest to the Z -boson mass. The resulting lepton pair is treated as invisible. The contribution from jets misidentified as leptons in this control region is estimated using MC samples and amounts to less than 10% [87].

Finally, to correctly estimate the single-top-quark background and, therefore, to reduce the systematic uncertainties arising from its modelling, a dedicated CR with two leptons and high E_T^{miss} is constructed. Most

$Z + \text{jets}$ events are removed by requiring $m_{\ell\ell}$ to be outside of the Z -boson mass range i.e. $\notin [71, 111]$ GeV. Events with a leptonically decaying W boson are selected by means of a low m_{T2} requirement built using both leptons in the event and E_T^{miss} . The variables $m_{b\ell}^{\text{min}}$ and $m_{b\ell}^t$ [39, 117] are built by combining the leptons and jets in the event and present an endpoint in the range 153–170 GeV, close to the mass of the top quark. They are highly efficient in separating the single-top-quark, $t\bar{t}$ and $t\bar{t}Z$ backgrounds and are used to increase this CR's purity in single-top-quark events.

A summary of all control region definitions can be found in Tables 3 and 4. Normalization factors for all of the aforementioned SM backgrounds are fitted simultaneously in these regions using the background-only fit configuration. Their values are $\mu_{t\bar{t}}^{\text{tW}_{0L}} = 1.00 \pm 0.12$, $\mu_{t\bar{t}}^{\text{tW}_{1L}} = 0.92 \pm 0.06$, $\mu_{Z+\text{jets}} = 0.98 \pm 0.07$, $\mu_{W+\text{jets}} = 1.08 \pm 0.09$, $\mu_{\text{single-top}} = 0.43 \pm 0.13$ and $\mu_{t\bar{t}Z} = 1.18 \pm 0.19$. There is a large discrepancy between the fitted value of the single-top normalization parameter and the Monte Carlo predicted value. This discrepancy is driven by the dominant contribution of the tW process to the single-top channel and related to the modelling of the interference between single-resonant and double-resonant top-quark production. It is found that the default scheme used to model this interference (diagram removal [118]) and the alternative scheme used to estimate the associated uncertainty (diagram subtraction, see Section 6 for details) bracket the observed number of events in the single-top CR data, with a large difference between the two predictions. The single-top CR allows $\mu_{\text{single-top}}$ to be constrained by data independently of the choice of default interference scheme. Residual shape differences between the two schemes are assigned as systematic uncertainties as described in Section 6.

Figure 3 shows the post-fit E_T^{miss} and $E_{T,\ell\ell}^{\text{miss}}$ distributions for all CRs, where good agreement between data and fitted predictions can be observed.

Validation regions are defined in order to verify that the background estimation strategy is robust. One or more VRs are designed to validate each background estimate from the CRs. The $tW_{0L} t\bar{t}$ background estimate is validated using a selection with zero reconstructed leptons. In order to ensure orthogonality to the SRs and a high $t\bar{t}$ background purity, the $m_{W\text{-tagged},b_1}$ and $\mathcal{S}_{E_T^{\text{miss}}}$ selection requirements are inverted. A similar strategy is used for the $Z + \text{jets}$ and $W + \text{jets}$ VRs, where the normalization factors are extrapolated from two-lepton and one-lepton control regions to a zero-lepton selection. However, since the definition of a $W + \text{jets}$ -enriched region using an event selection with no leptons poses a challenge due to its similarity to $Z + \text{jets}$, a combined $V + \text{jets}$ validation region is defined for $W + \text{jets}$ and $Z + \text{jets}$ with the goal of high acceptance for the sum of the two processes. In the $V + \text{jets}$ validation region, the selection requirement on $\Delta R_{W\text{-tagged},b_1}$ is also inverted to be orthogonal to the signal region, but the $\mathcal{S}_{E_T^{\text{miss}}}$ selection requirement is kept the same, as this ensures orthogonality to the $tW_{0L} t\bar{t}$ VR. Furthermore, in order to decrease statistical uncertainties, the $N_{W\text{-tagged}}^{J;R=1.0}$ selection requirement is relaxed, as shown in Figure 2, and requirements on $\min[\Delta\phi(j^{\text{all}}, E_T^{\text{miss}})]$ and $\Delta R_{j_1,j_2}$ are imposed to increase the $Z + \text{jets}$ and $W + \text{jets}$ purity.

To validate the $t\bar{t}$ prediction in the tW_{1L} channel, one validation region per SR is constructed. In both VRs, low am_{T2} is required, both to ensure orthogonality to the signal regions and to enhance the $t\bar{t}$ fraction. To increase the acceptance in the regions, the W -tagging requirement is dropped in the $\text{SR}_{tW_{1L}}^{\text{lep.top}} t\bar{t}$ validation region and the m_W^{had} requirement is dropped in the $\text{SR}_{tW_{1L}}^{\text{had.top}} t\bar{t}$ validation region. The $W + \text{jets}$ VR is kinematically close to $\text{SR}_{tW_{1L}}^{\text{had.top}}$. The acceptance of $W + \text{jets}$ events is increased by constraining $m_T(\ell, E_T^{\text{miss}})$ to be in the W -boson mass range and demanding high $\mathcal{S}_{E_T^{\text{miss}}}$. The resulting region has large $t\bar{t}$ and single-top-quark contributions and can be considered a simultaneous validation region for all three backgrounds. Good agreement between data and the $t\bar{t}Z$ background predicted by its CR was reported in Ref. [87], so no dedicated $t\bar{t}Z$ VR is considered in this analysis.

Table 3: Summary of W + jets, Z + jets, and both $t\bar{t}$ control regions. All variables used in Z + jets CR are calculated using a corrected version of the E_T^{miss} , denoted by $E_{T,\ell\ell}^{\text{miss}}$, treating all leptons in the event as invisible. ‘SF-OS’ indicates that the selected leptons are required to have the same flavour and opposite-sign electric charges, such that they are compatible with the decay of a Z boson.

Variable	$\text{CR}_{tW_{0L}}(t\bar{t})$	$\text{CR}_{tW_{1L}}(t\bar{t})$	CR (W + jets)	CR (Z + jets)
Trigger	E_T^{miss}	E_T^{miss}	E_T^{miss}	Single-lepton
E_T^{miss} [GeV]	≥ 250	≥ 250	≥ 250	≤ 120
$E_{T,\ell\ell}^{\text{miss}}$ [GeV]	–	–	–	≥ 250
$\mathcal{S}_{E_T^{\text{miss}}}$	–	–	≥ 15	–
$\mathcal{S}_{E_{T,\ell\ell}^{\text{miss}}}$	–	–	–	≥ 14
$\min[\Delta\phi(\text{jet}_{1-4}, E_T^{\text{miss}})]$	≥ 0.5	≥ 0.5	≥ 0.5	–
$\min[\Delta\phi(\text{jet}_{1-4}, E_{T,\ell\ell}^{\text{miss}})]$	–	–	–	≥ 0.5
Number of baseline leptons	1	1	1	2
Number of signal leptons	1	1	1	2 (SF-OS)
$p_T^{\ell_1}$ [GeV]	≥ 30	≥ 30	≥ 30	≥ 30
$p_T^{\ell_2}$ [GeV]	–	–	–	≥ 20
Number of signal jets	≥ 4	≥ 3	≥ 3	≥ 4
$p_T^{j_1}$ [GeV]	≥ 100	≥ 30	≥ 30	≥ 100
$p_T^{j_2}$ [GeV]	≥ 60	≥ 30	≥ 30	≥ 60
$p_T^{j_3}$ [GeV]	≥ 60	≥ 30	≥ 30	≥ 60
$p_T^{j_4}$ [GeV]	≥ 40	–	–	≥ 40
Number of b -tagged jets	≥ 1	≥ 2	≥ 1	≥ 1
$p_T^{b_1}$ [GeV]	≥ 50	≥ 50	≥ 50	≥ 50
$p_T^{b_2}$ [GeV]	≤ 50	≥ 50	≤ 50	≤ 50
Number of W -tagged jets ($N_{W\text{-tagged}}^{J;R=1.0}$)	≥ 1	–	$= 0$	≥ 0
$\Delta R_{W\text{-tagged},b_1}$	≥ 1.0	–	–	–
$m_{W\text{-tagged},b_1}$ [GeV]	≥ 220	–	–	–
$m_{\ell\ell}$ [GeV]	–	–	–	$\in [81, 101]$
$m_T(b_1, E_{T,\ell\ell}^{\text{miss}})$ [GeV]	–	–	–	≥ 180
$m_T(\ell, E_T^{\text{miss}})$ [GeV]	$\in [30, 130]$	≥ 130	$\in [40, 100]$	–
am_{T2} [GeV]	< 180	< 180	≥ 180	–
m_W^{had} [GeV]	–	–	< 60	–

Table 4: Summary of the single-top-quark and $t\bar{t}Z$ control regions. ‘SF’ and ‘OS’ indicate that the two leptons are required to have the same flavour and opposite-sign electric charges, respectively. For the $t\bar{t}V$ CR, the leptons treated as invisible in $E_{T,\ell\ell}^{\text{miss}}$ are the SF-OS pair with invariant mass closest to the Z-boson mass.

Variable	CR (Single t)	CR ($t\bar{t}Z$)
Trigger	E_T^{miss}	Single-lepton
E_T^{miss} [GeV]	≥ 250	–
$E_{T,\ell\ell}^{\text{miss}}$ [GeV]	–	≥ 140
$\min[\Delta\phi(\text{jet}_{1-4}, E_T^{\text{miss}})]$	≥ 0.5	–
Number of baseline leptons	2	3
Number of signal leptons	2 (OS)	3 (at least one SF-OS pair)
$p_T^{\ell_1}$ [GeV]	≥ 25	≥ 30
$p_T^{\ell_2}$ [GeV]	≥ 20	≥ 20
$p_T^{\ell_3}$ [GeV]	–	≥ 20
Number of signal jets	≥ 1	≥ 3
$p_T^{j_1}$ [GeV]	≥ 50	≥ 30
$p_T^{j_2}$ [GeV]	–	≥ 30
$p_T^{j_3}$ [GeV]	–	≥ 30
Number of b -tagged jets	≥ 1	≥ 2
$p_T^{b_1}$ [GeV]	≥ 50	≥ 30
$p_T^{b_2}$ [GeV]	–	≥ 30
$m_{\ell\ell}$ [GeV]	$\geq 40, \notin [71, 111]$ if SF	$\in [71, 111]$ for at least one SF-OS pair
$m_T(\ell, E_T^{\text{miss}})$ [GeV]	> 30	–
m_{T2} [GeV]	< 100	–
$m_{b\ell}^{\text{min}}$ [GeV]	> 170	–
$m_{b\ell}^t$ [GeV]	> 150	–

Table 5: Summary of the tW_{0L} $t\bar{t}$ and the $V+$ jets validation regions.

Variable	$VR_{tW_{0L}}(t\bar{t})$	$VR_{tW_{0L}}(V+\text{jets})$
Trigger	E_T^{miss}	E_T^{miss}
E_T^{miss} [GeV]	≥ 250	≥ 250
$\mathcal{S}_{E_T^{\text{miss}}}$	$\in [10, 14]$	≥ 14
$\min[\Delta\phi(\text{jet}_{1-4}, E_T^{\text{miss}})]$	≥ 0.9	≥ 0.5
Number of baseline leptons	0	0
Number of signal leptons	0	0
Number of signal jets	≥ 4	≥ 4
p_T^{j1} [GeV]	≥ 100	≥ 100
p_T^{j2} [GeV]	≥ 60	≥ 60
p_T^{j3} [GeV]	≥ 60	≥ 60
p_T^{j4} [GeV]	≥ 40	≥ 40
Number of b -tagged jets	≥ 1	≥ 1
p_T^{b1} [GeV]	≥ 50	≥ 50
p_T^{b2} [GeV]	≤ 50	≤ 50
Number of W -tagged jets ($N_{W\text{-tagged}}^{J;R=1.0}$)	≥ 1	≥ 0
$\Delta R_{W\text{-tagged}, b1}$	-	< 1.0
$m_{W\text{-tagged}, b1}$ [GeV]	< 220	-
$m_T(b1, E_T^{\text{miss}})$ [GeV]	≥ 180	≥ 180
$\min[\Delta\phi(j^{\text{all}}, E_T^{\text{miss}})]$	-	≥ 1.2
$\Delta R_{j1, j2}$	-	≥ 1.2

Finally, the single-top-quark prediction is validated in a one-lepton region. The single-top-quark acceptance is enhanced by applying a low $m_T(\ell, E_T^{\text{miss}})$ requirement. The $t\bar{t}$ events are suppressed by demanding high am_{T2} and $\mathcal{S}_{E_T^{\text{miss}}}$. The W +jets contribution is reduced by selecting events with high sub-leading b -jet transverse momentum.

A summary of all validation regions can be found in Tables 5 and 6. Figure 4 shows the post-fit E_T^{miss} distribution in each VR. In addition, observed data and predicted background yields in all control and validation regions are presented in Figure 5, together with the ratio of their difference to the estimated background uncertainty. Good agreement between data and the expected background predictions can be observed in both figures, thus validating the background estimation strategy of the analysis.

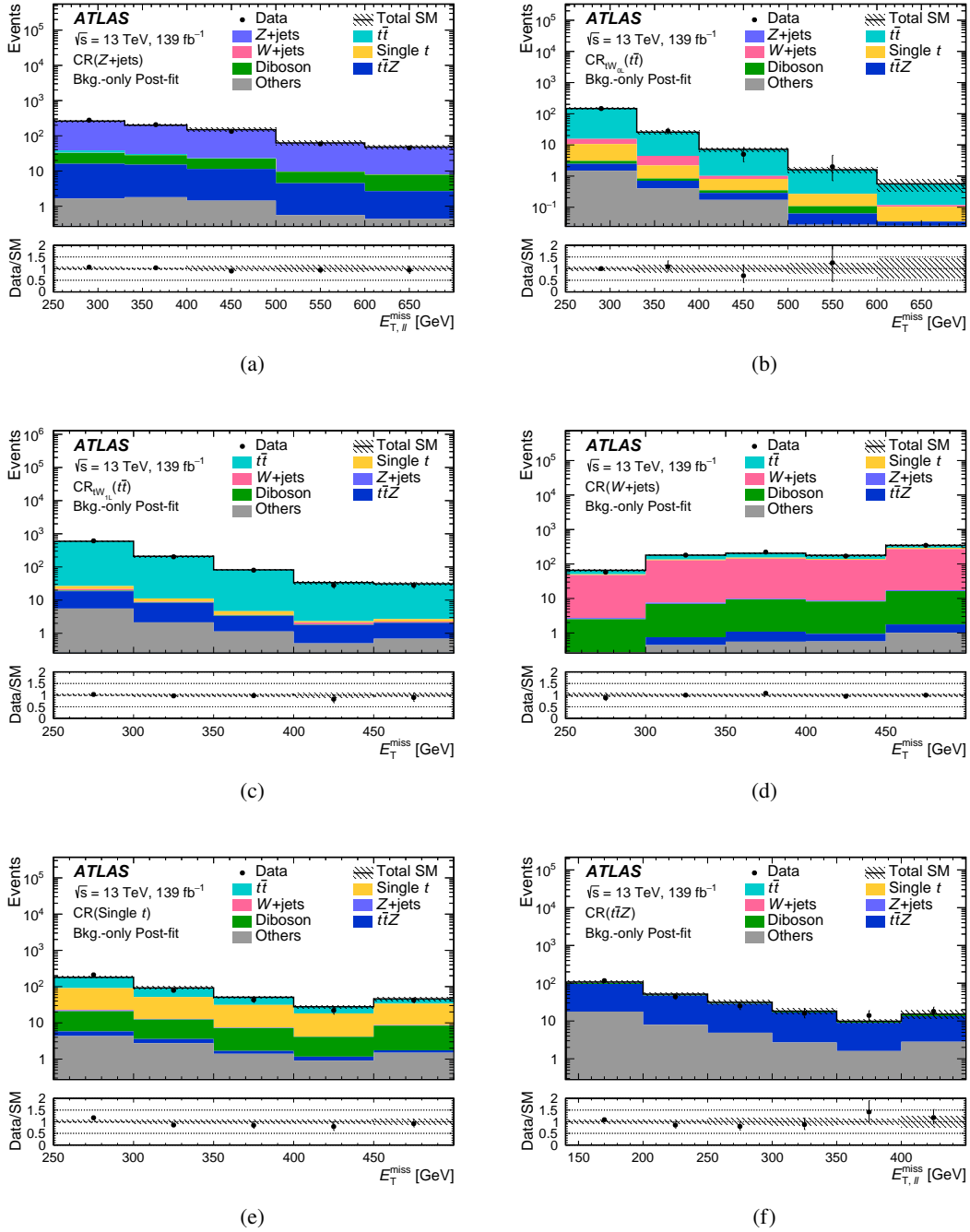


Figure 3: The post-fit E_T^{miss} and $E_{T,\ell\ell}^{\text{miss}}$ distributions in the (a) $Z+jets$, (b) $tW_{0L} t\bar{t}$, (c) $tW_{IL} t\bar{t}$, (d) $W+jets$, (e) single-top, and (f) $t\bar{t}Z$ control regions. The last bin in the histogram includes the overflow events. The bottom panel shows the ratio of data to total SM background. The uncertainties shown are the sum of the statistical and post-fit systematic uncertainties as detailed in Section 6. The fit set-up corresponds to the background-only fit configuration. The ‘Others’ category includes contributions from rare processes such as tWZ , tZ , triboson, ttt , $t\bar{t}\bar{t}$, $t\bar{t}W$ and $t\bar{t}H$.

Table 6: Summary of the tW_{1L} , $t\bar{t}$, W +jets and single-top-quark validation regions.

Variable	$VR_{tW_{1L}}^{\text{lep.top}}(t\bar{t})$	$VR_{tW_{1L}}^{\text{had.top}}(t\bar{t})$	$VR_{tW_{1L}}(W+\text{jets})$	VR (Single t)
Trigger	E_T^{miss}	E_T^{miss}	E_T^{miss}	E_T^{miss}
E_T^{miss} [GeV]	≥ 250	≥ 250	≥ 250	≥ 250
$\mathcal{S}_{E_T^{\text{miss}}}$	≥ 15	–	≥ 15	≥ 15
$\min[\Delta\phi(\text{jet}_{1-4}, E_T^{\text{miss}})]$	≥ 0.5	≥ 0.5	≥ 0.5	≥ 0.5
Number of baseline leptons	1	1	1	1
Number of signal leptons	1	1	1	1
$p_T^{\ell_1}$ [GeV]	≥ 30	≥ 30	≥ 30	≥ 30
Number of signal jets	≥ 2	≥ 3	≥ 3	≥ 3
Number of b -tagged jets	≥ 1	≥ 1	≥ 1	≥ 2
$p_T^{b_1}$ [GeV]	≥ 50	≥ 50	≥ 50	≥ 50
$p_T^{b_2}$ [GeV]	≤ 50	≤ 50	≤ 50	≥ 50
$m_T(\ell, E_T^{\text{miss}})$ [GeV]	≥ 130	≥ 200	$\in [40, 100]$	$\in [30, 100]$
m_{b_1, \cancel{b}_1} [GeV]	≥ 200	< 200	< 200	–
am_{T2} [GeV]	< 180	< 180	≥ 180	≥ 180
m_W^{had} [GeV]	–	–	≥ 60	–

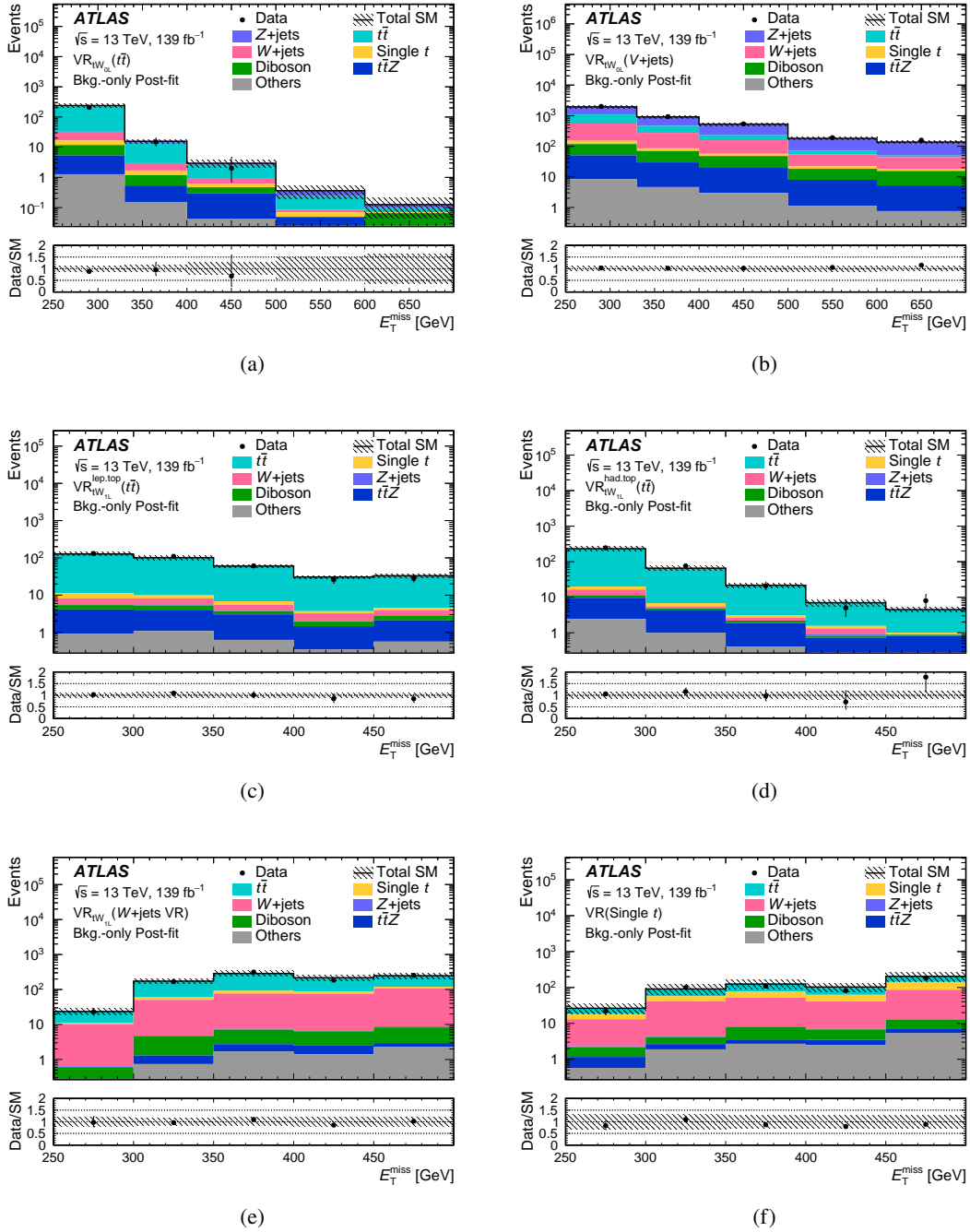


Figure 4: The post-fit E_T^{miss} distributions in the (a) $tW_{\text{OL}} t\bar{t}$, (b) $tW_{\text{OL}} V+jets$ (c) $SR_{\text{WIL}}^{\text{lep.top}} t\bar{t}$, (d) $SR_{\text{WIL}}^{\text{had.top}} t\bar{t}$, (e) $W+jets$ and (f) single-top-quark validation regions. The last bin in the histogram includes the overflow events. The bottom panel shows the ratio of data to the total SM background. The uncertainties shown are the sum of the statistical and post-fit systematic uncertainties as detailed in Section 6. The fit set-up corresponds to the background-only fit configuration. The ‘Others’ category includes contributions from rare processes such as tWZ , tZ , triboson, ttt , $t\bar{t}\bar{t}$, ttW and ttH .

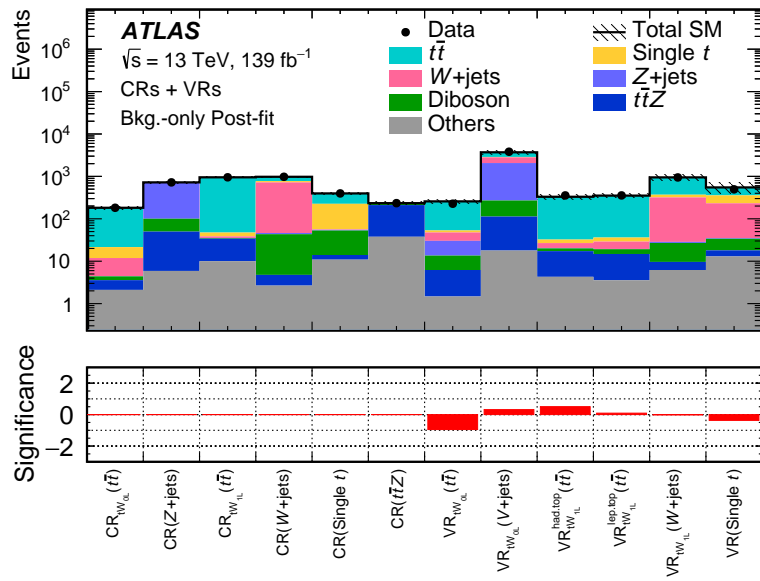


Figure 5: Summary of all control and validation regions comparing the post-fit predicted SM background with the observed number of events. The normalization parameters were extracted from the control regions. The fit set-up corresponds to the background-only fit configuration. Statistical and systematic uncertainties are included in the shaded region of the top panel as detailed in Section 6. The bottom panel shows the statistical significance [119] of the excesses and deficits of data relative to the predicted SM background.

5.3 Statistical combination

The SRs of the tW_{0L} and tW_{1L} channels are constructed to be statistically independent and they are combined to derive the final results in Section 7. The CRs are constructed to be in common for the two channels, with the exception of the $t\bar{t}$ CRs which are disjoint and the $t\bar{t}$ background is estimated in each channel with a separate normalization parameter. These two channels are also statistically independent of the tW_{2L} channel in Ref. [87]. For this reason the results are also derived using the statistical combination of the tW_{0L} and tW_{1L} channels with the tW_{2L} channel, in order to provide the most stringent constraints on the model considered in this paper. The dominant SM background in the tW_{2L} channel is $t\bar{t}Z$ production and it is estimated in Ref. [87] using a CR which is a subset of the $t\bar{t}Z$ CR in this paper. In the combination of the three channels, the $t\bar{t}Z$ background is estimated using a common normalization parameter fitted in the common tW_{0L} and tW_{1L} CR (Section 5.2). As the $t\bar{t}Z$ CR in this paper has less contamination from diboson processes than the tW_{2L} $t\bar{t}Z$ CR, the diboson CR of Ref. [87], which provides an estimate of the diboson processes in the $t\bar{t}Z$ CR, is not used. All other SM backgrounds in the tW_{2L} channel are estimated directly from the MC simulation, as in Ref. [87]. These CR orthogonalization choices impact the final tW_{2L} background estimate by up to 10%–15% because the normalization factor for the $t\bar{t}Z$ background in this channel changes from 0.8 ± 0.2 to 1.2 ± 0.2 .

6 Systematic uncertainties

This analysis considers several sources of uncertainty, of both experimental and theoretical nature, that affect the prediction of the SM background and the DM signal in all channels. Figure 6 provides an overview of the size of the tW_{0L} and tW_{1L} systematic uncertainties, estimated in a combined fit of the two channels.

The uncertainties related to the limited measurement precision of reconstructed objects, the estimate of the dataset luminosity and the modelling of the pile-up are broadly referred to as ‘detector systematic uncertainties’. The dominant contributions to these uncertainties arise from the small- R jet energy scale and resolution and the large- R jet W -tagging. The small- R jet energy scale and resolution uncertainties have a large impact on the high E_T^{miss} bins of the $\text{SR}_{tW_{1L}}^{\text{had.top}}$ and $\text{SR}_{tW_{1L}}^{\text{lep.top}}$ region, respectively. In addition, small- R jet energy resolution uncertainties are the source of the second-largest experimental uncertainty in the tW_{0L} SRs. The W -tagging uncertainties dominate across the tW_{0L} SRs, being the dominant experimental uncertainty in this channel. The uncertainties associated with trigger requirements, pile-up modelling, lepton reconstruction and energy measurements have a small or negligible impact on the final results. The lepton, photon and jet-related uncertainties are propagated to the calculation of the E_T^{miss} , along with additional uncertainties due to the energy scale and resolution of the soft term. These E_T^{miss} soft-term uncertainties are found to be small or negligible. Finally, as mentioned in Section 3, a 1.7% uncertainty in the combined 2015–2018 integrated luminosity is included.

Theoretical uncertainties are estimated for the modelling of SM background processes in the MC simulation. Their theoretical cross-section uncertainties are also taken into account. Modelling uncertainties are important for both channels. In the tW_{0L} channel, single-top-quark uncertainties are dominant in the bins of the SRs with highest E_T^{miss} requirements, while Z +jets theory uncertainties contribute significantly in the lowest E_T^{miss} bins. The $t\bar{t}$ and W +jets uncertainties are the dominant ones in the tW_{1L} channel. The Z +jets and W +jets modelling uncertainties are evaluated by varying the CKKW-L scale for matching of the matrix element and parton shower, and the resummation, renormalization and factorization scales independently

by factors of 0.5 and 2. The $t\bar{t}$ and single-top-quark uncertainties from the renormalization and factorization scales and initial- and final-state radiation parameters are evaluated similarly. In addition, uncertainties due to our choices of hard-scattering generator and parton-shower and hadronization models are estimated for these two processes. The impact of the latter is evaluated by comparing the nominal simulated sample with a sample generated using the same matrix element generator, POWHEG BOX, interfaced to an alternative shower generator, HERWIG 7 [120, 121]. This sample uses the H7UE set of tuned parameters [121]. To assess the uncertainty due to the choice of hard-scattering generator and matching scheme, an alternative generator set-up using MADGRAPH5_AMC@NLO [54] interfaced to PYTHIA 8 [55] is employed. An additional uncertainty is considered for the single-top-quark tW channel: the impact of interference between single-resonant and double-resonant top-quark production on the implementation of the W -boson lineshape in the generator is estimated by comparing the nominal sample generated using the diagram removal method with samples using the alternative diagram subtraction method [118]. For the $t\bar{t}Z$ background, uncertainties related to the choice of renormalization and factorization scales are assessed by varying the corresponding event generator parameters by factors of 0.5 and 2 from their nominal values. Overall, the total SM uncertainties vary from 11% to 42% across the tW_{0L} and tW_{1L} signal regions.

Detector and modelling uncertainties are also evaluated for the DM signal processes. Detector uncertainties are found to have an impact of 9%–43% on the expected signal yields across the $m_a-m_{H^\pm}$ and $m_a-\tan\beta$ planes for the signal regions of the tW_{0L} and tW_{1L} analysis channels. The largest uncertainties are found to be concentrated in the highest E_T^{miss} bins of the SRs for both channels. In all SRs, the dominant experimental uncertainties affecting signal yields are found to be the uncertainties associated with the jet energy scale and resolution and with W -tagging, as observed for the SM processes. These uncertainties are assumed to be fully correlated with those affecting the SM background. Modelling uncertainties include renormalization and factorization scale uncertainties and uncertainties related to the modelling of the parton shower. For the signal regions of the tW_{0L} (tW_{1L}) analysis channel, the average value of these modelling uncertainties lies between 3% and 30% (3% and 24%) across the $m_a-m_{H^\pm}$ and $m_a-\tan\beta$ planes, but can reach 50% for certain benchmark signals in the highest E_T^{miss} regions of the channel.

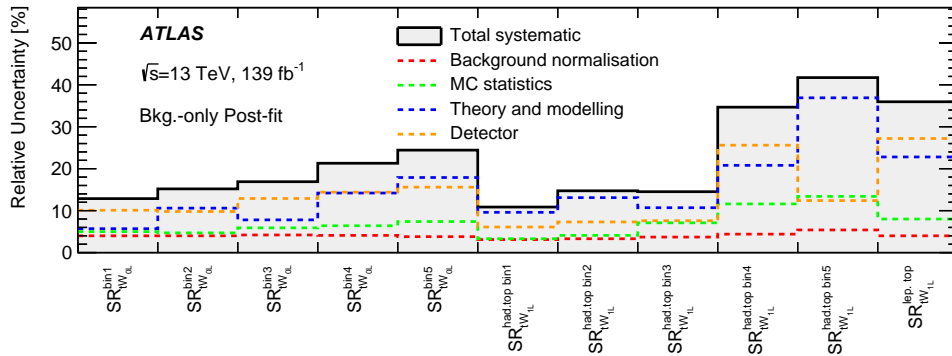


Figure 6: Relative uncertainties (in percent) in the total background yield in each signal region of the two analysis channels, including the contributions from the different sources of uncertainty. The ‘Detector’ category contains all detector-related systematic uncertainties. The ‘Background normalization’ represents the uncertainty in the fitted normalization factors, including the available data event counts in the CRs. Individual uncertainties can be correlated, and do not necessarily add up in quadrature to the total background uncertainty. The fit configuration used to estimate these uncertainties corresponds to the background-only fit explained in Section 7.

The effects of the various sources of systematic uncertainty on the signal and background estimates are introduced in the likelihood fit (see Section 5) through nuisance parameters (NPs) that affect the expectation values of the Poisson terms for each CR and SR bin. The probability density function of each nuisance parameter is described by a Gaussian distribution whose standard deviation corresponds to a specific experimental or theoretical modelling uncertainty. The preferred value of each nuisance parameter is determined as part of the likelihood fit and none of them is significantly altered or constrained by the fit. The uncertainties arising from the total number of data events in the CRs are also included in the fit for each region. Since the number of CRs matches the number of fitted background normalization parameters, the systematic uncertainties are not constrained in the background-only fit of this analysis.

All uncertainties arising from the same source, including background and signal modelling uncertainties, are treated as correlated across the tW_{0L} and tW_{1L} channels. For the statistical combination of the tW_{0L} and tW_{1L} channels with the tW_{2L} channel, a simplified approach which considers uncorrelated experimental and theoretical systematic uncertainties is adopted. This is supported by the large differences between the definitions of the physics objects, the selection and quality criteria, and uncertainty schemes which were used in the tW_{2L} channel and the analyses described in this paper. Only the modelling uncertainties for the DM signal are treated as correlated across all channels.

7 Results

The expected and observed numbers of events in the tW_{0L} and tW_{1L} SRs are shown in Tables 7 and 8, respectively, together with the SM prediction breakdown for the background processes. The expected yields are derived using the background-only fit configuration. All systematic and statistical uncertainties described in Section 6 are included in the predictions. A graphical representation of the tables is given in Figure 7, where the bottom panel shows the statistical significance [119] of the difference between the observation and prediction. No significant deviation of the observed data from the SM prediction is found. The largest difference appears in $SR_{tW_{0L}}^{\text{bin}4}$, corresponding to $500 < E_T^{\text{miss}} < 600$ GeV, and amounts to a data event deficit of around 2.5σ considering statistical and systematic uncertainties of the SM prediction. Since the data and predictions agree well in the bins below and above, this deficit is considered to be a statistical fluctuation.

Figure 8 shows the observed data and the SM prediction in the tW_{0L} channel for the E_T^{miss} distribution in the SR using the binning of the final fit. In the same figure, the W -tagged jet multiplicity, the $m_{W\text{-tagged},b_1}$ observable and the $m_T(b_1, E_T^{\text{miss}})$ observable are shown in a region that contains all SR requirements with the exception of the one on the variable shown in the plot. Small local deficits are seen in the $m_{W\text{-tagged},b_1}$ variable around 480 GeV, although no significant trend is observed in any of the distributions and overall, given the uncertainties, there is good agreement between data and predictions.

Figure 9 shows the observed data and the SM prediction in $SR_{tW_{1L}}^{\text{lep.top}}$ and $SR_{tW_{1L}}^{\text{had.top}}$ of the tW_{1L} channel. Panel (a) shows the E_T^{miss} distribution in $SR_{tW_{1L}}^{\text{had.top}}$, using the same bins as in the final fit. In the other panels, the W -tagged jet multiplicity in $SR_{tW_{1L}}^{\text{lep.top}}$ and the m_{b_1, \cancel{b}_1} observable in both $SR_{tW_{1L}}^{\text{lep.top}}$ and $SR_{tW_{1L}}^{\text{had.top}}$ are shown. In all cases, all SR requirements except the one on the shown quantity are applied. Similarly to the tW_{0L} channel, no significant trend is observed in the distributions and overall there is good agreement between data and prediction. In addition, Figures 9(c) and 9(d) show that $N_{W\text{-tagged}}^{J;R=1.0}$ and m_{b_1, \cancel{b}_1} are powerful discriminating variables for rejecting $t\bar{t}$ and $W+$ jets backgrounds for the considered signal benchmark models.

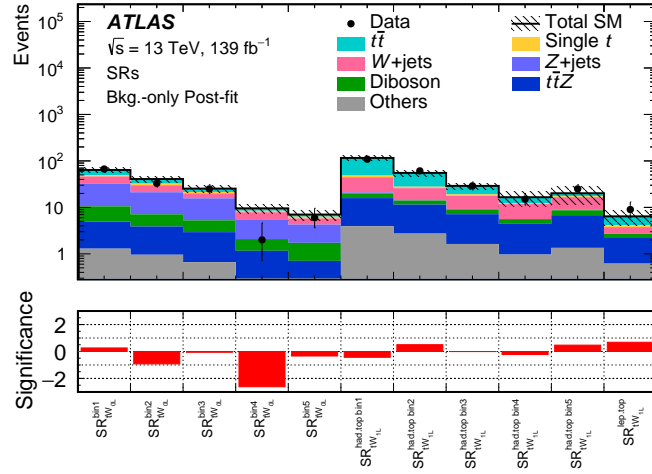


Figure 7: Comparison of the background-only fit SM predictions extrapolated to all SRs with the observed data. The normalization of the backgrounds is obtained from the fit to the CRs. The upper panel shows the observed number of events and the predicted background yields. The ‘Others’ category includes contributions from rare processes such as tWZ , tZ , triboson, ttt , $t\bar{t}t$, $t\bar{t}t$, $t\bar{t}t$ and $t\bar{t}t$. All uncertainties defined in Section 6 are included in the uncertainty band. The bottom panel shows the statistical significance [119] of the excesses and deficits of data events relative to the predicted SM background.

Table 7: Event yields showing the observed data and the background-only fit SM predictions in the tW_{0L} signal regions. Signal regions are defined according to the five E_T^{miss} bins presented in Section 5.1 for the tW_{0L} channel, corresponding to increasing E_T^{miss} values in bins 1–5. SM predictions are decomposed into the main backgrounds of the analysis. Smaller backgrounds (tWZ , tZ , triboson, ttt , $t\bar{t}t$, $t\bar{t}t$ and $t\bar{t}t$ events) are grouped together and labelled as ‘Others’. The quoted uncertainties in the fitted SM background include both the statistical and systematic uncertainties.

	SR ^{bin1} _{tW_{0L}}	SR ^{bin2} _{tW_{0L}}	SR ^{bin3} _{tW_{0L}}	SR ^{bin4} _{tW_{0L}}	SR ^{bin5} _{tW_{0L}}
Observed events	67	33	25	2	6
Fitted SM bkg. events	64 ± 8	41 ± 6	25 ± 4	9.6 ± 2.1	7.0 ± 1.7
Z + jets	22 ± 5	14.1 ± 2.9	10.4 ± 2.7	3.4 ± 0.9	2.5 ± 0.8
W + jets	14.2 ± 3.2	8.8 ± 1.8	4.4 ± 1.3	2.4 ± 0.8	1.51 ± 0.28
$t\bar{t}$	14.2 ± 2.6	8.3 ± 3.3	3.9 ± 1.2	1.1 ± 0.5	0.7 ± 0.6
$t\bar{t}Z$	3.6 ± 1.6	2.9 ± 1.1	2.3 ± 0.9	1.0 ^{+1.0} _{-1.0}	0.5 ± 0.4
Single-top	3.3 ± 2.5	2.5 ^{+3.1} _{-2.5}	1.4 ± 1.1	0.6 ^{+0.8} _{-0.6}	0.5 ^{+1.0} _{-0.5}
Diboson	5.6 ± 1.2	3.2 ± 0.8	2.3 ± 0.8	0.92 ± 0.26	1.02 ± 0.31
Others	1.29 ± 0.23	0.96 ± 0.17	0.66 ± 0.11	0.20 ± 0.04	0.20 ± 0.04

Table 8: Event yields showing the observed data and the background-only fit SM predictions in the tW_{1L} signal regions. Bin numbers for $SR_{tW_{1L}}^{\text{had.top}}$ refer to the five E_T^{miss} bins presented in Section 5.1 for the tW_{1L} channel, corresponding to increasing E_T^{miss} values in bins 1–5. SM predictions are decomposed into the main backgrounds of the analysis. Smaller backgrounds (tWZ , tZ , triboson, ttt , $t\bar{t}t\bar{t}$, ttW and ttH events) are grouped together and labelled as ‘Others’. The quoted uncertainties in the fitted SM background include both the statistical and systematic uncertainties.

	$SR_{tW_{1L}}^{\text{had.top bin1}}$	$SR_{tW_{1L}}^{\text{had.top bin2}}$	$SR_{tW_{1L}}^{\text{had.top bin3}}$	$SR_{tW_{1L}}^{\text{had.top bin4}}$	$SR_{tW_{1L}}^{\text{had.top bin5}}$	$SR_{tW_{1L}}^{\text{lep.top}}$
Observed events	109	61	29	15	25	9
Fitted SM bkg. events	116 ± 13	55 ± 8	29 ± 4	17 ± 6	20 ± 8	6.4 ± 2.3
Z + jets	$0.9^{+1.1}_{-0.9}$	0.22 ± 0.13	0.25 ± 0.25	$0.04^{+0.09}_{-0.04}$	0.25 ± 0.08	0.01 ± 0.00
W+ jets	24 ± 8	12 ± 5	8.6 ± 2.8	6 ± 5	8 ± 8	$1.1^{+1.6}_{-1.1}$
$t\bar{t}$	68 ± 8	27 ± 6	10.0 ± 2.1	4.2 ± 1.2	2.9 ± 1.2	2.3 ± 1.4
$t\bar{t}Z$	11.9 ± 3.4	8.8 ± 1.9	5.5 ± 2.4	3.5 ± 1.5	5.5 ± 1.7	1.6 ± 0.7
Single-top	4^{+4}_{-4}	$1.9^{+2.5}_{-1.9}$	$1.2^{+1.5}_{-1.2}$	$0.6^{+1.3}_{-0.6}$	0.7 ± 0.7	$0.4^{+0.7}_{-0.4}$
Diboson	4.2 ± 0.4	2.58 ± 0.32	1.9 ± 0.4	1.16 ± 0.22	1.88 ± 0.31	0.51 ± 0.09
Others	3.95 ± 0.28	2.72 ± 0.28	1.63 ± 0.17	0.96 ± 0.14	1.35 ± 0.32	0.62 ± 0.12

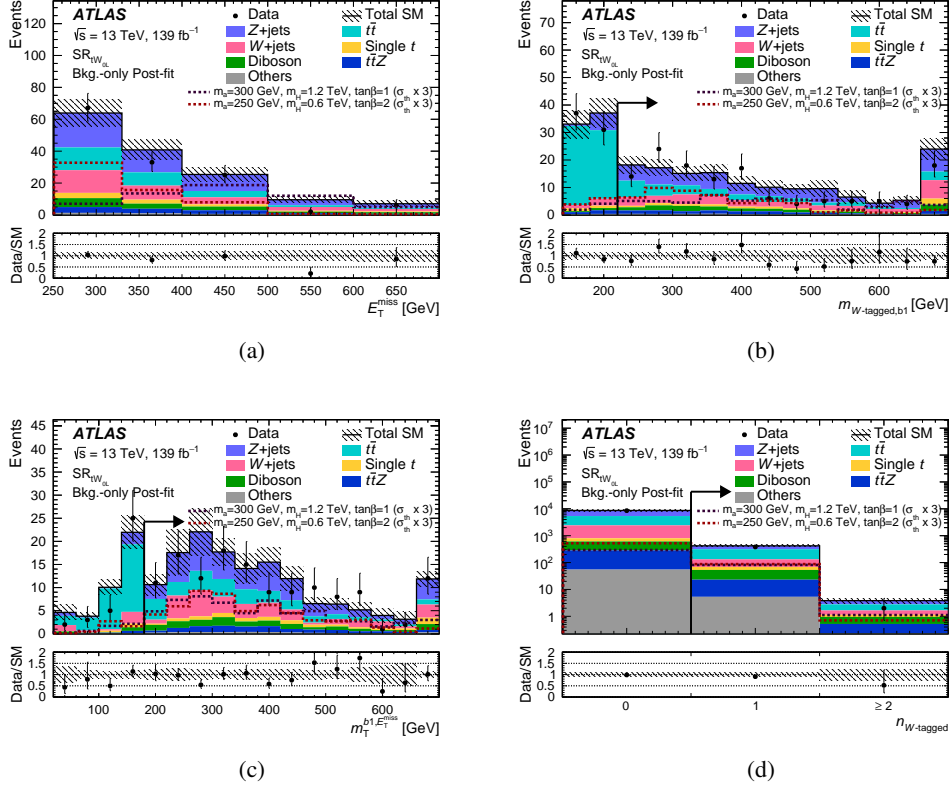


Figure 8: Representative distributions of (a) E_T^{miss} , (b) $m_{W\text{-tagged},b1}$, (c) $m_T(b1, E_T^{\text{miss}})$, and (d) the number of W -tagged large- R jets in the tW_{0L} signal region. Observed data are compared with the SM background predictions extrapolated from the background-only fit. The ‘Others’ category includes contributions from rare processes such as tWZ , tZ , triboson, ttt , $t\bar{t}\bar{t}$, ttW and ttH . The expected distributions for representative scenarios with different m_a , m_{H^\pm} , and $\tan\beta$ are shown for illustrative purposes. All signal theory cross-sections (σ_{th}) have been multiplied by three for better visibility. The overflow events, where present, are included in the last bin. The lower panels show the ratio of data to the background prediction. The hatched error bands indicate the combined experimental, theoretical and MC statistical uncertainties of these background predictions. The arrows, when present, indicate the value of the SR requirement on the quantity presented on the x -axis.

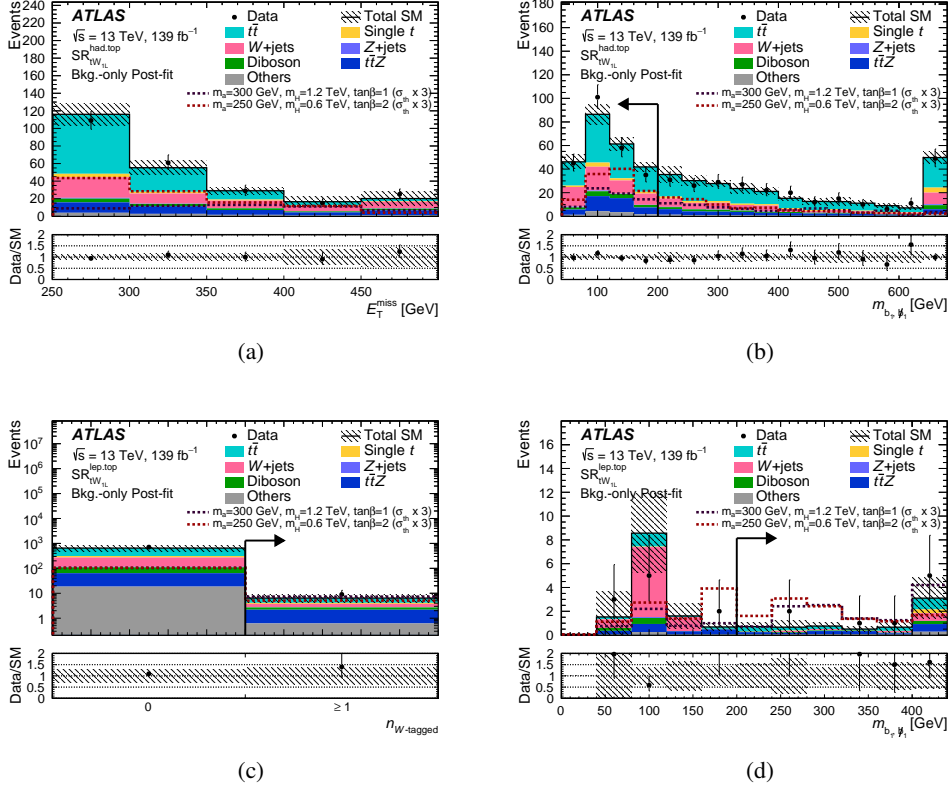


Figure 9: Representative distributions of (a) E_T^{miss} and (b) m_{b_1, \bar{b}_1} in $\text{SR}_{tW_{IL}}^{\text{had, top}}$, as well as (c) the number of W -tagged large- R jets and (d) m_{b_1, \bar{b}_1} in $\text{SR}_{tW_{IL}}^{\text{lep, top}}$. Observed data are compared with the SM background predictions extrapolated from the background-only fit. The ‘Others’ category includes contributions from rare processes such as tWZ , tZ , triboson, ttt , $t\bar{t}t\bar{t}$, ttW and ttH . The expected distributions for representative scenarios with different m_a , m_{H^\pm} , and $\tan\beta$ values are shown for illustrative purposes. All signal theory cross-sections (σ_{th}) have been multiplied by three for better visibility. The overflow events, where present, are included in the last bin. The lower panels show the ratio of data to the background prediction. The hatched error bands indicate the combined experimental, theoretical and MC statistical uncertainties of these background predictions. The arrows, when present, indicate the value of the SR requirement on the quantity presented on the x -axis.

7.1 Model-independent exclusion upper limits

Model-independent upper limits exclude the presence of a larger generic signal independently for each discovery region considered in this analysis. These limits are evaluated by extrapolating the SM background predictions obtained from the background-only fit configuration to the single-bin inclusive SR. Table 9 presents the results of this evaluation, provided in the form of CL_B representing the probability of the predicted SM background to fluctuate to at least the observed number of events. In addition, 95% CL upper limits are set on the observed (S_{obs}^{95}) and expected (S_{exp}^{95}) numbers of BSM events as well as on the visible cross-section (σ_{vis}) for all discovery regions.

7.2 Exclusion limits for the 2HDM+ a model

The tW_{OL} and tW_{IL} channels are statistically combined with the tW_{2L} channel of Ref. [39] as described in Sections 5 and 6, in order to provide the most stringent constraints for 2HDM+ a models using the tW +DM channel.

Exclusion limits on the 2HDM+ a model are derived as a function of the parameters m_a , m_{H^\pm} , and $\tan\beta$ in a combined likelihood fit to the events in all CRs and SRs of the three channels and are shown in Figure 10. The results are presented as a function of (m_a, m_{H^\pm}) assuming $\tan\beta = 1$ and as a function of $(m_{H^\pm}, \tan\beta)$ assuming $m_a = 150$ GeV or $m_a = 250$ GeV. Values of $\tan\beta$ up to 30 are considered in order to probe the local maximum at $\tan\beta \in [20, 30]$, as explained in Section 1. The 1σ uncertainty bands are shown as

Table 9: The first column presents the name of the treated discovery region. The next two columns present the observed number of data events and expected SM contribution from the background-only fit in the model-independent regions. The fourth and fifth columns present the 95% CL upper limits on the visible cross-section ($\langle\epsilon\sigma\rangle_{\text{obs}}^{95}$) and on the observed number of signal events (S_{obs}^{95}), respectively. The sixth column (S_{exp}^{95}) shows the 95% CL upper limit on the expected number of signal events, given the expected number of background events and $\pm 1\sigma$ excursions of the expectation. The last two columns indicate the CL_B value, i.e. the confidence level observed for the background-only hypothesis, and the discovery p -value ($p(s=0)$). These values are calculated using an asymptotic calculator based on a one-sided profile likelihood. Therefore, the p -values corresponding to regions with deficits are capped at 0.5.

Signal channel	Obs.	SM. exp	$\langle\epsilon\sigma\rangle_{\text{obs}}^{95}$ [fb]	S_{obs}^{95}	S_{exp}^{95}	CL_B	$p(s=0)$ (Z)
$\text{SR}_{tW_{\text{OL}}}(E_{\text{T}}^{\text{miss}} \geq 250 \text{ GeV})$	133	147 ± 15	0.21	29	36_{-10}^{+14}	0.24	0.50 (0.00)
$\text{SR}_{tW_{\text{OL}}}(E_{\text{T}}^{\text{miss}} \geq 330 \text{ GeV})$	66	83 ± 9	0.11	15.5	24_{-7}^{+10}	0.09	0.50 (0.00)
$\text{SR}_{tW_{\text{OL}}}(E_{\text{T}}^{\text{miss}} \geq 400 \text{ GeV})$	33	42 ± 6	0.08	11.7	16_{-5}^{+7}	0.15	0.50 (0.00)
$\text{SR}_{tW_{\text{OL}}}(E_{\text{T}}^{\text{miss}} \geq 500 \text{ GeV})$	8	16.6 ± 2.3	0.04	5.4	$9.7_{-2.8}^{+4.3}$	0.03	0.50 (0.00)
$\text{SR}_{tW_{\text{OL}}}(E_{\text{T}}^{\text{miss}} \geq 600 \text{ GeV})$	6	7.0 ± 1.7	0.05	6.5	$7.4_{-2.1}^{+3.3}$	0.38	0.50 (0.00)
$\text{SR}_{tW_{\text{IL}}}^{\text{had.top}}(E_{\text{T}}^{\text{miss}} \geq 250 \text{ GeV})$	239	237 ± 25	0.42	58	57_{-15}^{+21}	0.53	0.47 (0.06)
$\text{SR}_{tW_{\text{IL}}}^{\text{had.top}}(E_{\text{T}}^{\text{miss}} \geq 300 \text{ GeV})$	130	121 ± 17	0.33	46.4	40_{-11}^{+15}	0.67	0.33 (0.44)
$\text{SR}_{tW_{\text{IL}}}^{\text{had.top}}(E_{\text{T}}^{\text{miss}} \geq 350 \text{ GeV})$	69	66 ± 9	0.19	26.3	24_{-7}^{+10}	0.60	0.39 (0.27)
$\text{SR}_{tW_{\text{IL}}}^{\text{had.top}}(E_{\text{T}}^{\text{miss}} \geq 400 \text{ GeV})$	40	37 ± 9	0.17	23.7	22_{-6}^{+8}	0.62	0.38 (0.30)
$\text{SR}_{tW_{\text{IL}}}^{\text{had.top}}(E_{\text{T}}^{\text{miss}} \geq 450 \text{ GeV})$	25	20 ± 9	0.16	22.0	19_{-5}^{+6}	0.69	0.30 (0.51)
$\text{SR}_{tW_{\text{IL}}}^{\text{lep.top}}$	9	6.4 ± 2.3	0.07	10.2	$8.0_{-2.3}^{+3.8}$	0.74	0.24 (0.72)

shaded areas around the expected limit contour of the statistical combination. The typical acceptance, i.e. percentage of events passing the selection requirements defined in Section 5, times detector efficiency for the tW +DM benchmark signals is 0.02%–1.2% for the inclusive tW_{0L} SRs, 0.001%–0.4% for $SR_{tW_{1L}}^{\text{lep.top}}$ and 0.04%–1.1% for the $SR_{tW_{1L}}^{\text{had.top}}$ bins. Figure 10 also shows the sensitivity of each individual channel in both the (m_a, m_{H^\pm}) and $(m_{H^\pm}, \tan\beta)$ planes. For the fits in the individual channels, the non- $t\bar{t}$ background estimates in the signal regions are derived using all control regions defined in Section 5.2, including the common $t\bar{t}Z$ region for the tW_{2L} channel. For the $t\bar{t}$ process, the tW_{0L} fit uses the tW_{0L} $t\bar{t}$ CR, while the tW_{1L} $t\bar{t}$ CR is used in the tW_{1L} fit. The left panels in Figure 10 consider only the tW +DM process as signal for the interpretation of the results, while the right panels in the same figure consider the contributions of both the tW +DM and $t\bar{t}$ +DM processes as predicted by the 2HDM+ a model.

The introduction of the tW_{0L} channel and the statistical combination performed in this paper extend the sensitivity towards large H^\pm boson masses. Exclusion limits are placed in the high $\tan\beta$ parameter space for the first time in this final state. Signal models assuming H^\pm boson masses up to 1.5 TeV and a -boson masses up to 350 GeV can be excluded at 95% CL for $\tan\beta = 1$. For an a -boson mass of 150 (250) GeV, $\tan\beta$ values up to 2 are excluded for H^\pm masses between 300 (400) GeV and 1.5 TeV. Signals with $\tan\beta$ values between 20 and 30 are also excluded for H^\pm masses between 500 and 800 GeV (900 GeV) and a a -boson mass of 150 (250) GeV. If $t\bar{t}$ +DM contributions are considered together with tW +DM, a -boson masses up to 250 GeV can be excluded at 95% CL for an H^\pm mass of 1.5 TeV assuming $\tan\beta = 1$. For low H^\pm boson masses, the lower limit on m_a is 20–40 GeV higher than when considering only the tW +DM contribution at the same $\tan\beta$ value. Assuming an m_a value of 150 GeV or 250 GeV, H^\pm boson masses below 400 GeV can be excluded for $\tan\beta$ values lower than 1. No additional constraints are observed at $\tan\beta > 10$ when adding the $t\bar{t}$ +DM contribution to the tW +DM contribution since, as discussed in Refs. [15, 34], the $t\bar{t}$ +DM cross-section in the 2HDM+ a model is proportional to $1/\tan^2\beta$ and is expected to be subdominant at high $\tan\beta$ values.

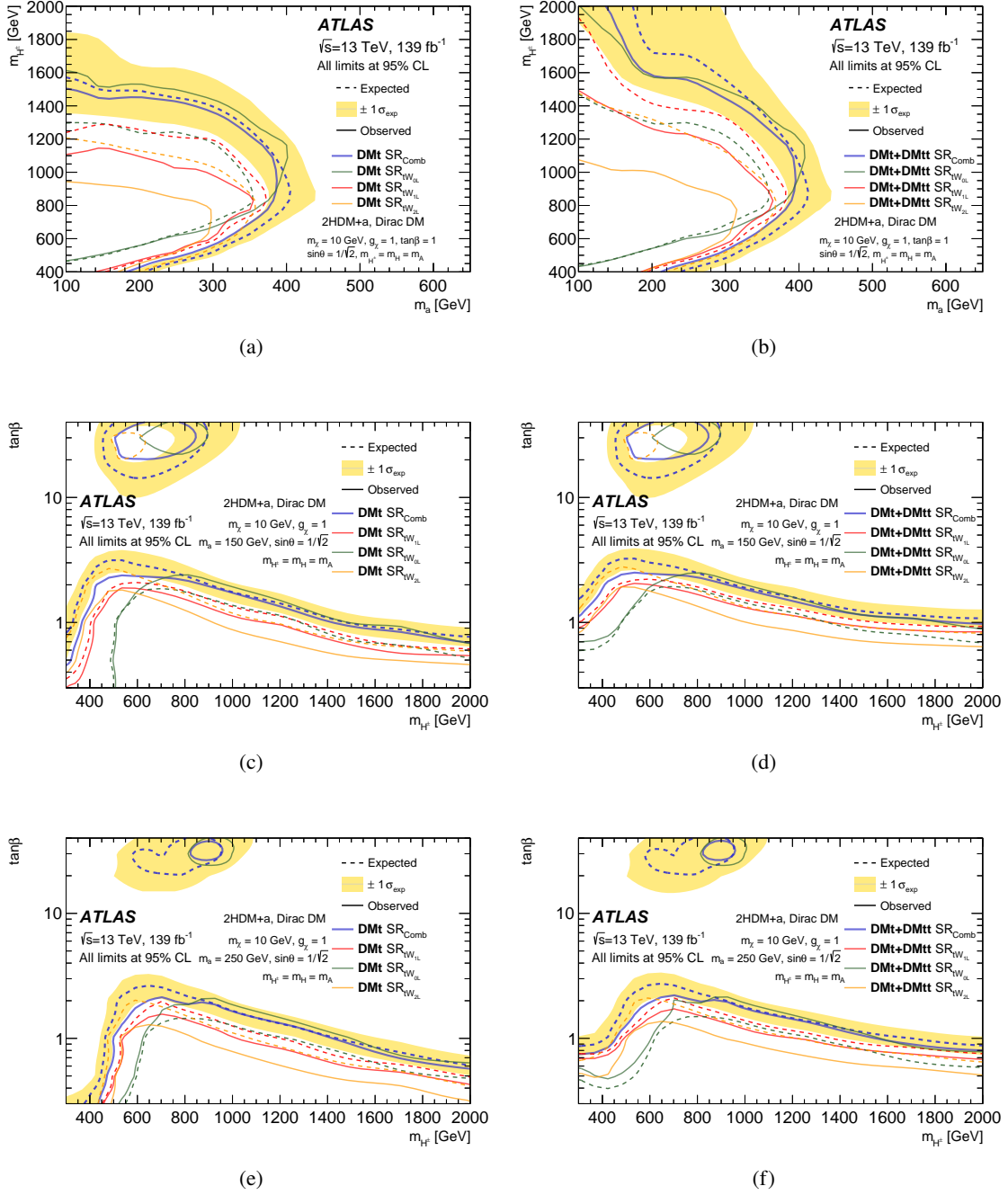


Figure 10: The expected and observed exclusion contours as a function of (a)–(b) (m_a, m_{H^\pm}) , (c)–(d) $(m_{H^\pm}, \tan\beta)$ assuming $m_a = 150$ GeV and (e)–(f) $(m_{H^\pm}, \tan\beta)$ assuming $m_a = 250$ GeV. The individual tW_{0L} (green line), tW_{1L} (red line) and tW_{2L} (orange line) analysis channels are shown together with their statistical combination (blue line). Only tW +DM contributions are considered in (a), (c) and (e), while (b), (d) and (f) consider tW +DM and $t\bar{t}$ +DM contributions. Experimental and theoretical systematic uncertainties, as described in Section 6, are applied to background and signal samples and illustrated by the ± 1 standard-deviation yellow band and the blue dashed contour lines, respectively, for the statistical combination.

8 Conclusions

A search for dark matter in final states with a single top quark and an energetic W boson using 139 fb^{-1} of pp collisions delivered by the LHC at a centre-of-mass energy of 13 TeV and collected by the ATLAS detector is presented. The search focuses on a two-Higgs-doublet model together with an additional pseudoscalar mediator, a , which decays into dark-matter particles. Final states which include either zero or one charged lepton (electron or muon) and a significant amount of missing transverse momentum are considered. No significant excess relative to Standard Model predictions was found and 95% confidence-level limits are set on the 2HDM+ a signal models considered. These limits exclude a -boson mediator masses up to 350 GeV and H^\pm boson masses up to 1.5 TeV for $\tan\beta = 1$ in comparison with the current 1.3 TeV bound, and are the most stringent limits on tW +DM signal models obtained so far at the LHC. This analysis also provides the first limits for a 2HDM+ a signal model assuming $\tan\beta \geq 10$ and using the single-top-quark production signature.

Acknowledgements

We thank CERN for the very successful operation of the LHC, as well as the support staff from our institutions without whom ATLAS could not be operated efficiently.

We acknowledge the support of ANPCyT, Argentina; YerPhI, Armenia; ARC, Australia; BMWFW and FWF, Austria; ANAS, Azerbaijan; CNPq and FAPESP, Brazil; NSERC, NRC and CFI, Canada; CERN; ANID, Chile; CAS, MOST and NSFC, China; Minciencias, Colombia; MEYS CR, Czech Republic; DNRF and DNSRC, Denmark; IN2P3-CNRS and CEA-DRF/IRFU, France; SRNSFG, Georgia; BMBF, HGF and MPG, Germany; GSRI, Greece; RGC and Hong Kong SAR, China; ISF and Benoziyo Center, Israel; INFN, Italy; MEXT and JSPS, Japan; CNRST, Morocco; NWO, Netherlands; RCN, Norway; MEiN, Poland; FCT, Portugal; MNE/IFA, Romania; MESTD, Serbia; MSSR, Slovakia; ARRS and MIZŠ, Slovenia; DSI/NRF, South Africa; MICINN, Spain; SRC and Wallenberg Foundation, Sweden; SERI, SNSF and Cantons of Bern and Geneva, Switzerland; MOST, Taiwan; TENMAK, Türkiye; STFC, United Kingdom; DOE and NSF, United States of America. In addition, individual groups and members have received support from BCKDF, CANARIE, Compute Canada and CRC, Canada; PRIMUS 21/SCI/017 and UNCE SCI/013, Czech Republic; COST, ERC, ERDF, Horizon 2020 and Marie Skłodowska-Curie Actions, European Union; Investissements d’Avenir Labex, Investissements d’Avenir IDEX and ANR, France; DFG and AvH Foundation, Germany; Herakleitos, Thales and Aristeia programmes co-financed by EU-ESF and the Greek NSRF, Greece; BSF-NSF and MINERVA, Israel; Norwegian Financial Mechanism 2014-2021, Norway; NCN and NAWA, Poland; La Caixa Banking Foundation, CERCA Programme Generalitat de Catalunya and PROMETEO and GenT Programmes Generalitat Valenciana, Spain; Göran Gustafssons Stiftelse, Sweden; The Royal Society and Leverhulme Trust, United Kingdom.

The crucial computing support from all WLCG partners is acknowledged gratefully, in particular from CERN, the ATLAS Tier-1 facilities at TRIUMF (Canada), NDGF (Denmark, Norway, Sweden), CC-IN2P3 (France), KIT/GridKA (Germany), INFN-CNAF (Italy), NL-T1 (Netherlands), PIC (Spain), ASGC (Taiwan), RAL (UK) and BNL (USA), the Tier-2 facilities worldwide and large non-WLCG resource providers. Major contributors of computing resources are listed in Ref. [122].

References

- [1] F. Zwicky, *Die Rotverschiebung von extragalaktischen Nebeln*, *Helv. Phys. Acta* **6** (1933) 110.
- [2] G. Bertone, D. Hooper and J. Silk, *Particle dark matter: Evidence, candidates and constraints*, *Phys. Rept.* **405** (2005) 279, arXiv: [hep-ph/0404175](#).
- [3] G. Hinshaw et al., *Nine-Year Wilkinson Microwave Anisotropy Probe (WMAP) Observations: Cosmological Parameter Results*, *Astrophys. J. Suppl.* **208** (2013) 19, arXiv: [1212.5226 \[astro-ph.CO\]](#).
- [4] N. Aghanim et al., *Planck 2018 results. I. Overview and the cosmological legacy of Planck*, *Astron. Astrophys.* **641** (2020) A1, arXiv: [1807.06205 \[astro-ph.CO\]](#).
- [5] G. Steigman and M. S. Turner, *Cosmological constraints on the properties of weakly interacting massive particles*, *Nucl. Phys. B* **253** (1985) 375.
- [6] S. Ipek, D. McKeen and A. E. Nelson, *Renormalizable model for the Galactic Center gamma-ray excess from dark matter annihilation*, *Phys. Rev. D* **90** (2014) 055021, arXiv: [1404.3716 \[hep-ph\]](#).
- [7] J. M. No, *Looking through the pseudoscalar portal into dark matter: Novel mono-Higgs and mono-Z signatures at the LHC*, *Phys. Rev. D* **93** (2016) 031701, arXiv: [1509.01110 \[hep-ph\]](#).
- [8] D. Gonçalves, P. A. N. Machado and J. M. No, *Simplified models for dark matter face their consistent completions*, *Phys. Rev. D* **95** (2017) 055027, arXiv: [1611.04593 \[hep-ph\]](#).
- [9] N. F. Bell, G. Busoni and I. W. Sanderson, *Self-consistent Dark Matter Simplified Models with an s-channel scalar mediator*, *JCAP* **1703** (2017) 015, arXiv: [1612.03475 \[hep-ph\]](#).
- [10] M. Bauer, U. Haisch and F. Kahlhoefer, *Simplified dark matter models with two Higgs doublets: I. Pseudoscalar mediators*, *JHEP* **05** (2017) 138, arXiv: [1701.07427 \[hep-ph\]](#).
- [11] M. Bauer, M. Klassen and V. Tenorth, *Universal properties of pseudoscalar mediators in dark matter extensions of 2HDMs*, *JHEP* **07** (2018) 107, arXiv: [1712.06597 \[hep-ph\]](#).
- [12] U. Haisch and A. Malinauskas, *Let there be light from a second light Higgs doublet*, *JHEP* **03** (2018) 135, arXiv: [1712.06599 \[hep-ph\]](#).
- [13] G. Arcadi, M. Lindner, F. S. Queiroz, W. Rodejohann and S. Vogl, *Pseudoscalar mediators: A WIMP model at the neutrino floor*, *JCAP* **1803** (2018) 042, arXiv: [1711.02110 \[hep-ph\]](#).
- [14] N. F. Bell, G. Busoni and I. W. Sanderson, *Two Higgs doublet dark matter portal*, *JCAP* **1801** (2018) 015, arXiv: [1710.10764 \[hep-ph\]](#).
- [15] T. Abe et al., *LHC Dark Matter Working Group: Next-generation spin-0 dark matter models*, *Phys. Dark Univ.* **27** (2020) 100351, arXiv: [1810.09420 \[hep-ex\]](#).
- [16] J. Abdallah et al., *Simplified models for dark matter searches at the LHC*, *Phys. Dark Univ.* **9-10** (2015) 8, arXiv: [1506.03116 \[hep-ph\]](#).

- [17] D. Abercrombie et al., *Dark Matter benchmark models for early LHC Run-2 Searches: Report of the ATLAS/CMS Dark Matter Forum*, *Phys. Dark Univ.* **27** (2020) 100371, arXiv: 1507.00966 [hep-ex].
- [18] K. Cheung, K. Mawatari, E. Senaha, P.-Y. Tseng and T.-C. Yuan, *The top window for dark matter*, *JHEP* **10** (2010) 081, arXiv: 1009.0618 [hep-ph].
- [19] U. Haisch, A. Hibbs and E. Re, *Determining the structure of dark-matter couplings at the LHC*, *Phys. Rev. D* **89** (2014) 034009, arXiv: 1311.7131 [hep-ph].
- [20] M. R. Buckley, D. Feld and D. Gonçalves, *Scalar simplified models for dark matter*, *Phys. Rev. D* **91** (2015) 015017, arXiv: 1410.6497 [hep-ph].
- [21] M. R. Buckley and D. Gonçalves, *Constraining the strength and CP structure of dark production at the LHC: The associated top-pair channel*, *Phys. Rev. D* **93** (2016) 034003, arXiv: 1511.06451 [hep-ph].
- [22] U. Haisch and E. Re, *Simplified dark matter top-quark interactions at the LHC*, *JHEP* **06** (2015) 078, arXiv: 1503.00691 [hep-ph].
- [23] M. Backović et al., *Higher-order QCD predictions for dark matter production at the LHC in simplified models with s-channel mediators*, *Eur. Phys. J. C* **75** (2015) 482, arXiv: 1508.05327 [hep-ph].
- [24] C. Arina et al., *A comprehensive approach to dark matter studies: exploration of simplified top-philic models*, *JHEP* **11** (2016) 111, arXiv: 1605.09242 [hep-ph].
- [25] U. Haisch, P. Pani and G. Polesello, *Determining the CP nature of spin-0 mediators in associated production of dark matter and $t\bar{t}$ pairs*, *JHEP* **02** (2017) 131, arXiv: 1611.09841 [hep-ph].
- [26] S. Banerjee et al., *Cornering pseudoscalar-mediated dark matter with the LHC and cosmology*, *JHEP* **07** (2017) 080, arXiv: 1705.02327 [hep-ph].
- [27] U. Haisch and G. Polesello, *Searching for production of dark matter in association with top quarks at the LHC*, *JHEP* **02** (2019) 029, arXiv: 1812.00694 [hep-ph].
- [28] P. Pani and G. Polesello, *Dark matter production in association with a single top-quark at the LHC in a two-Higgs-doublet model with a pseudoscalar mediator*, *Phys. Dark Univ.* **21** (2018) 8, arXiv: 1712.03874 [hep-ph].
- [29] X. Cid Vidal et al., *Report from Working Group 3: Beyond the Standard Model physics at the HL-LHC and HE-LHC*, *CERN Yellow Rep. Monogr.* **7** (2019) 585, arXiv: 1812.07831 [hep-ph].
- [30] ATLAS Collaboration, *ATLAS sensitivity to Two-Higgs-Doublet models with an additional pseudoscalar exploiting four top quark signatures with $3ab^{-1}$ of $\sqrt{s} = 14$ TeV proton-proton collisions*, ATL-PHYS-PUB-2018-027, 2018, URL: <https://cds.cern.ch/record/2645845>.
- [31] U. Haisch and G. Polesello, *Searching for heavy Higgs bosons in the $t\bar{t}Z$ and tbW final states*, *JHEP* **09** (2018) 151, arXiv: 1807.07734 [hep-ph].
- [32] J. M. Butterworth, M. Habedank, P. Pani and A. Vaitkus, *A study of collider signatures for two Higgs doublet models with a Pseudoscalar mediator to Dark Matter*, *SciPost Phys. Core* **4** (2021) 003, arXiv: 2009.02220 [hep-ph].

- [33] T. Robens, *The THDMa Revisited*, *Symmetry* **13** (2021) 2341, arXiv: 2106.02962 [hep-ph].
- [34] ATLAS Collaboration, *Constraints on mediator-based dark matter and scalar dark energy models using $\sqrt{s} = 13$ TeV pp collision data collected by the ATLAS detector*, *JHEP* **05** (2019) 142, arXiv: 1903.01400 [hep-ex].
- [35] CMS Collaboration, *Search for dark matter produced in association with a Higgs boson decaying to a pair of bottom quarks in proton–proton collisions at $\sqrt{s} = 13$ TeV*, *Eur. Phys. J. C* **79** (2019) 280, arXiv: 1811.06562 [hep-ex].
- [36] ATLAS Collaboration, *Search for dark matter produced in association with a Standard Model Higgs boson decaying into b -quarks using the full Run 2 dataset from the ATLAS detector*, *JHEP* **11** (2021) 209, arXiv: 2108.13391 [hep-ex].
- [37] CMS Collaboration, *Search for dark matter produced in association with a leptonically decaying Z boson in proton–proton collisions at $\sqrt{s} = 13$ TeV*, *Eur. Phys. J. C* **81** (2021) 13, arXiv: 2008.04735 [hep-ex].
- [38] ATLAS Collaboration, *Search for dark matter in events with missing transverse momentum and a Higgs boson decaying into two photons in pp collisions at $\sqrt{s} = 13$ TeV with the ATLAS detector*, *JHEP* **10** (2021) 013, arXiv: 2104.13240 [hep-ex].
- [39] ATLAS Collaboration, *Search for dark matter produced in association with a single top quark in $\sqrt{s} = 13$ TeV pp collisions with the ATLAS detector*, *Eur. Phys. J. C* **81** (2020) 860, arXiv: 2011.09308 [hep-ex].
- [40] CMS Collaboration, *Search for dark matter produced in association with a single top quark or a top quark pair in proton–proton collisions at $\sqrt{s} = 13$ TeV*, *JHEP* **03** (2019) 141, arXiv: 1901.01553 [hep-ex].
- [41] ATLAS Collaboration, *The ATLAS Experiment at the CERN Large Hadron Collider*, *JINST* **3** (2008) S08003.
- [42] ATLAS Collaboration, *ATLAS Insertable B-Layer Technical Design Report*, ATLAS-TDR-19; CERN-LHCC-2010-013, 2010, URL: <https://cds.cern.ch/record/1291633>, Addendum: ATLAS-TDR-19-ADD-1; CERN-LHCC-2012-009, 2012, URL: <https://cds.cern.ch/record/1451888>.
- [43] B. Abbott et al., *Production and integration of the ATLAS Insertable B-Layer*, *JINST* **13** (2018) T05008, arXiv: 1803.00844 [physics.ins-det].
- [44] ATLAS Collaboration, *Performance of the ATLAS trigger system in 2015*, *Eur. Phys. J. C* **77** (2017) 317, arXiv: 1611.09661 [hep-ex].
- [45] ATLAS Collaboration, *The ATLAS Collaboration Software and Firmware*, ATL-SOFT-PUB-2021-001, 2021, URL: <https://cds.cern.ch/record/2767187>.
- [46] ATLAS Collaboration, *Luminosity determination in pp collisions at $\sqrt{s} = 13$ TeV using the ATLAS detector at the LHC*, ATLAS-CONF-2019-021, 2019, URL: <https://cds.cern.ch/record/2677054>.
- [47] G. Avoni et al., *The new LUCID-2 detector for luminosity measurement and monitoring in ATLAS*, *JINST* **13** (2018) P07017. 33 p, URL: <https://cds.cern.ch/record/2633501>.
- [48] ATLAS Collaboration, *ATLAS data quality operations and performance for 2015–2018 data-taking*, *JINST* **15** (2020) P04003, arXiv: 1911.04632 [physics.ins-det].

- [49] ATLAS Collaboration, *Performance of the missing transverse momentum triggers for the ATLAS detector during Run-2 data taking*, *JHEP* **08** (2020) 080, arXiv: [2005.09554 \[hep-ex\]](#).
- [50] ATLAS Collaboration, *Performance of electron and photon triggers in ATLAS during LHC Run 2*, *Eur. Phys. J. C* **80** (2020) 47, arXiv: [1909.00761 \[hep-ex\]](#).
- [51] ATLAS Collaboration, *Performance of the ATLAS muon triggers in Run 2*, *JINST* **15** (2020) P09015, arXiv: [2004.13447 \[hep-ex\]](#).
- [52] J. F. Gunion and H. E. Haber, *CP-conserving two-Higgs-doublet model: The approach to the decoupling limit*, *Phys. Rev. D* **67** (2003) 075019, arXiv: [hep-ph/0207010 \[hep-ph\]](#).
- [53] G. C. Branco et al., *Theory and phenomenology of two-Higgs-doublet models*, *Phys. Rept.* **516** (2012) 1, arXiv: [1106.0034 \[hep-ph\]](#).
- [54] J. Alwall et al., *The automated computation of tree-level and next-to-leading order differential cross sections, and their matching to parton shower simulations*, *JHEP* **07** (2014) 079, arXiv: [1405.0301 \[hep-ph\]](#).
- [55] T. Sjöstrand et al., *An introduction to PYTHIA 8.2*, *Comput. Phys. Commun.* **191** (2015) 159, arXiv: [1410.3012 \[hep-ph\]](#).
- [56] ATLAS Collaboration, *ATLAS Pythia 8 tunes to 7 TeV data*, ATL-PHYS-PUB-2014-021, 2014, URL: <https://cds.cern.ch/record/1966419>.
- [57] R. D. Ball et al., *Parton distributions for the LHC Run II*, *JHEP* **04** (2015) 040, arXiv: [1410.8849 \[hep-ph\]](#).
- [58] P. Artoisenet, R. Frederix, O. Mattelaer and R. Rietkerk, *Automatic spin-entangled decays of heavy resonances in Monte Carlo simulations*, *JHEP* **03** (2013) 015, arXiv: [1212.3460 \[hep-ph\]](#).
- [59] R. D. Ball et al., *Parton distributions with LHC data*, *Nucl. Phys. B* **867** (2013) 244, arXiv: [1207.1303 \[hep-ph\]](#).
- [60] T. Gleisberg et al., *Event generation with SHERPA 1.1*, *JHEP* **02** (2009) 007, arXiv: [0811.4622 \[hep-ph\]](#).
- [61] T. Gleisberg and S. Höche, *Comix, a new matrix element generator*, *JHEP* **12** (2008) 039, arXiv: [0808.3674 \[hep-ph\]](#).
- [62] F. Cascioli, P. Maierhöfer and S. Pozzorini, *Scattering Amplitudes with Open Loops*, *Phys. Rev. Lett.* **108** (2012) 111601, arXiv: [1111.5206 \[hep-ph\]](#).
- [63] S. Schumann and F. Krauss, *A parton shower algorithm based on Catani–Seymour dipole factorisation*, *JHEP* **03** (2008) 038, arXiv: [0709.1027 \[hep-ph\]](#).
- [64] S. Höche, F. Krauss, M. Schönherr and F. Siegert, *QCD matrix elements + parton showers. The NLO case*, *JHEP* **04** (2013) 027, arXiv: [1207.5030 \[hep-ph\]](#).
- [65] E. Bothmann et al., *Event generation with Sherpa 2.2*, *SciPost Phys.* **7** (2019) 034, arXiv: [1905.09127 \[hep-ph\]](#).
- [66] D. J. Lange, *The EvtGen particle decay simulation package*, *Nucl. Instrum. Meth. A* **462** (2001) 152.

- [67] ATLAS Collaboration, *The ATLAS Simulation Infrastructure*, *Eur. Phys. J. C* **70** (2010) 823, arXiv: [1005.4568 \[physics.ins-det\]](#).
- [68] GEANT4 Collaboration, S. Agostinelli et al., *GEANT4 – a simulation toolkit*, *Nucl. Instrum. Meth. A* **506** (2003) 250.
- [69] T. Sjöstrand, S. Mrenna and P. Skands, *A brief introduction to PYTHIA 8.1*, *Comput. Phys. Commun.* **178** (2008) 852, arXiv: [0710.3820 \[hep-ph\]](#).
- [70] ATLAS Collaboration, *The Pythia 8 A3 tune description of ATLAS minimum bias and inelastic measurements incorporating the Donnachie–Landshoff diffractive model*, ATL-PHYS-PUB-2016-017, 2016, URL: <https://cds.cern.ch/record/2206965>.
- [71] S. Frixione, G. Ridolfi and P. Nason, *A positive-weight next-to-leading-order Monte Carlo for heavy flavour hadroproduction*, *JHEP* **09** (2007) 126, arXiv: [0707.3088 \[hep-ph\]](#).
- [72] P. Nason, *A new method for combining NLO QCD with shower Monte Carlo algorithms*, *JHEP* **11** (2004) 040, arXiv: [hep-ph/0409146](#).
- [73] S. Frixione, P. Nason and C. Oleari, *Matching NLO QCD computations with parton shower simulations: the POWHEG method*, *JHEP* **11** (2007) 070, arXiv: [0709.2092 \[hep-ph\]](#).
- [74] S. Alioli, P. Nason, C. Oleari and E. Re, *A general framework for implementing NLO calculations in shower Monte Carlo programs: the POWHEG BOX*, *JHEP* **06** (2010) 043, arXiv: [1002.2581 \[hep-ph\]](#).
- [75] M. Czakon and A. Mitov, *Top++: A program for the calculation of the top-pair cross-section at hadron colliders*, *Comput. Phys. Commun.* **185** (2014) 2930, arXiv: [1112.5675 \[hep-ph\]](#).
- [76] R. Frederix, E. Re and P. Torrielli, *Single-top t -channel hadroproduction in the four-flavour scheme with POWHEG and aMC@NLO*, *JHEP* **09** (2012) 130, arXiv: [1207.5391 \[hep-ph\]](#).
- [77] N. Kidonakis, *Next-to-next-to-leading-order collinear and soft gluon corrections for t -channel single top quark production*, *Phys. Rev. D* **83** (2011) 091503, arXiv: [1103.2792 \[hep-ph\]](#).
- [78] E. Re, *Single-top Wt -channel production matched with parton showers using the POWHEG method*, *Eur. Phys. J. C* **71** (2011) 1547, arXiv: [1009.2450 \[hep-ph\]](#).
- [79] N. Kidonakis, *Two-loop soft anomalous dimensions for single top quark associated production with a W^- or H^-* , *Phys. Rev. D* **82** (2010) 054018, arXiv: [1005.4451 \[hep-ph\]](#).
- [80] N. Kidonakis, *Next-to-next-to-leading logarithm resummation for s -channel single top quark production*, *Phys. Rev. D* **81** (2010) 054028, arXiv: [1001.5034 \[hep-ph\]](#).
- [81] S. Catani, L. Cieri, G. Ferrera, D. de Florian and M. Grazzini, *Vector Boson Production at Hadron Colliders: A Fully Exclusive QCD Calculation at Next-to-Next-to-Leading Order*, *Phys. Rev. Lett.* **103** (2009) 082001, arXiv: [0903.2120 \[hep-ph\]](#).
- [82] D. de Florian et al., *Handbook of LHC Higgs Cross Sections: 4. Deciphering the Nature of the Higgs Sector*, **2/2017** (2016), arXiv: [1610.07922 \[hep-ph\]](#).

- [83] ATLAS Collaboration, *Vertex Reconstruction Performance of the ATLAS Detector at $\sqrt{s} = 13$ TeV*, ATL-PHYS-PUB-2015-026, 2015, URL: <https://cds.cern.ch/record/2037717>.
- [84] ATLAS Collaboration, *Selection of jets produced in 13 TeV proton–proton collisions with the ATLAS detector*, ATLAS-CONF-2015-029, 2015, URL: <https://cds.cern.ch/record/2037702>.
- [85] ATLAS Collaboration, *E_T^{miss} performance in the ATLAS detector using 2015–2016 LHC pp collisions*, ATLAS-CONF-2018-023, 2018, URL: <https://cds.cern.ch/record/2625233>.
- [86] ATLAS Collaboration, *Topological cell clustering in the ATLAS calorimeters and its performance in LHC Run 1*, *Eur. Phys. J. C* **77** (2017) 490, arXiv: [1603.02934](https://arxiv.org/abs/1603.02934) [hep-ex].
- [87] ATLAS Collaboration, *Search for new phenomena in events with two opposite-charge leptons, jets and missing transverse momentum in pp collisions at $\sqrt{s} = 13$ TeV with the ATLAS detector*, *JHEP* **04** (2021) 165, arXiv: [2102.01444](https://arxiv.org/abs/2102.01444) [hep-ex].
- [88] ATLAS Collaboration, *Electron reconstruction and identification in the ATLAS experiment using the 2015 and 2016 LHC proton–proton collision data at $\sqrt{s} = 13$ TeV*, *Eur. Phys. J. C* **79** (2019) 639, arXiv: [1902.04655](https://arxiv.org/abs/1902.04655) [hep-ex].
- [89] ATLAS Collaboration, *Electron and photon performance measurements with the ATLAS detector using the 2015–2017 LHC proton–proton collision data*, *JINST* **14** (2019) P12006, arXiv: [1908.00005](https://arxiv.org/abs/1908.00005) [hep-ex].
- [90] ATLAS Collaboration, *Muon reconstruction and identification efficiency in ATLAS using the full Run 2 pp collision data set at $\sqrt{s} = 13$ TeV*, *Eur. Phys. J. C* **81** (2021) 578, arXiv: [2012.00578](https://arxiv.org/abs/2012.00578) [hep-ex].
- [91] M. Cacciari, G. P. Salam and G. Soyez, *The anti- k_t jet clustering algorithm*, *JHEP* **04** (2008) 063, arXiv: [0802.1189](https://arxiv.org/abs/0802.1189) [hep-ph].
- [92] M. Cacciari, G. P. Salam and G. Soyez, *FastJet user manual*, *Eur. Phys. J. C* **72** (2012) 1896, arXiv: [1111.6097](https://arxiv.org/abs/1111.6097) [hep-ph].
- [93] ATLAS Collaboration, *Jet reconstruction and performance using particle flow with the ATLAS Detector*, *Eur. Phys. J. C* **77** (2017) 466, arXiv: [1703.10485](https://arxiv.org/abs/1703.10485) [hep-ex].
- [94] ATLAS Collaboration, *Jet energy scale and resolution measured in proton–proton collisions at $\sqrt{s} = 13$ TeV with the ATLAS detector*, *Eur. Phys. J. C* **81** (2020) 689, arXiv: [2007.02645](https://arxiv.org/abs/2007.02645) [hep-ex].
- [95] ATLAS Collaboration, *Performance of pile-up mitigation techniques for jets in pp collisions at $\sqrt{s} = 8$ TeV using the ATLAS detector*, *Eur. Phys. J. C* **76** (2016) 581, arXiv: [1510.03823](https://arxiv.org/abs/1510.03823) [hep-ex].
- [96] ATLAS Collaboration, *Identification and rejection of pile-up jets at high pseudorapidity with the ATLAS detector*, *Eur. Phys. J. C* **77** (2017) 580, arXiv: [1705.02211](https://arxiv.org/abs/1705.02211) [hep-ex], Erratum: *Eur. Phys. J. C* **77** (2017) 712.
- [97] ATLAS Collaboration, *ATLAS b-jet identification performance and efficiency measurement with $t\bar{t}$ events in pp collisions at $\sqrt{s} = 13$ TeV*, *Eur. Phys. J. C* **79** (2019) 970, arXiv: [1907.05120](https://arxiv.org/abs/1907.05120) [hep-ex].

- [98] ATLAS Collaboration, *Optimisation of large-radius jet reconstruction for the ATLAS detector in 13 TeV proton–proton collisions*, *Eur. Phys. J. C* **81** (2020) 334, arXiv: [2009.04986 \[hep-ex\]](#).
- [99] D. Krohn, J. Thaler and L.-T. Wang, *Jet trimming*, *JHEP* **02** (2010) 084, arXiv: [0912.1342 \[hep-ph\]](#).
- [100] S. D. Ellis and D. E. Soper, *Successive combination jet algorithm for hadron collisions*, *Phys. Rev. D* **48** (1993) 3160, arXiv: [hep-ph/9305266](#).
- [101] ATLAS Collaboration, *In situ calibration of large-radius jet energy and mass in 13 TeV proton–proton collisions with the ATLAS detector*, *Eur. Phys. J. C* **79** (2019) 135, arXiv: [1807.09477 \[hep-ex\]](#).
- [102] ATLAS Collaboration, *Measurement of the ATLAS Detector Jet Mass Response using Forward Folding with 80 fb^{-1} of $\sqrt{s} = 13\text{ TeV}$ pp data*, ATLAS-CONF-2020-022, 2020, URL: <https://cds.cern.ch/record/2724442>.
- [103] ATLAS Collaboration, *Performance of top-quark and W-boson tagging with ATLAS in Run 2 of the LHC*, *Eur. Phys. J. C* **79** (2019) 375, arXiv: [1808.07858 \[hep-ex\]](#).
- [104] A. J. Larkoski, I. Moult and D. Neill, *Power Counting to Better Jet Observables*, *JHEP* **12** (2014) 009, arXiv: [1409.6298 \[hep-ph\]](#).
- [105] ATLAS Collaboration, *Measurements of b-jet tagging efficiency with the ATLAS detector using $t\bar{t}$ events at $\sqrt{s} = 13\text{ TeV}$* , *JHEP* **08** (2018) 089, arXiv: [1805.01845 \[hep-ex\]](#).
- [106] ATLAS Collaboration, *Boosted hadronic vector boson and top quark tagging with ATLAS using Run 2 data*, ATL-PHYS-PUB-2020-017, 2020, URL: <https://cds.cern.ch/record/2724149>.
- [107] M. Baak et al., *HistFitter software framework for statistical data analysis*, *Eur. Phys. J. C* **75** (2015) 153, arXiv: [1410.1280 \[hep-ex\]](#).
- [108] P. Liashchynskyy and P. Liashchynskyy, *Grid Search, Random Search, Genetic Algorithm: A Big Comparison for NAS*, 2019, arXiv: [1912.06059 \[cs.LG\]](#).
- [109] ATLAS Collaboration, *Object-based missing transverse momentum significance in the ATLAS Detector*, ATLAS-CONF-2018-038, 2018, URL: <https://cds.cern.ch/record/2630948>.
- [110] ATLAS Collaboration, *Search for a scalar partner of the top quark in the all-hadronic $t\bar{t}$ plus missing transverse momentum final state at $\sqrt{s} = 13\text{ TeV}$ with the ATLAS detector*, *Eur. Phys. J. C* **80** (2020) 737, arXiv: [2004.14060 \[hep-ex\]](#).
- [111] G. Brooijmans et al., *Les Houches 2017: Physics at TeV Colliders New Physics Working Group Report*, 2018, arXiv: [1803.10379 \[hep-ph\]](#), URL: <http://lss.fnal.gov/archive/2017/conf/fermilab-conf-17-664-ppd.pdf>.
- [112] P. Konar, K. Kong, K. T. Matchev and M. Park, *Dark Matter particle spectroscopy at the LHC: generalizing M_{T2} to asymmetric event topologies*, *JHEP* **04** (2010) 086, arXiv: [0911.4126 \[hep-ph\]](#).

- [113] C. G. Lester and B. Nachman, *Bisection-based asymmetric M_{T2} computation: a higher precision calculator than existing symmetric methods*, *JHEP* **03** (2015) 100, arXiv: [1411.4312 \[hep-ph\]](#).
- [114] C. Lester and D. Summers, *Measuring masses of semiinvisibly decaying particles pair produced at hadron colliders*, *Phys. Lett. B* **463** (1999) 99, arXiv: [hep-ph/9906349](#).
- [115] A. Barr, C. Lester and P. Stephens, *A variable for measuring masses at hadron colliders when missing energy is expected; m_{T2} : the truth behind the glamour*, *J. Phys. G* **29** (2003) 2343, arXiv: [hep-ph/0304226](#).
- [116] ATLAS Collaboration, *Search for top-squark pair production in final states with one lepton, jets, and missing transverse momentum using 36fb^{-1} of $\sqrt{s} = 13\text{ TeV}$ pp collision data with the ATLAS detector*, *JHEP* **06** (2018) 108, arXiv: [1711.11520 \[hep-ex\]](#).
- [117] ATLAS Collaboration, *Probing the Quantum Interference between Singly and Doubly Resonant Top-Quark Production in pp Collisions at $\sqrt{s} = 13\text{ TeV}$ with the ATLAS Detector*, *Phys. Rev. Lett.* **121** (2018) 152002, arXiv: [1806.04667 \[hep-ex\]](#).
- [118] S. Frixione, E. Laenen, P. Motylinski, C. White and B. R. Webber, *Single-top hadroproduction in association with a W boson*, *JHEP* **07** (2008) 029, arXiv: [0805.3067 \[hep-ph\]](#).
- [119] ATLAS Collaboration, *Formulae for Estimating Significance*, ATL-PHYS-PUB-2020-025, 2020, URL: <https://cds.cern.ch/record/2736148>.
- [120] M. Bähr et al., *Herwig++ physics and manual*, *Eur. Phys. J. C* **58** (2008) 639, arXiv: [0803.0883 \[hep-ph\]](#).
- [121] J. Bellm et al., *Herwig 7.0/Herwig++ 3.0 release note*, *Eur. Phys. J. C* **76** (2016) 196, arXiv: [1512.01178 \[hep-ph\]](#).
- [122] ATLAS Collaboration, *ATLAS Computing Acknowledgements*, ATL-SOFT-PUB-2021-003, 2021, URL: <https://cds.cern.ch/record/2776662>.

The ATLAS Collaboration

G. Aad ¹⁰¹, B. Abbott ¹¹⁹, D.C. Abbott ¹⁰², K. Abeling ⁵⁵, S.H. Abidi ²⁹, A. Abouhorma ^{35e}, H. Abramowicz ¹⁵⁰, H. Abreu ¹⁴⁹, Y. Abulaiti ¹¹⁶, A.C. Abusleme Hoffman ^{136a}, B.S. Acharya ^{68a,68b,o}, B. Achkar ⁵⁵, L. Adam ⁹⁹, C. Adam Bourdarios ⁴, L. Adamczyk ^{84a}, L. Adamek ¹⁵⁴, S.V. Addepalli ²⁶, J. Adelman ¹¹⁴, A. Adiguzel ^{21c}, S. Adorni ⁵⁶, T. Adye ¹³³, A.A. Affolder ¹³⁵, Y. Afik ³⁶, M.N. Agaras ¹³, J. Agarwala ^{72a,72b}, A. Aggarwal ⁹⁹, C. Agheorghiesei ^{27c}, J.A. Aguilar-Saavedra ^{129f}, A. Ahmad ³⁶, F. Ahmadov ^{38,x}, W.S. Ahmed ¹⁰³, X. Ai ⁴⁸, G. Aielli ^{75a,75b}, I. Aizenberg ¹⁶⁸, M. Akbiyik ⁹⁹, T.P.A. Åkesson ⁹⁷, A.V. Akimov ³⁷, K. Al Khoury ⁴¹, G.L. Alberghi ^{23b}, J. Albert ¹⁶⁴, P. Albicocco ⁵³, M.J. Alconada Verzini ⁸⁹, S. Alderweireldt ⁵², M. Aleksa ³⁶, I.N. Aleksandrov ³⁸, C. Alexa ^{27b}, T. Alexopoulos ¹⁰, A. Alfonsi ¹¹³, F. Alfonsi ^{23b}, M. Alhroob ¹¹⁹, B. Ali ¹³¹, S. Ali ¹⁴⁷, M. Aliev ³⁷, G. Alimonti ^{70a}, C. Allaire ³⁶, B.M.M. Allbrooke ¹⁴⁵, P.P. Allport ²⁰, A. Aloisio ^{71a,71b}, F. Alonso ⁸⁹, C. Alpigiani ¹³⁷, E. Alunno Camelia ^{75a,75b}, M. Alvarez Estevez ⁹⁸, M.G. Alvigi ^{71a,71b}, Y. Amaral Coutinho ^{81b}, A. Ambler ¹⁰³, C. Amelung ³⁶, C.G. Ames ¹⁰⁸, D. Amidei ¹⁰⁵, S.P. Amor Dos Santos ^{129a}, S. Amoroso ⁴⁸, K.R. Amos ¹⁶², C.S. Amrouche ⁵⁶, V. Ananiev ¹²⁴, C. Anastopoulos ¹³⁸, N. Andari ¹³⁴, T. Andeen ¹¹, J.K. Anders ¹⁹, S.Y. Andrean ^{47a,47b}, A. Andreatza ^{70a,70b}, S. Angelidakis ⁹, A. Angerami ^{41,aa}, A.V. Anisenkov ³⁷, A. Annovi ^{73a}, C. Antel ⁵⁶, M.T. Anthony ¹³⁸, E. Antipov ¹²⁰, M. Antonelli ⁵³, D.J.A. Antrim ^{17a}, F. Anulli ^{74a}, M. Aoki ⁸², J.A. Aparisi Pozo ¹⁶², M.A. Aparo ¹⁴⁵, L. Aperio Bella ⁴⁸, C. Appelt ¹⁸, N. Aranzabal ³⁶, V. Araujo Ferraz ^{81a}, C. Arcangeletti ⁵³, A.T.H. Arce ⁵¹, E. Arena ⁹¹, J-F. Arguin ¹⁰⁷, S. Argyropoulos ⁵⁴, J.-H. Arling ⁴⁸, A.J. Armbruster ³⁶, O. Arnaez ¹⁵⁴, H. Arnold ¹¹³, Z.P. Arrubarrena Tame ¹⁰⁸, G. Artoni ^{74a,74b}, H. Asada ¹¹⁰, K. Asai ¹¹⁷, S. Asai ¹⁵², N.A. Asbah ⁶¹, E.M. Asimakopoulou ¹⁶⁰, J. Assahsah ^{35d}, K. Assamagan ²⁹, R. Astalos ^{28a}, R.J. Atkin ^{33a}, M. Atkinson ¹⁶¹, N.B. Atlay ¹⁸, H. Atmani ^{62b}, P.A. Atlasiddha ¹⁰⁵, K. Augsten ¹³¹, S. Auricchio ^{71a,71b}, A.D. Auriol ²⁰, V.A. Austrup ¹⁷⁰, G. Avner ¹⁴⁹, G. Avolio ³⁶, K. Axiotis ⁵⁶, M.K. Ayoub ^{14c}, G. Azuelos ^{107,af}, D. Babal ^{28a}, H. Bachacou ¹³⁴, K. Bachas ^{151,r}, A. Bachiu ³⁴, F. Backman ^{47a,47b}, A. Badea ⁶¹, P. Bagnaia ^{74a,74b}, M. Bahmani ¹⁸, A.J. Bailey ¹⁶², V.R. Bailey ¹⁶¹, J.T. Baines ¹³³, C. Bakalis ¹⁰, O.K. Baker ¹⁷¹, P.J. Bakker ¹¹³, E. Bakos ¹⁵, D. Bakshi Gupta ⁸, S. Balaji ¹⁴⁶, R. Balasubramanian ¹¹³, E.M. Baldin ³⁷, P. Balek ¹³², E. Ballabene ^{70a,70b}, F. Balli ¹³⁴, L.M. Baltos ^{63a}, W.K. Balunas ³², J. Balz ⁹⁹, E. Banas ⁸⁵, M. Bandieramonte ¹²⁸, A. Bandyopadhyay ²⁴, S. Bansal ²⁴, L. Barak ¹⁵⁰, E.L. Barberio ¹⁰⁴, D. Barberis ^{57b,57a}, M. Barbero ¹⁰¹, G. Barbour ⁹⁵, K.N. Barends ^{33a}, T. Barillari ¹⁰⁹, M-S. Barisits ³⁶, J. Barkeloo ¹²², T. Barklow ¹⁴², R.M. Barnett ^{17a}, P. Baron ¹²¹, D.A. Baron Moreno ¹⁰⁰, A. Baroncelli ^{62a}, G. Barone ²⁹, A.J. Barr ¹²⁵, L. Barranco Navarro ^{47a,47b}, F. Barreiro ⁹⁸, J. Barreiro Guimarães da Costa ^{14a}, U. Barron ¹⁵⁰, M.G. Barros Teixeira ^{129a}, S. Barsov ³⁷, F. Bartels ^{63a}, R. Bartoldus ¹⁴², A.E. Barton ⁹⁰, P. Bartos ^{28a}, A. Basalaeu ⁴⁸, A. Basan ⁹⁹, M. Baselga ⁴⁹, I. Bashta ^{76a,76b}, A. Bassalat ^{66,ac}, M.J. Basso ¹⁵⁴, C.R. Basson ¹⁰⁰, R.L. Bates ⁵⁹, S. Batlamous ^{35e}, J.R. Batley ³², B. Batool ¹⁴⁰, M. Battaglia ¹³⁵, M. Bauge ^{74a,74b}, P. Bauer ²⁴, A. Bayirli ^{21a}, J.B. Beacham ⁵¹, T. Beau ¹²⁶, P.H. Beauchemin ¹⁵⁷, F. Becherer ⁵⁴, P. Bechtel ²⁴, H.P. Beck ^{19,q}, K. Becker ¹⁶⁶, C. Becot ⁴⁸, A.J. Beddall ^{21d}, V.A. Bednyakov ³⁸, C.P. Bee ¹⁴⁴, L.J. Beemster ¹⁵, T.A. Beermann ³⁶, M. Begalli ^{81b,81d}, M. Begel ²⁹, A. Behera ¹⁴⁴, J.K. Behr ⁴⁸, C. Beirao Da Cruz E Silva ³⁶, J.F. Beirer ^{55,36}, F. Beisiegel ²⁴, M. Belfkir ¹⁵⁸, G. Bella ¹⁵⁰, L. Bellagamba ^{23b}, A. Bellerive ³⁴, P. Bellos ²⁰, K. Beloborodov ³⁷, K. Belotskiy ³⁷, N.L. Belyaev ³⁷, D. Benckekroun ^{35a},

F. Bendebba ^{35a}, Y. Benhammou ¹⁵⁰, D.P. Benjamin ²⁹, M. Benoit ²⁹, J.R. Bensinger ²⁶,
 S. Bentvelsen ¹¹³, L. Beresford ³⁶, M. Beretta ⁵³, D. Berge ¹⁸, E. Bergeaas Kuutmann ¹⁶⁰,
 N. Berger ⁴, B. Bergmann ¹³¹, J. Beringer ^{17a}, S. Berlendis ⁷, G. Bernardi ⁵, C. Bernius ¹⁴²,
 F.U. Bernlochner ²⁴, T. Berry ⁹⁴, P. Berta ¹³², A. Berthold ⁵⁰, I.A. Bertram ⁹⁰,
 O. Bessidskaia Bylund ¹⁷⁰, S. Bethke ¹⁰⁹, A. Betti ⁴⁴, A.J. Bevan ⁹³, M. Bhamjee ^{33c},
 S. Bhatta ¹⁴⁴, D.S. Bhattacharya ¹⁶⁵, P. Bhattarai ²⁶, V.S. Bhopatkar ⁶, R. Bi ¹²⁸, R. Bi ^{29,ai},
 R.M. Bianchi ¹²⁸, O. Biebel ¹⁰⁸, R. Bielski ¹²², N.V. Biesuz ^{73a,73b}, M. Biglietti ^{76a},
 T.R.V. Billoud ¹³¹, M. Bindi ⁵⁵, A. Bingul ^{21b}, C. Bini ^{74a,74b}, S. Biondi ^{23b,23a}, A. Biondini ⁹¹,
 C.J. Birch-sykes ¹⁰⁰, G.A. Bird ^{20,133}, M. Birman ¹⁶⁸, T. Bisanz ³⁶, D. Biswas ^{169,k},
 A. Bitadze ¹⁰⁰, K. Bjørke ¹²⁴, I. Bloch ⁴⁸, C. Blocker ²⁶, A. Blue ⁵⁹, U. Blumenschein ⁹³,
 J. Blumenthal ⁹⁹, G.J. Bobbink ¹¹³, V.S. Bobrovnikov ³⁷, M. Boehler ⁵⁴, D. Bogavac ³⁶,
 A.G. Bogdanchikov ³⁷, C. Bohm ^{47a}, V. Boisvert ⁹⁴, P. Bokan ⁴⁸, T. Bold ^{84a}, M. Bomben ⁵,
 M. Bona ⁹³, M. Boonekamp ¹³⁴, C.D. Booth ⁹⁴, A.G. Borbély ⁵⁹, H.M. Borecka-Bielska ¹⁰⁷,
 L.S. Borgna ⁹⁵, G. Borissov ⁹⁰, D. Bortoletto ¹²⁵, D. Boscherini ^{23b}, M. Bosman ¹³,
 J.D. Bossio Sola ³⁶, K. Bouaouda ^{35a}, J. Boudreau ¹²⁸, E.V. Bouhova-Thacker ⁹⁰,
 D. Boumediene ⁴⁰, R. Bouquet ⁵, A. Boveia ¹¹⁸, J. Boyd ³⁶, D. Boye ²⁹, I.R. Boyko ³⁸,
 J. Bracinik ²⁰, N. Brahimy ^{62d,62c}, G. Brandt ¹⁷⁰, O. Brandt ³², F. Braren ⁴⁸, B. Brau ¹⁰²,
 J.E. Brau ¹²², W.D. Breaden Madden ⁵⁹, K. Brendlinger ⁴⁸, R. Brenner ¹⁶⁸, L. Brenner ³⁶,
 R. Brenner ¹⁶⁰, S. Bressler ¹⁶⁸, B. Brickwedde ⁹⁹, D. Britton ⁵⁹, D. Britzger ¹⁰⁹, I. Brock ²⁴,
 G. Brooijmans ⁴¹, W.K. Brooks ^{136f}, E. Brost ²⁹, P.A. Bruckman de Renstrom ⁸⁵, B. Brüers ⁴⁸,
 D. Bruncko ^{28b,*}, A. Bruni ^{23b}, G. Bruni ^{23b}, M. Bruschi ^{23b}, N. Brusino ^{74a,74b},
 L. Bryngemark ¹⁴², T. Buanes ¹⁶, Q. Buat ¹³⁷, P. Buchholz ¹⁴⁰, A.G. Buckley ⁵⁹,
 I.A. Budagov ^{38,*}, M.K. Bugge ¹²⁴, O. Bulekov ³⁷, B.A. Bullard ⁶¹, S. Burdin ⁹¹,
 C.D. Burgard ⁴⁸, A.M. Burger ⁴⁰, B. Burghgrave ⁸, J.T.P. Burr ³², C.D. Burton ¹¹,
 J.C. Burzynski ¹⁴¹, E.L. Busch ⁴¹, V. Büscher ⁹⁹, P.J. Bussey ⁵⁹, J.M. Butler ²⁵, C.M. Buttar ⁵⁹,
 J.M. Butterworth ⁹⁵, W. Buttinger ¹³³, C.J. Buxo Vazquez ¹⁰⁶, A.R. Buzykaev ³⁷, G. Cabras ^{23b},
 S. Cabrera Urbán ¹⁶², D. Caforio ⁵⁸, H. Cai ¹²⁸, Y. Cai ^{14a,14d}, V.M.M. Cairo ³⁶, O. Cakir ^{3a},
 N. Calace ³⁶, P. Calafiura ^{17a}, G. Calderini ¹²⁶, P. Calfayan ⁶⁷, G. Callea ⁵⁹, L.P. Caloba ^{81b},
 D. Calvet ⁴⁰, S. Calvet ⁴⁰, T.P. Calvet ¹⁰¹, M. Calvetti ^{73a,73b}, R. Camacho Toro ¹²⁶,
 S. Camarda ³⁶, D. Camarero Munoz ⁹⁸, P. Camarri ^{75a,75b}, M.T. Camerlingo ^{76a,76b},
 D. Cameron ¹²⁴, C. Camincher ¹⁶⁴, M. Campanelli ⁹⁵, A. Camplani ⁴², V. Canale ^{71a,71b},
 A. Canesse ¹⁰³, M. Cano Bret ⁷⁹, J. Cantero ¹⁶², Y. Cao ¹⁶¹, F. Capocasa ²⁶, M. Capua ^{43b,43a},
 A. Carbone ^{70a,70b}, R. Cardarelli ^{75a}, J.C.J. Cardenas ⁸, F. Cardillo ¹⁶², T. Carli ³⁶,
 G. Carlino ^{71a}, B.T. Carlson ^{128,s}, E.M. Carlson ^{164,155a}, L. Carminati ^{70a,70b}, M. Carnesale ^{74a,74b},
 S. Caron ¹¹², E. Carquin ^{136f}, S. Carrá ^{70a,70b}, G. Carratta ^{23b,23a}, F. Carrio Argos ^{33g},
 J.W.S. Carter ¹⁵⁴, T.M. Carter ⁵², M.P. Casado ^{13,h}, A.F. Casha ¹⁵⁴, E.G. Castiglia ¹⁷¹,
 F.L. Castillo ^{63a}, L. Castillo Garcia ¹³, V. Castillo Gimenez ¹⁶², N.F. Castro ^{129a,129e},
 A. Catinaccio ³⁶, J.R. Catmore ¹²⁴, V. Cavaliere ²⁹, N. Cavalli ^{23b,23a}, V. Cavasinni ^{73a,73b},
 E. Celebi ^{21a}, F. Celli ¹²⁵, M.S. Centonze ^{69a,69b}, K. Cerny ¹²¹, A.S. Cerqueira ^{81a}, A. Cerri ¹⁴⁵,
 L. Cerrito ^{75a,75b}, F. Cerutti ^{17a}, A. Cervelli ^{23b}, S.A. Cetin ^{21d}, Z. Chadi ^{35a},
 D. Chakraborty ¹¹⁴, M. Chala ^{129f}, J. Chan ¹⁶⁹, W.S. Chan ¹¹³, W.Y. Chan ¹⁵²,
 J.D. Chapman ³², B. Chargeishvili ^{148b}, D.G. Charlton ²⁰, T.P. Charman ⁹³, M. Chatterjee ¹⁹,
 S. Chekanov ⁶, S.V. Chekulaev ^{155a}, G.A. Chelkov ^{38,a}, A. Chen ¹⁰⁵, B. Chen ¹⁵⁰, B. Chen ¹⁶⁴,
 C. Chen ^{62a}, H. Chen ^{14c}, H. Chen ²⁹, J. Chen ^{62c}, J. Chen ²⁶, S. Chen ¹⁵², S.J. Chen ^{14c},
 X. Chen ^{62c}, X. Chen ^{14b,ae}, Y. Chen ^{62a}, C.L. Cheng ¹⁶⁹, H.C. Cheng ^{64a}, A. Cheplakov ³⁸,
 E. Cheremushkina ⁴⁸, E. Cherepanova ¹¹³, R. Cherkaoui El Moursli ^{35e}, E. Cheu ⁷, K. Cheung ⁶⁵,
 L. Chevalier ¹³⁴, V. Chiarella ⁵³, G. Chiarelli ^{73a}, G. Chiodini ^{69a}, A.S. Chisholm ²⁰,

A. Chitan ^{27b}, Y.H. Chiu ¹⁶⁴, M.V. Chizhov ³⁸, K. Choi ¹¹, A.R. Chomont ^{74a,74b}, Y. Chou ¹⁰²,
 E.Y.S. Chow ¹¹³, T. Chowdhury ^{33g}, L.D. Christopher ^{33g}, K.L. Chu ^{64a}, M.C. Chu ^{64a},
 X. Chu ^{14a,14d}, J. Chudoba ¹³⁰, J.J. Chwastowski ⁸⁵, D. Cieri ¹⁰⁹, K.M. Ciesla ^{84a}, V. Cindro ⁹²,
 A. Ciocio ^{17a}, F. Cirotto ^{71a,71b}, Z.H. Citron ^{168,1}, M. Citterio ^{70a}, D.A. Ciubotaru ^{27b},
 B.M. Ciungu ¹⁵⁴, A. Clark ⁵⁶, P.J. Clark ⁵², J.M. Clavijo Columbie ⁴⁸, S.E. Clawson ¹⁰⁰,
 C. Clement ^{47a,47b}, J. Clercx ⁴⁸, L. Clissa ^{23b,23a}, Y. Coadou ¹⁰¹, M. Cobal ^{68a,68c},
 A. Coccaro ^{57b}, R.F. Coelho Barrue ^{129a}, R. Coelho Lopes De Sa ¹⁰², S. Coelli ^{70a}, H. Cohen ¹⁵⁰,
 A.E.C. Coimbra ^{70a,70b}, B. Cole ⁴¹, J. Collot ⁶⁰, P. Conde Muiño ^{129a,129g}, S.H. Connell ^{33c},
 I.A. Connelly ⁵⁹, E.I. Conroy ¹²⁵, F. Conventi ^{71a,ag}, H.G. Cooke ²⁰, A.M. Cooper-Sarkar ¹²⁵,
 F. Cormier ¹⁶³, L.D. Corpe ³⁶, M. Corradi ^{74a,74b}, E.E. Corrigan ⁹⁷, F. Corriveau ^{103,w},
 A. Cortes-Gonzalez ¹⁸, M.J. Costa ¹⁶², F. Costanza ⁴, D. Costanzo ¹³⁸, B.M. Cote ¹¹⁸,
 G. Cowan ⁹⁴, J.W. Cowley ³², K. Cranmer ¹¹⁶, S. Crépe-Renaudin ⁶⁰, F. Crescioli ¹²⁶,
 M. Cristinziani ¹⁴⁰, M. Cristoforetti ^{77a,77b,c}, V. Croft ¹⁵⁷, G. Crosetti ^{43b,43a}, A. Cueto ³⁶,
 T. Cuhadar Donszelmann ¹⁵⁹, H. Cui ^{14a,14d}, Z. Cui ⁷, A.R. Cukierman ¹⁴², W.R. Cunningham ⁵⁹,
 F. Curcio ^{43b,43a}, P. Czodrowski ³⁶, M.M. Czurylo ^{63b}, M.J. Da Cunha Sargedas De Sousa ^{62a},
 J.V. Da Fonseca Pinto ^{81b}, C. Da Via ¹⁰⁰, W. Dabrowski ^{84a}, T. Dado ⁴⁹, S. Dahbi ^{33g},
 T. Dai ¹⁰⁵, C. Dallapiccola ¹⁰², M. Dam ⁴², G. D'amen ²⁹, V. D'Amico ^{76a,76b}, J. Damp ⁹⁹,
 J.R. Dandoy ¹²⁷, M.F. Daneri ³⁰, M. Danninger ¹⁴¹, V. Dao ³⁶, G. Darbo ^{57b}, S. Darmora ⁶,
 S.J. Das ^{29,ai}, A. Dattagupta ¹²², S. D'Auria ^{70a,70b}, C. David ^{155b}, T. Davidek ¹³²,
 D.R. Davis ⁵¹, B. Davis-Purcell ³⁴, I. Dawson ⁹³, K. De ⁸, R. De Asmundis ^{71a},
 M. De Beurs ¹¹³, S. De Castro ^{23b,23a}, N. De Groot ¹¹², P. de Jong ¹¹³, H. De la Torre ¹⁰⁶,
 A. De Maria ^{14c}, A. De Salvo ^{74a}, U. De Sanctis ^{75a,75b}, M. De Santis ^{75a,75b}, A. De Santo ¹⁴⁵,
 J.B. De Vivie De Regie ⁶⁰, D.V. Dedovich ³⁸, J. Degens ¹¹³, A.M. Deiana ⁴⁴, F. Del Corso ^{23b,23a},
 J. Del Peso ⁹⁸, F. Del Rio ^{63a}, F. Deliot ¹³⁴, C.M. Delitzsch ⁴⁹, M. Della Pietra ^{71a,71b},
 D. Della Volpe ⁵⁶, A. Dell'Acqua ³⁶, L. Dell'Asta ^{70a,70b}, M. Delmastro ⁴, P.A. Delsart ⁶⁰,
 S. Demers ¹⁷¹, M. Demichev ³⁸, S.P. Denisov ³⁷, L. D'Eramo ¹¹⁴, D. Derendarz ⁸⁵,
 F. Derue ¹²⁶, P. Dervan ⁹¹, K. Desch ²⁴, K. Dette ¹⁵⁴, C. Deutsch ²⁴, P.O. Deviveiros ³⁶,
 F.A. Di Bello ^{74a,74b}, A. Di Ciaccio ^{75a,75b}, L. Di Ciaccio ⁴, A. Di Domenico ^{74a,74b},
 C. Di Donato ^{71a,71b}, A. Di Girolamo ³⁶, G. Di Gregorio ^{73a,73b}, A. Di Luca ^{77a,77b},
 B. Di Micco ^{76a,76b}, R. Di Nardo ^{76a,76b}, C. Diaconu ¹⁰¹, F.A. Dias ¹¹³, T. Dias Do Vale ¹⁴¹,
 M.A. Diaz ^{136a,136b}, F.G. Diaz Capriles ²⁴, M. Didenko ¹⁶², E.B. Diehl ¹⁰⁵, L. Diehl ⁵⁴,
 S. Díez Cornell ⁴⁸, C. Diez Pardos ¹⁴⁰, C. Dimitriadi ^{24,160}, A. Dimitrievska ^{17a}, W. Ding ^{14b},
 J. Dingfelder ²⁴, I-M. Dinu ^{27b}, S.J. Dittmeier ^{63b}, F. Dittus ³⁶, F. Djama ¹⁰¹, T. Djobava ^{148b},
 J.I. Djuvsland ¹⁶, D. Dodsworth ²⁶, C. Doglioni ^{100,97}, J. Dolejsi ¹³², Z. Dolezal ¹³²,
 M. Donadelli ^{81c}, B. Dong ^{62c}, J. Donini ⁴⁰, A. D'Onofrio ^{14c}, M. D'Onofrio ⁹¹, J. Dopke ¹³³,
 A. Doria ^{71a}, M.T. Dova ⁸⁹, A.T. Doyle ⁵⁹, M.A. Draguet ¹²⁵, E. Drechsler ¹⁴¹, E. Dreyer ¹⁶⁸,
 I. Drivas-koulouris ¹⁰, A.S. Drobac ¹⁵⁷, D. Du ^{62a}, T.A. du Pree ¹¹³, F. Dubinin ³⁷,
 M. Dubovsky ^{28a}, E. Duchovni ¹⁶⁸, G. Duckeck ¹⁰⁸, O.A. Ducu ³⁶, D. Duda ¹⁰⁹, A. Dudarev ³⁶,
 M. D'uffizi ¹⁰⁰, L. Dufflot ⁶⁶, M. Dührssen ³⁶, C. Dülsen ¹⁷⁰, A.E. Dumitriu ^{27b}, M. Dunford ^{63a},
 S. Dungs ⁴⁹, K. Dunne ^{47a,47b}, A. Duperrin ¹⁰¹, H. Duran Yildiz ^{3a}, M. Düren ⁵⁸,
 A. Durglishvili ^{148b}, B.L. Dwyer ¹¹⁴, G.I. Dyckes ^{17a}, M. Dyndal ^{84a}, S. Dysch ¹⁰⁰,
 B.S. Dziedzic ⁸⁵, Z.O. Earnshaw ¹⁴⁵, B. Eckerova ^{28a}, M.G. Eggleston ⁵¹,
 E. Egidio Purcino De Souza ^{81b}, L.F. Ehrke ⁵⁶, G. Eigen ¹⁶, K. Einsweiler ^{17a}, T. Ekelof ¹⁶⁰,
 P.A. Ekman ⁹⁷, Y. El Ghazali ^{35b}, H. El Jarrari ^{35e,147}, A. El Moussaouy ^{35a}, V. Ellajosyula ¹⁶⁰,
 M. Ellert ¹⁶⁰, F. Ellinghaus ¹⁷⁰, A.A. Elliot ⁹³, N. Ellis ³⁶, J. Elmsheuser ²⁹, M. Elsing ³⁶,
 D. Emelianov ¹³³, A. Emerman ⁴¹, Y. Enari ¹⁵², I. Ene ^{17a}, S. Epari ¹³, J. Erdmann ⁴⁹,
 A. Ereditato ¹⁹, P.A. Erland ⁸⁵, M. Errenst ¹⁷⁰, M. Escalier ⁶⁶, C. Escobar ¹⁶², E. Etzion ¹⁵⁰,

G. Evans [id](#)^{129a}, H. Evans [id](#)⁶⁷, M.O. Evans [id](#)¹⁴⁵, A. Ezhilov [id](#)³⁷, S. Ezzarqtouni [id](#)^{35a}, F. Fabbri [id](#)⁵⁹, L. Fabbri [id](#)^{23b,23a}, G. Facini [id](#)⁹⁵, V. Fadeyev [id](#)¹³⁵, R.M. Fakhruddinov [id](#)³⁷, S. Falciano [id](#)^{74a}, P.J. Falke [id](#)²⁴, S. Falke [id](#)³⁶, J. Faltova [id](#)¹³², Y. Fan [id](#)^{14a}, Y. Fang [id](#)^{14a,14d}, G. Fanourakis [id](#)⁴⁶, M. Fanti [id](#)^{70a,70b}, M. Faraj [id](#)^{68a,68b}, A. Farbin [id](#)⁸, A. Farilla [id](#)^{76a}, T. Farooque [id](#)¹⁰⁶, S.M. Farrington [id](#)⁵², F. Fassi [id](#)^{35e}, D. Fassouliotis [id](#)⁹, M. Fauci Giannelli [id](#)^{75a,75b}, W.J. Fawcett [id](#)³², L. Fayard [id](#)⁶⁶, O.L. Fedin [id](#)^{37,a}, G. Fedotov [id](#)³⁷, M. Feickert [id](#)¹⁶¹, L. Feligioni [id](#)¹⁰¹, A. Fell [id](#)¹³⁸, D.E. Fellers [id](#)¹²², C. Feng [id](#)^{62b}, M. Feng [id](#)^{14b}, M.J. Fenton [id](#)¹⁵⁹, A.B. Fenyuk [id](#)³⁷, L. Ferencz [id](#)⁴⁸, S.W. Ferguson [id](#)⁴⁵, J. Ferrando [id](#)⁴⁸, A. Ferrari [id](#)¹⁶⁰, P. Ferrari [id](#)¹¹³, R. Ferrari [id](#)^{72a}, D. Ferrere [id](#)⁵⁶, C. Ferretti [id](#)¹⁰⁵, F. Fiedler [id](#)⁹⁹, A. Filipič [id](#)⁹², E.K. Filmer [id](#)¹, F. Filthaut [id](#)¹¹², M.C.N. Fiolhais [id](#)^{129a,129c,b}, L. Fiorini [id](#)¹⁶², F. Fischer [id](#)¹⁴⁰, W.C. Fisher [id](#)¹⁰⁶, T. Fitschen [id](#)^{20,66}, I. Fleck [id](#)¹⁴⁰, P. Fleischmann [id](#)¹⁰⁵, T. Flick [id](#)¹⁷⁰, L. Flores [id](#)¹²⁷, M. Flores [id](#)^{33d,ab}, L.R. Flores Castillo [id](#)^{64a}, F.M. Follega [id](#)^{77a,77b}, N. Fomin [id](#)¹⁶, J.H. Foo [id](#)¹⁵⁴, B.C. Forland [id](#)⁶⁷, A. Formica [id](#)¹³⁴, A.C. Forti [id](#)¹⁰⁰, E. Fortin [id](#)¹⁰¹, A.W. Fortman [id](#)⁶¹, M.G. Foti [id](#)^{17a}, L. Fountas [id](#)^{9,i}, D. Fournier [id](#)⁶⁶, H. Fox [id](#)⁹⁰, P. Francavilla [id](#)^{73a,73b}, S. Francescato [id](#)⁶¹, M. Franchini [id](#)^{23b,23a}, S. Franchino [id](#)^{63a}, D. Francis [id](#)³⁶, L. Franco [id](#)¹¹², L. Franconi [id](#)¹⁹, M. Franklin [id](#)⁶¹, G. Frattari [id](#)²⁶, A.C. Fregard [id](#)⁹³, P.M. Freeman [id](#)²⁰, W.S. Freund [id](#)^{81b}, N. Fritzsche [id](#)⁵⁰, A. Froch [id](#)⁵⁴, D. Froidevaux [id](#)³⁶, J.A. Frost [id](#)¹²⁵, Y. Fu [id](#)^{62a}, M. Fujimoto [id](#)¹¹⁷, E. Fullana Torregrosa [id](#)^{162,*}, J. Fuster [id](#)¹⁶², A. Gabrielli [id](#)^{23b,23a}, A. Gabrielli [id](#)³⁶, P. Gadow [id](#)⁴⁸, G. Gagliardi [id](#)^{57b,57a}, L.G. Gagnon [id](#)^{17a}, G.E. Gallardo [id](#)¹²⁵, E.J. Gallas [id](#)¹²⁵, B.J. Gallop [id](#)¹³³, R. Gamboa Goni [id](#)⁹³, K.K. Gan [id](#)¹¹⁸, S. Ganguly [id](#)¹⁵², J. Gao [id](#)^{62a}, Y. Gao [id](#)⁵², F.M. Garay Walls [id](#)^{136a,136b}, B. Garcia [id](#)^{29,ai}, C. García [id](#)¹⁶², J.E. García Navarro [id](#)¹⁶², J.A. García Pascual [id](#)^{14a}, M. Garcia-Sciveres [id](#)^{17a}, R.W. Gardner [id](#)³⁹, D. Garg [id](#)⁷⁹, R.B. Garg [id](#)^{142,p}, S. Gargiulo [id](#)⁵⁴, C.A. Garner [id](#)¹⁵⁴, V. Garonne [id](#)²⁹, S.J. Gasiorowski [id](#)¹³⁷, P. Gaspar [id](#)^{81b}, G. Gaudio [id](#)^{72a}, V. Gautam [id](#)¹³, P. Gauzzi [id](#)^{74a,74b}, I.L. Gavrilenko [id](#)³⁷, A. Gavrilyuk [id](#)³⁷, C. Gay [id](#)¹⁶³, G. Gaycken [id](#)⁴⁸, E.N. Gazis [id](#)¹⁰, A.A. Geanta [id](#)^{27b}, C.M. Gee [id](#)¹³⁵, J. Geisen [id](#)⁹⁷, M. Geisen [id](#)⁹⁹, C. Gemme [id](#)^{57b}, M.H. Genest [id](#)⁶⁰, S. Gentile [id](#)^{74a,74b}, S. George [id](#)⁹⁴, W.F. George [id](#)²⁰, T. Geralis [id](#)⁴⁶, L.O. Gerlach [id](#)⁵⁵, P. Gessinger-Befurt [id](#)³⁶, M. Ghasemi Bostanabad [id](#)¹⁶⁴, M. Ghneimat [id](#)¹⁴⁰, A. Ghosal [id](#)¹⁴⁰, A. Ghosh [id](#)¹⁵⁹, A. Ghosh [id](#)⁷, B. Giacobbe [id](#)^{23b}, S. Giagu [id](#)^{74a,74b}, N. Giangiacomi [id](#)¹⁵⁴, P. Giannetti [id](#)^{73a}, A. Giannini [id](#)^{62a}, S.M. Gibson [id](#)⁹⁴, M. Gignac [id](#)¹³⁵, D.T. Gil [id](#)^{84b}, A.K. Gilbert [id](#)^{84a}, B.J. Gilbert [id](#)⁴¹, D. Gillberg [id](#)³⁴, G. Gilles [id](#)¹¹³, N.E.K. Gillwald [id](#)⁴⁸, L. Ginabat [id](#)¹²⁶, D.M. Gingrich [id](#)^{2,af}, M.P. Giordani [id](#)^{68a,68c}, P.F. Giraud [id](#)¹³⁴, G. Giugliarelli [id](#)^{68a,68c}, D. Giugni [id](#)^{70a}, F. Giuli [id](#)³⁶, I. Gkialas [id](#)^{9,i}, L.K. Gladilin [id](#)³⁷, C. Glasman [id](#)⁹⁸, G.R. Gledhill [id](#)¹²², M. Glisic [id](#)¹²², I. Gnesi [id](#)^{43b,e}, Y. Go [id](#)^{29,ai}, M. Goblirsch-Kolb [id](#)²⁶, D. Godin [id](#)¹⁰⁷, S. Goldfarb [id](#)¹⁰⁴, T. Golling [id](#)⁵⁶, M.G.D. Gololo [id](#)^{33g}, D. Golubkov [id](#)³⁷, J.P. Gombas [id](#)¹⁰⁶, A. Gomes [id](#)^{129a,129b}, G. Gomes Da Silva [id](#)¹⁴⁰, A.J. Gomez Delegido [id](#)¹⁶², R. Goncalves Gama [id](#)⁵⁵, R. Gonçalo [id](#)^{129a,129c}, G. Gonella [id](#)¹²², L. Gonella [id](#)²⁰, A. Gongadze [id](#)³⁸, F. Gonnella [id](#)²⁰, J.L. Gonski [id](#)⁴¹, R.Y. González Andana [id](#)⁵², S. González de la Hoz [id](#)¹⁶², S. Gonzalez Fernandez [id](#)¹³, R. Gonzalez Lopez [id](#)⁹¹, C. Gonzalez Renteria [id](#)^{17a}, R. Gonzalez Suarez [id](#)¹⁶⁰, S. Gonzalez-Sevilla [id](#)⁵⁶, G.R. Gonzalvo Rodriguez [id](#)¹⁶², L. Goossens [id](#)³⁶, N.A. Gorasia [id](#)²⁰, P.A. Gorbounov [id](#)³⁷, B. Gorini [id](#)³⁶, E. Gorini [id](#)^{69a,69b}, A. Gorišek [id](#)⁹², A.T. Goshaw [id](#)⁵¹, M.I. Gostkin [id](#)³⁸, C.A. Gottardo [id](#)¹¹², M. Goughri [id](#)^{35b}, V. Goumarre [id](#)⁴⁸, A.G. Goussiou [id](#)¹³⁷, N. Govender [id](#)^{33c}, C. Goy [id](#)⁴, I. Grabowska-Bold [id](#)^{84a}, K. Graham [id](#)³⁴, E. Gramstad [id](#)¹²⁴, S. Grancagnolo [id](#)¹⁸, M. Grandi [id](#)¹⁴⁵, V. Gratchev [id](#)^{37,*}, P.M. Gravila [id](#)^{27f}, F.G. Gravili [id](#)^{69a,69b}, H.M. Gray [id](#)^{17a}, M. Greco [id](#)^{69a,69b}, C. Grefe [id](#)²⁴, I.M. Gregor [id](#)⁴⁸, P. Grenier [id](#)¹⁴², C. Grieco [id](#)¹³, A.A. Grillo [id](#)¹³⁵, K. Grimm [id](#)^{31,m}, S. Grinstein [id](#)^{13,u}, J.-F. Grivaz [id](#)⁶⁶, E. Gross [id](#)¹⁶⁸, J. Grosse-Knetter [id](#)⁵⁵, C. Grud [id](#)¹⁰⁵, A. Grummer [id](#)¹¹¹, J.C. Grundy [id](#)¹²⁵, L. Guan [id](#)¹⁰⁵, W. Guan [id](#)¹⁶⁹, C. Gubbels [id](#)¹⁶³, J.G.R. Guerrero Rojas [id](#)¹⁶², G. Guerrieri [id](#)^{68a,68c}, F. Guescini [id](#)¹⁰⁹, R. Gugel [id](#)⁹⁹, J.A.M. Guhit [id](#)¹⁰⁵, A. Guida [id](#)⁴⁸, T. Guillemain [id](#)⁴, E. Guilloton [id](#)^{166,133}, S. Guindon [id](#)³⁶, F. Guo [id](#)^{14a,14d}, J. Guo [id](#)^{62c}, L. Guo [id](#)⁶⁶, Y. Guo [id](#)¹⁰⁵,

R. Gupta ⁴⁸, S. Gurbuz ²⁴, S.S. Gurdasani ⁵⁴, G. Gustavino ³⁶, M. Guth ⁵⁶, P. Gutierrez ¹¹⁹, L.F. Gutierrez Zagazeta ¹²⁷, C. Gutschow ⁹⁵, C. Guyot ¹³⁴, C. Gwenlan ¹²⁵, C.B. Gwilliam ⁹¹, E.S. Haaland ¹²⁴, A. Haas ¹¹⁶, M. Habedank ⁴⁸, C. Haber ^{17a}, H.K. Hadavand ⁸, A. Hadeif ⁹⁹, S. Hadzic ¹⁰⁹, M. Haleem ¹⁶⁵, J. Haley ¹²⁰, J.J. Hall ¹³⁸, G.D. Hallowell ¹⁰¹, L. Halser ¹⁹, K. Hamano ¹⁶⁴, H. Hamdaoui ^{35e}, M. Hamer ²⁴, G.N. Hamity ⁵², J. Han ^{62b}, K. Han ^{62a}, L. Han ^{14c}, L. Han ^{62a}, S. Han ^{17a}, Y.F. Han ¹⁵⁴, K. Hanagaki ⁸², M. Hance ¹³⁵, D.A. Hangal ^{41,aa}, M.D. Hank ³⁹, R. Hankache ¹⁰⁰, J.B. Hansen ⁴², J.D. Hansen ⁴², P.H. Hansen ⁴², K. Hara ¹⁵⁶, D. Harada ⁵⁶, T. Harenberg ¹⁷⁰, S. Harkusha ³⁷, Y.T. Harris ¹²⁵, P.F. Harrison ¹⁶⁶, N.M. Hartman ¹⁴², N.M. Hartmann ¹⁰⁸, Y. Hasegawa ¹³⁹, A. Hasib ⁵², S. Haug ¹⁹, R. Hauser ¹⁰⁶, M. Havranek ¹³¹, C.M. Hawkes ²⁰, R.J. Hawkins ³⁶, S. Hayashida ¹¹⁰, D. Hayden ¹⁰⁶, C. Hayes ¹⁰⁵, R.L. Hayes ¹⁶³, C.P. Hays ¹²⁵, J.M. Hays ⁹³, H.S. Hayward ⁹¹, F. He ^{62a}, Y. He ¹⁵³, Y. He ¹²⁶, M.P. Heath ⁵², V. Hedberg ⁹⁷, A.L. Heggelund ¹²⁴, N.D. Hehir ⁹³, C. Heidegger ⁵⁴, K.K. Heidegger ⁵⁴, W.D. Heidorn ⁸⁰, J. Heilman ³⁴, S. Heim ⁴⁸, T. Heim ^{17a}, J.G. Heinlein ¹²⁷, J.J. Heinrich ¹²², L. Heinrich ³⁶, J. Hejbal ¹³⁰, L. Helary ⁴⁸, A. Held ¹¹⁶, S. Hellesund ¹²⁴, C.M. Helling ¹⁶³, S. Hellman ^{47a,47b}, C. Hensens ³⁶, R.C.W. Henderson ⁹⁰, L. Henkelmann ³², A.M. Henriques Correia ³⁶, H. Herde ¹⁴², Y. Hernández Jiménez ¹⁴⁴, H. Herr ⁹⁹, M.G. Herrmann ¹⁰⁸, T. Herrmann ⁵⁰, G. Herten ⁵⁴, R. Hertenberger ¹⁰⁸, L. Hervas ³⁶, N.P. Hessey ^{155a}, H. Hibi ⁸³, E. Higón-Rodríguez ¹⁶², S.J. Hillier ²⁰, I. Hinchliffe ^{17a}, F. Hinterkeuser ²⁴, M. Hirose ¹²³, S. Hirose ¹⁵⁶, D. Hirschbuehl ¹⁷⁰, T.G. Hitchings ¹⁰⁰, B. Hiti ⁹², J. Hobbs ¹⁴⁴, R. Hobincu ^{27e}, N. Hod ¹⁶⁸, M.C. Hodgkinson ¹³⁸, B.H. Hodgkinson ³², A. Hoecker ³⁶, J. Hofer ⁴⁸, D. Hohn ⁵⁴, T. Holm ²⁴, M. Holzbock ¹⁰⁹, L.B.A.H. Hommels ³², B.P. Honan ¹⁰⁰, J. Hong ^{62c}, T.M. Hong ¹²⁸, Y. Hong ⁵⁵, J.C. Honig ⁵⁴, A. Hönle ¹⁰⁹, B.H. Hooberman ¹⁶¹, W.H. Hopkins ⁶, Y. Horii ¹¹⁰, S. Hou ¹⁴⁷, A.S. Howard ⁹², J. Howarth ⁵⁹, J. Hoya ⁸⁹, M. Hrabovsky ¹²¹, A. Hrynevich ³⁷, T. Hryn'ova ⁴, P.J. Hsu ⁶⁵, S.-C. Hsu ¹³⁷, Q. Hu ^{41,aa}, Y.F. Hu ^{14a,14d,ah}, D.P. Huang ⁹⁵, S. Huang ^{64b}, X. Huang ^{14c}, Y. Huang ^{62a}, Y. Huang ^{14a}, Z. Huang ¹⁰⁰, Z. Hubacek ¹³¹, M. Huebner ²⁴, F. Huegging ²⁴, T.B. Huffman ¹²⁵, M. Huhtinen ³⁶, S.K. Huiberts ¹⁶, R. Hulsken ¹⁰³, N. Huseynov ^{12,a}, J. Huston ¹⁰⁶, J. Huth ⁶¹, R. Hyneman ¹⁴², S. Hyrych ^{28a}, G. Iacobucci ⁵⁶, G. Iakovidis ²⁹, I. Ibragimov ¹⁴⁰, L. Iconomidou-Fayard ⁶⁶, P. Inengo ^{71a,71b}, R. Iguchi ¹⁵², T. Iizawa ⁵⁶, Y. Ikegami ⁸², A. Ilg ¹⁹, N. Ilic ¹⁵⁴, H. Imam ^{35a}, T. Ingebretsen Carlson ^{47a,47b}, G. Introzzi ^{72a,72b}, M. Iodice ^{76a}, V. Ippolito ^{74a,74b}, M. Ishino ¹⁵², W. Islam ¹⁶⁹, C. Issever ^{18,48}, S. Istin ^{21a,aj}, H. Ito ¹⁶⁷, J.M. Iturbe Ponce ^{64a}, R. Iuppa ^{77a,77b}, A. Ivina ¹⁶⁸, J.M. Izen ⁴⁵, V. Izzo ^{71a}, P. Jacka ^{130,131}, P. Jackson ¹, R.M. Jacobs ⁴⁸, B.P. Jaeger ¹⁴¹, C.S. Jagfeld ¹⁰⁸, G. Jäkel ¹⁷⁰, K. Jakobs ⁵⁴, T. Jakoubek ¹⁶⁸, J. Jamieson ⁵⁹, K.W. Janas ^{84a}, G. Jarlskog ⁹⁷, A.E. Jaspan ⁹¹, T. Javůrek ³⁶, M. Javurkova ¹⁰², F. Jeanneau ¹³⁴, L. Jeanty ¹²², J. Jejelava ^{148a,y}, P. Jenni ^{54,f}, C.E. Jessiman ³⁴, S. Jézéquel ⁴, J. Jia ¹⁴⁴, X. Jia ⁶¹, X. Jia ^{14a,14d}, Z. Jia ^{14c}, Y. Jiang ^{62a}, S. Jiggins ⁵², J. Jimenez Pena ¹⁰⁹, S. Jin ^{14c}, A. Jinaru ^{27b}, O. Jinnouchi ¹⁵³, H. Jivan ^{33g}, P. Johansson ¹³⁸, K.A. Johns ⁷, C.A. Johnson ⁶⁷, D.M. Jones ³², E. Jones ¹⁶⁶, P. Jones ³², R.W.L. Jones ⁹⁰, T.J. Jones ⁹¹, J. Jovicevic ¹⁵, X. Ju ^{17a}, J.J. Junggeburth ³⁶, A. Juste Rozas ^{13,u}, S. Kabana ^{136e}, A. Kaczmarska ⁸⁵, M. Kado ^{74a,74b}, H. Kagan ¹¹⁸, M. Kagan ¹⁴², A. Kahn ⁴¹, A. Kahn ¹²⁷, C. Kahra ⁹⁹, T. Kaji ¹⁶⁷, E. Kajomovitz ¹⁴⁹, N. Kakati ¹⁶⁸, C.W. Kalderon ²⁹, A. Kamenshchikov ¹⁵⁴, N.J. Kang ¹³⁵, Y. Kano ¹¹⁰, D. Kar ^{33g}, K. Karava ¹²⁵, M.J. Kareem ^{155b}, E. Karentzos ⁵⁴, I. Karkanias ¹⁵¹, S.N. Karpov ³⁸, Z.M. Karpova ³⁸, V. Kartvelishvili ⁹⁰, A.N. Karyukhin ³⁷, E. Kasimi ¹⁵¹, C. Kato ^{62d}, J. Katzy ⁴⁸, S. Kaur ³⁴, K. Kawade ¹³⁹, K. Kawagoe ⁸⁸, T. Kawaguchi ¹¹⁰, T. Kawamoto ¹³⁴, G. Kawamura ⁵⁵, E.F. Kay ¹⁶⁴, F.I. Kaya ¹⁵⁷, S. Kazakos ¹³, V.F. Kazanin ³⁷, Y. Ke ¹⁴⁴, J.M. Keaveney ^{33a}, R. Keeler ¹⁶⁴, G.V. Kehris ⁶¹, J.S. Keller ³⁴, A.S. Kelly ⁹⁵,

D. Kelsey ¹⁴⁵, J.J. Kempster ²⁰, J. Kendrick ²⁰, K.E. Kennedy ⁴¹, O. Kepka ¹³⁰,
 B.P. Kerridge ¹⁶⁶, S. Kersten ¹⁷⁰, B.P. Kerševan ⁹², L. Keszezhova ^{28a}, S. Ketabchi Haghighat ¹⁵⁴,
 M. Khandoga ¹²⁶, A. Khanov ¹²⁰, A.G. Kharlamov ³⁷, T. Kharlamova ³⁷, E.E. Khoda ¹³⁷,
 T.J. Khoo ¹⁸, G. Khoriali ¹⁶⁵, J. Khubua ^{148b}, Y.A.R. Khwaira ⁶⁶, M. Kiehn ³⁶,
 A. Kilgallon ¹²², D.W. Kim ^{47a,47b}, E. Kim ¹⁵³, Y.K. Kim ³⁹, N. Kimura ⁹⁵, A. Kirchhoff ⁵⁵,
 D. Kirchmeier ⁵⁰, C. Kirfel ²⁴, J. Kirk ¹³³, A.E. Kiryunin ¹⁰⁹, T. Kishimoto ¹⁵², D.P. Kisliuk ¹⁵⁴,
 C. Kitsaki ¹⁰, O. Kivernyk ²⁴, M. Klassen ^{63a}, C. Klein ³⁴, L. Klein ¹⁶⁵, M.H. Klein ¹⁰⁵,
 M. Klein ⁹¹, U. Klein ⁹¹, P. Klimek ³⁶, A. Klimentov ²⁹, F. Klimpel ¹⁰⁹, T. Klingl ²⁴,
 T. Klioutchnikova ³⁶, F.F. Klitzner ¹⁰⁸, P. Kluit ¹¹³, S. Kluth ¹⁰⁹, E. Kneringer ⁷⁸,
 T.M. Knight ¹⁵⁴, A. Knue ⁵⁴, D. Kobayashi ⁸⁸, R. Kobayashi ⁸⁶, M. Kocian ¹⁴², T. Kodama ¹⁵²,
 P. Kodyš ¹³², D.M. Koeck ¹⁴⁵, P.T. Koenig ²⁴, T. Koffas ³⁴, N.M. Köhler ³⁶, M. Kolb ¹³⁴,
 I. Koletsou ⁴, T. Komarek ¹²¹, K. Köneke ⁵⁴, A.X.Y. Kong ¹, T. Kono ¹¹⁷, N. Konstantinidis ⁹⁵,
 B. Konya ⁹⁷, R. Kopeliansky ⁶⁷, S. Koperny ^{84a}, K. Korcyl ⁸⁵, K. Kordas ¹⁵¹, G. Koren ¹⁵⁰,
 A. Korn ⁹⁵, S. Korn ⁵⁵, I. Korolkov ¹³, N. Korotkova ³⁷, B. Kortman ¹¹³, O. Kortner ¹⁰⁹,
 S. Kortner ¹⁰⁹, W.H. Kostecka ¹¹⁴, V.V. Kostyukhin ¹⁴⁰, A. Kotsokechagia ⁶⁶, A. Kotwal ⁵¹,
 A. Koulouris ³⁶, A. Kourkoumeli-Charalampidi ^{72a,72b}, C. Kourkoumelis ⁹, E. Kourlitis ⁶,
 O. Kovanda ¹⁴⁵, R. Kowalewski ¹⁶⁴, W. Kozanecki ¹³⁴, A.S. Kozhin ³⁷, V.A. Kramarenko ³⁷,
 G. Kramberger ⁹², P. Kramer ⁹⁹, M.W. Krasny ¹²⁶, A. Krasznahorkay ³⁶, J.A. Kremer ⁹⁹,
 T. Kresse ⁵⁰, J. Kretschmar ⁹¹, K. Kreul ¹⁸, P. Krieger ¹⁵⁴, F. Krieter ¹⁰⁸,
 S. Krishnamurthy ¹⁰², A. Krishnan ^{63b}, M. Krivos ¹³², K. Krizka ^{17a}, K. Kroeninger ⁴⁹,
 H. Kroha ¹⁰⁹, J. Kroll ¹³⁰, J. Kroll ¹²⁷, K.S. Krowpman ¹⁰⁶, U. Kruchonak ³⁸, H. Krüger ²⁴,
 N. Krumnack ⁸⁰, M.C. Kruse ⁵¹, J.A. Krzysiak ⁸⁵, A. Kubota ¹⁵³, O. Kuchinskaja ³⁷, S. Kuday ^{3a},
 D. Kuechler ⁴⁸, J.T. Kuechler ⁴⁸, S. Kuehn ³⁶, T. Kuhl ⁴⁸, V. Kukhtin ³⁸, Y. Kulchitsky ^{37,a},
 S. Kuleshov ^{136d,136b}, M. Kumar ^{33g}, N. Kumari ¹⁰¹, M. Kuna ⁶⁰, A. Kupco ¹³⁰, T. Kupfer ⁴⁹,
 A. Kupich ³⁷, O. Kuprash ⁵⁴, H. Kurashige ⁸³, L.L. Kurchaninov ^{155a}, Y.A. Kurochkin ³⁷,
 A. Kurova ³⁷, E.S. Kuwertz ³⁶, M. Kuze ¹⁵³, A.K. Kvam ¹⁰², J. Kvita ¹²¹, T. Kwan ¹⁰³,
 K.W. Kwok ^{64a}, C. Lacasta ¹⁶², F. Lacava ^{74a,74b}, H. Lacker ¹⁸, D. Lacour ¹²⁶, N.N. Lad ⁹⁵,
 E. Ladygin ³⁸, B. Laforge ¹²⁶, T. Lagouri ^{136e}, S. Lai ⁵⁵, I.K. Lakomic ^{84a}, N. Lalloue ⁶⁰,
 J.E. Lambert ¹¹⁹, S. Lammers ⁶⁷, W. Lampl ⁷, C. Lampoudis ¹⁵¹, A.N. Lancaster ¹¹⁴,
 E. Lançon ²⁹, U. Landgraf ⁵⁴, M.P.J. Landon ⁹³, V.S. Lang ⁵⁴, R.J. Langenberg ¹⁰²,
 A.J. Lankford ¹⁵⁹, F. Lanni ²⁹, K. Lantzsch ²⁴, A. Lanza ^{72a}, A. Lapertosa ^{57b,57a},
 J.F. Laporte ¹³⁴, T. Lari ^{70a}, F. Lasagni Manghi ^{23b}, M. Lassnig ³⁶, V. Latonova ¹³⁰, T.S. Lau ^{64a},
 A. Laudrain ⁹⁹, A. Laurier ³⁴, S.D. Lawlor ⁹⁴, Z. Lawrence ¹⁰⁰, M. Lazzaroni ^{70a,70b}, B. Le ¹⁰⁰,
 B. Leban ⁹², A. Lebedev ⁸⁰, M. LeBlanc ³⁶, T. LeCompte ⁶, F. Ledroit-Guillon ⁶⁰, A.C.A. Lee ⁹⁵,
 G.R. Lee ¹⁶, L. Lee ⁶¹, S.C. Lee ¹⁴⁷, S. Lee ^{47a,47b}, L.L. Leeuw ^{33c}, H.P. Lefebvre ⁹⁴,
 M. Lefebvre ¹⁶⁴, C. Leggett ^{17a}, K. Lehmann ¹⁴¹, G. Lehmann Miotto ³⁶, W.A. Leight ¹⁰²,
 A. Leisos ^{151,t}, M.A.L. Leite ^{81c}, C.E. Leitgeb ⁴⁸, R. Leitner ¹³², K.J.C. Leney ⁴⁴, T. Lenz ²⁴,
 S. Leone ^{73a}, C. Leonidopoulos ⁵², A. Leopold ¹⁴³, C. Leroy ¹⁰⁷, R. Les ¹⁰⁶, C.G. Lester ³²,
 M. Levchenko ³⁷, J. Levêque ⁴, D. Levin ¹⁰⁵, L.J. Levinson ¹⁶⁸, D.J. Lewis ²⁰, B. Li ^{14b},
 B. Li ^{62b}, C. Li ^{62a}, C-Q. Li ^{62c,62d}, H. Li ^{62a}, H. Li ^{62b}, H. Li ^{14c}, H. Li ^{62b}, J. Li ^{62c},
 K. Li ¹³⁷, L. Li ^{62c}, M. Li ^{14a,14d}, Q.Y. Li ^{62a}, S. Li ^{62d,62c,d}, T. Li ^{62b}, X. Li ¹⁰³, Z. Li ^{62b},
 Z. Li ¹²⁵, Z. Li ¹⁰³, Z. Li ⁹¹, Z. Liang ^{14a}, M. Liberatore ⁴⁸, B. Liberti ^{75a}, K. Lie ^{64c},
 J. Lieber Marin ^{81b}, K. Lin ¹⁰⁶, R.A. Linck ⁶⁷, R.E. Lindley ⁷, J.H. Lindon ², A. Linss ⁴⁸,
 E. Lipeles ¹²⁷, A. Lipniacka ¹⁶, T.M. Liss ^{161,ad}, A. Lister ¹⁶³, J.D. Little ⁴, B. Liu ^{14a},
 B.X. Liu ¹⁴¹, D. Liu ^{62d,62c}, J.B. Liu ^{62a}, J.K.K. Liu ³², K. Liu ^{62d,62c}, M. Liu ^{62a},
 M.Y. Liu ^{62a}, P. Liu ^{14a}, Q. Liu ^{62d,137,62c}, X. Liu ^{62a}, Y. Liu ⁴⁸, Y. Liu ^{14c,14d}, Y.L. Liu ¹⁰⁵,
 Y.W. Liu ^{62a}, M. Livan ^{72a,72b}, J. Llorente Merino ¹⁴¹, S.L. Lloyd ⁹³, E.M. Lobodzinska ⁴⁸,






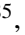
















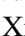

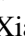
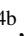

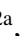
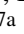
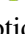
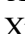








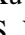
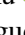
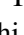






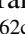

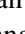


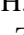

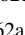
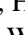

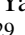

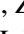
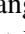


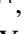
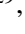
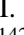
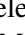


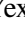

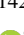





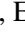
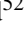


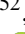
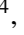
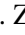

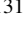

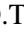
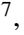
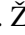

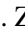





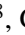





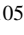


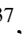



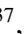





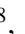




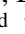



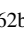
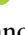

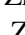

P. Loch ⁷, S. Loffredo ^{75a,75b}, T. Lohse ¹⁸, K. Lohwasser ¹³⁸, M. Lokajicek ^{130,*}, J.D. Long ¹⁶¹,
 I. Longarini ^{74a,74b}, L. Longo ^{69a,69b}, R. Longo ¹⁶¹, I. Lopez Paz ³⁶, A. Lopez Solis ⁴⁸,
 J. Lorenz ¹⁰⁸, N. Lorenzo Martinez ⁴, A.M. Lory ¹⁰⁸, A. Lösle ⁵⁴, X. Lou ^{47a,47b}, X. Lou ^{14a,14d},
 A. Lounis ⁶⁶, J. Love ⁶, P.A. Love ⁹⁰, J.J. Lozano Bahilo ¹⁶², G. Lu ^{14a,14d}, M. Lu ⁷⁹,
 S. Lu ¹²⁷, Y.J. Lu ⁶⁵, H.J. Lubatti ¹³⁷, C. Luci ^{74a,74b}, F.L. Lucio Alves ^{14c}, A. Lucotte ⁶⁰,
 F. Luehring ⁶⁷, I. Luise ¹⁴⁴, O. Lukianchuk ⁶⁶, O. Lundberg ¹⁴³, B. Lund-Jensen ¹⁴³,
 N.A. Luongo ¹²², M.S. Lutz ¹⁵⁰, D. Lynn ²⁹, H. Lyons ⁹¹, R. Lysak ¹³⁰, E. Lytken ⁹⁷, F. Lyu ^{14a},
 V. Lyubushkin ³⁸, T. Lyubushkina ³⁸, H. Ma ²⁹, L.L. Ma ^{62b}, Y. Ma ⁹⁵, D.M. Mac Donell ¹⁶⁴,
 G. Maccarrone ⁵³, J.C. MacDonald ¹³⁸, R. Madar ⁴⁰, W.F. Mader ⁵⁰, J. Maeda ⁸³, T. Maeno ²⁹,
 M. Maerker ⁵⁰, V. Magerl ⁵⁴, J. Magro ^{68a,68c}, H. Maguire ¹³⁸, D.J. Mahon ⁴¹,
 C. Maidantchik ^{81b}, A. Maio ^{129a,129b,129d}, K. Maj ^{84a}, O. Majersky ^{28a}, S. Majewski ¹²²,
 N. Makovec ⁶⁶, V. Maksimovic ¹⁵, B. Malaescu ¹²⁶, Pa. Malecki ⁸⁵, V.P. Maleev ³⁷,
 F. Malek ⁶⁰, D. Malito ^{43b,43a}, U. Mallik ⁷⁹, C. Malone ³², S. Maltezos ¹⁰, S. Malyukov ³⁸,
 J. Mamuzic ¹³, G. Mancini ⁵³, G. Manco ^{72a,72b}, J.P. Mandalia ⁹³, I. Mandić ⁹²,
 L. Manhaes de Andrade Filho ^{81a}, I.M. Maniatis ¹⁵¹, M. Manisha ¹³⁴, J. Manjarres Ramos ⁵⁰,
 D.C. Mankad ¹⁶⁸, K.H. Mankinen ⁹⁷, A. Mann ¹⁰⁸, A. Manousos ⁷⁸, B. Mansoulie ¹³⁴,
 S. Manzoni ³⁶, A. Marantis ^{151,t}, G. Marchiori ⁵, M. Marcisovsky ¹³⁰, L. Marcoccia ^{75a,75b},
 C. Marcon ⁹⁷, M. Marinescu ²⁰, M. Marjanovic ¹¹⁹, Z. Marshall ^{17a}, S. Marti-Garcia ¹⁶²,
 T.A. Martin ¹⁶⁶, V.J. Martin ⁵², B. Martin dit Latour ¹⁶, L. Martinelli ^{74a,74b}, M. Martinez ^{13,u},
 P. Martinez Agullo ¹⁶², V.I. Martinez Outschoorn ¹⁰², P. Martinez Suarez ¹³, S. Martin-Haugh ¹³³,
 V.S. Martoiu ^{27b}, A.C. Martyniuk ⁹⁵, A. Marzin ³⁶, S.R. Maschek ¹⁰⁹, L. Masetti ⁹⁹,
 T. Mashimo ¹⁵², J. Masik ¹⁰⁰, A.L. Maslennikov ³⁷, L. Massa ^{23b}, P. Massarotti ^{71a,71b},
 P. Mastrandrea ^{73a,73b}, A. Mastroberardino ^{43b,43a}, T. Masubuchi ¹⁵², T. Mathisen ¹⁶⁰,
 A. Matic ¹⁰⁸, N. Matsuzawa ¹⁵², J. Maurer ^{27b}, B. Maček ⁹², D.A. Maximov ³⁷, R. Mazini ¹⁴⁷,
 I. Maznas ¹⁵¹, M. Mazza ¹⁰⁶, S.M. Mazza ¹³⁵, C. Mc Ginn ²⁹, J.P. Mc Gowan ¹⁰³,
 S.P. Mc Kee ¹⁰⁵, T.G. McCarthy ¹⁰⁹, W.P. McCormack ^{17a}, E.F. McDonald ¹⁰⁴,
 A.E. McDougall ¹¹³, J.A. Mcfayden ¹⁴⁵, G. Mchedlidze ^{148b}, R.P. Mckenzie ^{33g},
 T.C. McLachlan ⁴⁸, D.J. McLaughlin ⁹⁵, K.D. McLean ¹⁶⁴, S.J. McMahon ¹³³, P.C. McNamara ¹⁰⁴,
 R.A. McPherson ^{164,w}, J.E. Mdhluli ^{33g}, S. Meehan ³⁶, T. Megy ⁴⁰, S. Mehlhase ¹⁰⁸,
 A. Mehta ⁹¹, B. Meirose ⁴⁵, D. Melini ¹⁴⁹, B.R. Mellado Garcia ^{33g}, A.H. Melo ⁵⁵,
 F. Meloni ⁴⁸, E.D. Mendes Gouveia ^{129a}, A.M. Mendes Jacques Da Costa ²⁰, H.Y. Meng ¹⁵⁴,
 L. Meng ⁹⁰, S. Menke ¹⁰⁹, M. Mentink ³⁶, E. Meoni ^{43b,43a}, C. Merlassino ¹²⁵,
 L. Merola ^{71a,71b}, C. Meroni ^{70a}, G. Merz ¹⁰⁵, O. Meshkov ³⁷, J.K.R. Meshreki ¹⁴⁰, J. Metcalfe ⁶,
 A.S. Mete ⁶, C. Meyer ⁶⁷, J-P. Meyer ¹³⁴, M. Michetti ¹⁸, R.P. Middleton ¹³³, L. Mijović ⁵²,
 G. Mikenberg ¹⁶⁸, M. Migestikova ¹³⁰, M. Mikuž ⁹², H. Mildner ¹³⁸, A. Milic ¹⁵⁴,
 C.D. Milke ⁴⁴, D.W. Miller ³⁹, L.S. Miller ³⁴, A. Milov ¹⁶⁸, D.A. Milstead ^{47a,47b}, T. Min ^{14c},
 A.A. Minaenko ³⁷, I.A. Minashvili ^{148b}, L. Mince ⁵⁹, A.I. Mincer ¹¹⁶, B. Mindur ^{84a},
 M. Mineev ³⁸, Y. Minegishi ¹⁵², Y. Mino ⁸⁶, L.M. Mir ¹³, M. Miralles Lopez ¹⁶²,
 M. Mironova ¹²⁵, T. Mitani ¹⁶⁷, A. Mitra ¹⁶⁶, V.A. Mitsou ¹⁶², O. Miu ¹⁵⁴, P.S. Miyagawa ⁹³,
 Y. Miyazaki ⁸⁸, A. Mizukami ⁸², J.U. Mjörnmark ⁹⁷, T. Mkrtchyan ^{63a}, M. Mlynarikova ¹¹⁴,
 T. Moa ^{47a,47b}, S. Mobius ⁵⁵, K. Mochizuki ¹⁰⁷, P. Moder ⁴⁸, P. Mogg ¹⁰⁸,
 A.F. Mohammed ^{14a,14d}, S. Mohapatra ⁴¹, G. Mokgatitswane ^{33g}, B. Mondal ¹⁴⁰, S. Mondal ¹³¹,
 K. Mönig ⁴⁸, E. Monnier ¹⁰¹, L. Monsonis Romero ¹⁶², J. Montejo Berlingen ³⁶, M. Montella ¹¹⁸,
 F. Monticelli ⁸⁹, N. Morange ⁶⁶, A.L. Moreira De Carvalho ^{129a}, M. Moreno Llácer ¹⁶²,
 C. Moreno Martinez ¹³, P. Morettini ^{57b}, S. Morgenstern ¹⁶⁶, M. Morii ⁶¹, M. Morinaga ¹⁵²,
 V. Morisbak ¹²⁴, A.K. Morley ³⁶, F. Morodei ^{74a,74b}, L. Morvaj ³⁶, P. Moschovakos ³⁶,
 B. Moser ³⁶, M. Mosidze ^{148b}, T. Moskalets ⁵⁴, P. Moskvitina ¹¹², J. Moss ^{31,n}, E.J.W. Moyses ¹⁰²,

S. Muanza ¹⁰¹, J. Mueller ¹²⁸, D. Muenstermann ⁹⁰, R. Müller ¹⁹, G.A. Mullier ⁹⁷, J.J. Mullin ¹²⁷,
 D.P. Mungo ^{70a,70b}, J.L. Munoz Martinez ¹³, D. Munoz Perez ¹⁶², F.J. Munoz Sanchez ¹⁰⁰,
 M. Murin ¹⁰⁰, W.J. Murray ^{166,133}, A. Murrone ^{70a,70b}, J.M. Muse ¹¹⁹, M. Muškinja ^{17a},
 C. Mwewa ²⁹, A.G. Myagkov ^{37,a}, A.J. Myers ⁸, A.A. Myers ¹²⁸, G. Myers ⁶⁷, M. Myska ¹³¹,
 B.P. Nachman ^{17a}, O. Nackenhorst ⁴⁹, A. Nag ⁵⁰, K. Nagai ¹²⁵, K. Nagano ⁸², J.L. Nagle ^{29,ai},
 E. Nagy ¹⁰¹, A.M. Nairz ³⁶, Y. Nakahama ⁸², K. Nakamura ⁸², H. Nanjo ¹²³, R. Narayan ⁴⁴,
 E.A. Narayanan ¹¹¹, I. Naryshkin ³⁷, M. Naseri ³⁴, C. Nass ²⁴, G. Navarro ^{22a},
 J. Navarro-Gonzalez ¹⁶², R. Nayak ¹⁵⁰, P.Y. Nechaeva ³⁷, F. Nechansky ⁴⁸, T.J. Neep ²⁰,
 A. Negri ^{72a,72b}, M. Negrini ^{23b}, C. Nellist ¹¹², C. Nelson ¹⁰³, K. Nelson ¹⁰⁵, S. Nemecek ¹³⁰,
 M. Nessi ^{36,g}, M.S. Neubauer ¹⁶¹, F. Neuhaus ⁹⁹, J. Neundorf ⁴⁸, R. Newhouse ¹⁶³,
 P.R. Newman ²⁰, C.W. Ng ¹²⁸, Y.S. Ng ¹⁸, Y.W.Y. Ng ¹⁵⁹, B. Ngair ^{35e}, H.D.N. Nguyen ¹⁰⁷,
 R.B. Nickerson ¹²⁵, R. Nicolaidou ¹³⁴, J. Nielsen ¹³⁵, M. Niemeyer ⁵⁵, N. Nikiforou ³⁶,
 V. Nikolaenko ^{37,a}, I. Nikolic-Audit ¹²⁶, K. Nikolopoulos ²⁰, P. Nilsson ²⁹, H.R. Nindhito ⁵⁶,
 A. Nisati ^{74a}, N. Nishu ², R. Nisius ¹⁰⁹, J-E. Nitschke ⁵⁰, E.K. Nkadimeng ^{33g},
 S.J. Noacco Rosende ⁸⁹, T. Nobe ¹⁵², D.L. Noel ³², Y. Noguchi ⁸⁶, T. Nommensen ¹⁴⁶,
 M.A. Nomura ²⁹, M.B. Norfolk ¹³⁸, R.R.B. Norisam ⁹⁵, B.J. Norman ³⁴, J. Novak ⁹², T. Novak ⁴⁸,
 O. Novgorodova ⁵⁰, L. Novotny ¹³¹, R. Novotny ¹¹¹, L. Nozka ¹²¹, K. Ntekas ¹⁵⁹, E. Nurse ⁹⁵,
 F.G. Oakham ^{34,af}, J. Ocariz ¹²⁶, A. Ochi ⁸³, I. Ochoa ^{129a}, S. Oda ⁸⁸, S. Oerdek ¹⁶⁰,
 A. Ogrodnik ^{84a}, A. Oh ¹⁰⁰, C.C. Ohm ¹⁴³, H. Oide ¹⁵³, R. Oishi ¹⁵², M.L. Ojeda ⁴⁸,
 Y. Okazaki ⁸⁶, M.W. O'Keefe ⁹¹, Y. Okumura ¹⁵², A. Olariu ^{27b}, L.F. Oleiro Seabra ^{129a},
 S.A. Olivares Pino ^{136e}, D. Oliveira Damazio ²⁹, D. Oliveira Goncalves ^{81a}, J.L. Oliver ¹⁵⁹,
 M.J.R. Olsson ¹⁵⁹, A. Olszewski ⁸⁵, J. Olszowska ^{85,*}, Ö.O. Öncel ⁵⁴, D.C. O'Neil ¹⁴¹,
 A.P. O'Neill ¹⁹, A. Onofre ^{129a,129e}, P.U.E. Onyisi ¹¹, M.J. Oreglia ³⁹, G.E. Orellana ⁸⁹,
 D. Orestano ^{76a,76b}, N. Orlando ¹³, R.S. Orr ¹⁵⁴, V. O'Shea ⁵⁹, R. Ospanov ^{62a},
 G. Otero y Garzon ³⁰, H. Otono ⁸⁸, P.S. Ott ^{63a}, G.J. Ottino ^{17a}, M. Ouchrif ^{35d},
 J. Ouellette ^{29,ai}, F. Ould-Saada ¹²⁴, M. Owen ⁵⁹, R.E. Owen ¹³³, K.Y. Oyulmaz ^{21a},
 V.E. Ozcan ^{21a}, N. Ozturk ⁸, S. Ozturk ^{21d}, J. Pacalt ¹²¹, H.A. Pacey ³², K. Pachal ⁵¹,
 A. Pacheco Pages ¹³, C. Padilla Aranda ¹³, G. Padovano ^{74a,74b}, S. Pagan Griso ^{17a},
 G. Palacino ⁶⁷, A. Palazzo ^{69a,69b}, S. Palazzo ⁵², S. Palestini ³⁶, M. Palka ^{84b}, J. Pan ¹⁷¹,
 T. Pan ^{64a}, D.K. Panchal ¹¹, C.E. Pandini ¹¹³, J.G. Panduro Vazquez ⁹⁴, P. Pani ⁴⁸,
 G. Panizzo ^{68a,68c}, L. Paolozzi ⁵⁶, C. Papadatos ¹⁰⁷, S. Parajuli ⁴⁴, A. Paramonov ⁶,
 C. Paraskevopoulos ¹⁰, D. Paredes Hernandez ^{64b}, T.H. Park ¹⁵⁴, M.A. Parker ³², F. Parodi ^{57b,57a},
 E.W. Parrish ¹¹⁴, V.A. Parrish ⁵², J.A. Parsons ⁴¹, U. Parzefall ⁵⁴, B. Pascual Dias ¹⁰⁷,
 L. Pascual Dominguez ¹⁵⁰, V.R. Pascuzzi ^{17a}, F. Pasquali ¹¹³, E. Pasqualucci ^{74a}, S. Passaggio ^{57b},
 F. Pastore ⁹⁴, P. Pasuwan ^{47a,47b}, J.R. Pater ¹⁰⁰, J. Patton ⁹¹, T. Pauly ³⁶, J. Pearkes ¹⁴²,
 M. Pedersen ¹²⁴, R. Pedro ^{129a}, S.V. Peleganchuk ³⁷, O. Penc ¹³⁰, C. Peng ^{64b}, H. Peng ^{62a},
 M. Penzin ³⁷, B.S. Peralva ^{81a,81d}, A.P. Pereira Peixoto ⁶⁰, L. Pereira Sanchez ^{47a,47b},
 D.V. Perepelitsa ^{29,ai}, E. Perez Codina ^{155a}, M. Perganti ¹⁰, L. Perini ^{70a,70b,*}, H. Pernegger ³⁶,
 S. Perrella ³⁶, A. Perrevoort ¹¹², O. Perrin ⁴⁰, K. Peters ⁴⁸, R.F.Y. Peters ¹⁰⁰, B.A. Petersen ³⁶,
 T.C. Petersen ⁴², E. Petit ¹⁰¹, V. Petousis ¹³¹, C. Petridou ¹⁵¹, A. Petrukhin ¹⁴⁰, M. Pettee ^{17a},
 N.E. Pettersson ³⁶, A. Petukhov ³⁷, K. Petukhova ¹³², A. Peyaud ¹³⁴, R. Pezoa ^{136f},
 L. Pezzotti ³⁶, G. Pezzullo ¹⁷¹, T. Pham ¹⁰⁴, P.W. Phillips ¹³³, M.W. Phipps ¹⁶¹,
 G. Piacquadio ¹⁴⁴, E. Pianori ^{17a}, F. Piazza ^{70a,70b}, R. Piegaia ³⁰, D. Pietreanu ^{27b},
 A.D. Pilkington ¹⁰⁰, M. Pinamonti ^{68a,68c}, J.L. Pinfold ², B.C. Pinheiro Pereira ^{129a},
 C. Pitman Donaldson ⁹⁵, D.A. Pizzi ³⁴, L. Pizzimento ^{75a,75b}, A. Pizzini ¹¹³, M.-A. Pleier ²⁹,
 V. Plesanovs ⁵⁴, V. Pleskot ¹³², E. Plotnikova ³⁸, G. Poddar ⁴, R. Poettgen ⁹⁷, R. Poggi ⁵⁶,
 L. Poggioli ¹²⁶, I. Pogrebnyak ¹⁰⁶, D. Pohl ²⁴, I. Pokharel ⁵⁵, S. Polacek ¹³², G. Polesello ^{72a},

A. Poley ^{141,155a}, R. Polifka ¹³¹, A. Polini ^{23b}, C.S. Pollard ¹²⁵, Z.B. Pollock ¹¹⁸,
 V. Polychronakos ²⁹, D. Ponomarenko ³⁷, L. Pontecorvo ³⁶, S. Popa ^{27a}, G.A. Popeneciu ^{27d},
 D.M. Portillo Quintero ^{155a}, S. Pospisil ¹³¹, P. Postolache ^{27c}, K. Potamianos ¹²⁵, I.N. Potrap ³⁸,
 C.J. Potter ³², H. Potti ¹, T. Poulsen ⁴⁸, J. Poveda ¹⁶², G. Pownall ⁴⁸, M.E. Pozo Astigarraga ³⁶,
 A. Prades Ibanez ¹⁶², M.M. Prapa ⁴⁶, J. Pretel ⁵⁴, D. Price ¹⁰⁰, M. Primavera ^{69a},
 M.A. Principe Martin ⁹⁸, M.L. Proffitt ¹³⁷, N. Proklova ³⁷, K. Prokofiev ^{64c}, G. Proto ^{75a,75b},
 S. Protopopescu ²⁹, J. Proudfoot ⁶, M. Przybycien ^{84a}, J.E. Puddefoot ¹³⁸, D. Pudzha ³⁷,
 P. Puzo ⁶⁶, D. Pyatiizbyantseva ³⁷, J. Qian ¹⁰⁵, Y. Qin ¹⁰⁰, T. Qiu ⁹³, A. Quadt ⁵⁵,
 M. Queitsch-Maitland ²⁴, G. Rabanal Bolanos ⁶¹, D. Rafanoharana ⁵⁴, F. Ragusa ^{70a,70b},
 J.L. Rainbolt ³⁹, J.A. Raine ⁵⁶, S. Rajagopalan ²⁹, E. Ramakoti ³⁷, K. Ran ^{14a,14d},
 V. Raskina ¹²⁶, D.F. Rassloff ^{63a}, S. Rave ⁹⁹, B. Ravina ⁵⁹, I. Ravinovich ¹⁶⁸, M. Raymond ³⁶,
 A.L. Read ¹²⁴, N.P. Readioff ¹³⁸, D.M. Rebutzi ^{72a,72b}, G. Redlinger ²⁹, K. Reeves ⁴⁵,
 J.A. Reidelsturz ¹⁷⁰, D. Reikher ¹⁵⁰, A. Reiss ⁹⁹, A. Rej ¹⁴⁰, C. Rembser ³⁶, A. Renardi ⁴⁸,
 M. Renda ^{27b}, M.B. Rendel ¹⁰⁹, A.G. Rennie ⁵⁹, S. Resconi ^{70a}, M. Ressegotti ^{57b,57a},
 E.D. Resseguie ^{17a}, S. Rettie ⁹⁵, B. Reynolds ¹¹⁸, E. Reynolds ^{17a}, M. Rezaei Estabragh ¹⁷⁰,
 O.L. Rezanova ³⁷, P. Reznicek ¹³², E. Ricci ^{77a,77b}, R. Richter ¹⁰⁹, S. Richter ^{47a,47b},
 E. Richter-Was ^{84b}, M. Ridel ¹²⁶, P. Rieck ¹¹⁶, P. Riedler ³⁶, M. Rijssenbeek ¹⁴⁴,
 A. Rimoldi ^{72a,72b}, M. Rimoldi ⁴⁸, L. Rinaldi ^{23b,23a}, T.T. Rinn ²⁹, M.P. Rinnagel ¹⁰⁸,
 G. Ripellino ¹⁴³, I. Riu ¹³, P. Rivadeneira ⁴⁸, J.C. Rivera Vergara ¹⁶⁴, F. Rizatdinova ¹²⁰,
 E. Rizvi ⁹³, C. Rizzi ⁵⁶, B.A. Roberts ¹⁶⁶, B.R. Roberts ^{17a}, S.H. Robertson ^{103,w}, M. Robin ⁴⁸,
 D. Robinson ³², C.M. Robles Gajardo ^{136f}, M. Robles Manzano ⁹⁹, A. Robson ⁵⁹, A. Rocchi ^{75a,75b},
 C. Roda ^{73a,73b}, S. Rodriguez Bosca ^{63a}, Y. Rodriguez Garcia ^{22a}, A. Rodriguez Rodriguez ⁵⁴,
 A.M. Rodríguez Vera ^{155b}, S. Roe ³⁶, J.T. Roemer ¹⁵⁹, A.R. Roepe-Gier ¹¹⁹, J. Roggel ¹⁷⁰,
 O. Røhne ¹²⁴, R.A. Rojas ¹⁶⁴, B. Roland ⁵⁴, C.P.A. Roland ⁶⁷, J. Roloff ²⁹, A. Romaniouk ³⁷,
 E. Romano ^{72a,72b}, M. Romano ^{23b}, A.C. Romero Hernandez ¹⁶¹, N. Rompotis ⁹¹, L. Roos ¹²⁶,
 S. Rosati ^{74a}, B.J. Rosser ³⁹, E. Rossi ⁴, E. Rossi ^{71a,71b}, L.P. Rossi ^{57b}, L. Rossini ⁴⁸,
 R. Rosten ¹¹⁸, M. Rotaru ^{27b}, B. Rottler ⁵⁴, D. Rousseau ⁵⁶, D. Rousso ³², G. Rovelli ^{72a,72b},
 A. Roy ¹⁶¹, A. Rozanov ¹⁰¹, Y. Rozen ¹⁴⁹, X. Ruan ^{33g}, A. Rubio Jimenez ¹⁶², A.J. Ruby ⁹¹,
 T.A. Ruggeri ¹, F. Rühr ⁵⁴, A. Ruiz-Martinez ¹⁶², A. Rummler ³⁶, Z. Rurikova ⁵⁴,
 N.A. Rusakovich ³⁸, H.L. Russell ¹⁶⁴, J.P. Rutherford ⁷, E.M. Rüttinger ¹³⁸, K. Rybacki ⁹⁰,
 M. Rybar ¹³², E.B. Rye ¹²⁴, A. Ryzhov ³⁷, J.A. Sabater Iglesias ⁵⁶, P. Sabatini ¹⁶²,
 L. Sabetta ^{74a,74b}, H.F-W. Sadrozinski ¹³⁵, F. Safai Tehrani ^{74a}, B. Safarzadeh Samani ¹⁴⁵,
 M. Safdari ¹⁴², S. Saha ¹⁰³, M. Sahinsoy ¹⁰⁹, M. Saimpert ¹³⁴, M. Saito ¹⁵², T. Saito ¹⁵²,
 D. Salamani ³⁶, G. Salamanna ^{76a,76b}, A. Salnikov ¹⁴², J. Salt ¹⁶², A. Salvador Salas ¹³,
 D. Salvatore ^{43b,43a}, F. Salvatore ¹⁴⁵, A. Salzburger ³⁶, D. Sammel ⁵⁴, D. Sampsonidis ¹⁵¹,
 D. Sampsonidou ^{62d,62c}, J. Sánchez ¹⁶², A. Sanchez Pineda ⁴, V. Sanchez Sebastian ¹⁶²,
 H. Sandaker ¹²⁴, C.O. Sander ⁴⁸, J.A. Sandesara ¹⁰², M. Sandhoff ¹⁷⁰, C. Sandoval ^{22b},
 D.P.C. Sankey ¹³³, A. Sansoni ⁵³, L. Santi ^{74a,74b}, C. Santoni ⁴⁰, H. Santos ^{129a,129b},
 S.N. Santpur ^{17a}, A. Santra ¹⁶⁸, K.A. Saoucha ¹³⁸, J.G. Saraiva ^{129a,129d}, J. Sardain ¹⁰¹,
 O. Sasaki ⁸², K. Sato ¹⁵⁶, C. Sauer ^{63b}, F. Sauerburger ⁵⁴, E. Sauvan ⁴, P. Savard ^{154,af},
 R. Sawada ¹⁵², C. Sawyer ¹³³, L. Sawyer ⁹⁶, I. Sayago Galvan ¹⁶², C. Sbarra ^{23b}, A. Sbrizzi ^{23b,23a},
 T. Scanlon ⁹⁵, J. Schaarschmidt ¹³⁷, P. Schacht ¹⁰⁹, D. Schaefer ³⁹, U. Schäfer ⁹⁹,
 A.C. Schaffer ⁶⁶, D. Schaile ¹⁰⁸, R.D. Schamberger ¹⁴⁴, E. Schanet ¹⁰⁸, C. Scharf ¹⁸,
 V.A. Schegelsky ³⁷, D. Scheirich ¹³², F. Schenck ¹⁸, M. Schernau ¹⁵⁹, C. Scheulen ⁵⁵,
 C. Schiavi ^{57b,57a}, Z.M. Schillaci ²⁶, E.J. Schioppa ^{69a,69b}, M. Schioppa ^{43b,43a}, B. Schlag ⁹⁹,
 K.E. Schleicher ⁵⁴, S. Schlenker ³⁶, K. Schmieden ⁹⁹, C. Schmitt ⁹⁹, S. Schmitt ⁴⁸,
 L. Schoeffel ¹³⁴, A. Schoening ^{63b}, P.G. Scholer ⁵⁴, E. Schopf ¹²⁵, M. Schott ⁹⁹,

J. Schovancova [ID36](#), S. Schramm [ID56](#), F. Schroeder [ID170](#), H-C. Schultz-Coulon [ID63a](#), M. Schumacher [ID54](#),
 B.A. Schumm [ID135](#), Ph. Schune [ID134](#), A. Schwartzman [ID142](#), T.A. Schwarz [ID105](#), Ph. Schwemling [ID134](#),
 R. Schwienhorst [ID106](#), A. Sciandra [ID135](#), G. Sciolla [ID26](#), F. Scuri [ID73a](#), F. Scutti [ID104](#), C.D. Sebastiani [ID91](#),
 K. Sedlaczek [ID49](#), P. Seema [ID18](#), S.C. Seidel [ID111](#), A. Seiden [ID135](#), B.D. Seidlitz [ID41](#), T. Seiss [ID39](#),
 C. Seitz [ID48](#), J.M. Seixas [ID81b](#), G. Sekhniaidze [ID71a](#), S.J. Sekula [ID44](#), L. Selem [ID4](#),
 N. Semprini-Cesari [ID23b,23a](#), S. Sen [ID51](#), D. Sengupta [ID56](#), V. Senthilkumar [ID162](#), L. Serin [ID66](#),
 L. Serkin [ID68a,68b](#), M. Sessa [ID76a,76b](#), H. Severini [ID119](#), S. Sevova [ID142](#), F. Sforza [ID57b,57a](#), A. Sfyrla [ID56](#),
 E. Shabalina [ID55](#), R. Shaheen [ID143](#), J.D. Shahinian [ID127](#), N.W. Shaikh [ID47a,47b](#), D. Shaked Renous [ID168](#),
 L.Y. Shan [ID14a](#), M. Shapiro [ID17a](#), A. Sharma [ID36](#), A.S. Sharma [ID163](#), P. Sharma [ID79](#), S. Sharma [ID48](#),
 P.B. Shatalov [ID37](#), K. Shaw [ID145](#), S.M. Shaw [ID100](#), Q. Shen [ID62c](#), P. Sherwood [ID95](#), L. Shi [ID95](#),
 C.O. Shimmin [ID171](#), Y. Shimogama [ID167](#), J.D. Shinner [ID94](#), I.P.J. Shipsey [ID125](#), S. Shirabe [ID60](#),
 M. Shiyakova [ID38](#), J. Shlomi [ID168](#), M.J. Shochet [ID39](#), J. Shojaii [ID104](#), D.R. Shope [ID143](#), S. Shrestha [ID118](#),
 E.M. Shrif [ID33g](#), M.J. Shroff [ID164](#), P. Sicho [ID130](#), A.M. Sickles [ID161](#), E. Sideras Haddad [ID33g](#),
 O. Sidiropoulou [ID36](#), A. Sidoti [ID23b](#), F. Siegert [ID50](#), Dj. Sijacki [ID15](#), R. Sikora [ID84a](#), F. Sili [ID89](#),
 J.M. Silva [ID20](#), M.V. Silva Oliveira [ID36](#), S.B. Silverstein [ID47a](#), S. Simion [ID66](#), R. Simoniello [ID36](#),
 E.L. Simpson [ID59](#), N.D. Simpson [ID97](#), S. Simsek [ID21d](#), S. Sindhu [ID55](#), P. Sinervo [ID154](#), V. Sinetckii [ID37](#),
 S. Singh [ID141](#), S. Singh [ID154](#), S. Sinha [ID48](#), S. Sinha [ID33g](#), M. Sioli [ID23b,23a](#), I. Siral [ID122](#),
 S.Yu. Sivoklov [ID37,*](#), J. Sjölin [ID47a,47b](#), A. Skaf [ID55](#), E. Skorda [ID97](#), P. Skubic [ID119](#), M. Slawinska [ID85](#),
 V. Smakhtin [ID168](#), B.H. Smart [ID133](#), J. Smiesko [ID132](#), S.Yu. Smirnov [ID37](#), Y. Smirnov [ID37](#),
 L.N. Smirnova [ID37,a](#), O. Smirnova [ID97](#), E.A. Smith [ID39](#), H.A. Smith [ID125](#), J.L. Smith [ID91](#), R. Smith [ID142](#),
 M. Smizanska [ID90](#), K. Smolek [ID131](#), A. Smykiewicz [ID85](#), A.A. Snesarev [ID37](#), H.L. Snoek [ID113](#),
 S. Snyder [ID29](#), R. Sobie [ID164,w](#), A. Soffer [ID150](#), C.A. Solans Sanchez [ID36](#), E.Yu. Soldatov [ID37](#),
 U. Soldevila [ID162](#), A.A. Solodkov [ID37](#), S. Solomon [ID54](#), A. Soloshenko [ID38](#), K. Solovieva [ID54](#),
 O.V. Solovyanov [ID37](#), V. Solovyev [ID37](#), P. Sommer [ID36](#), A. Sonay [ID13](#), W.Y. Song [ID155b](#),
 A. Sopczak [ID131](#), A.L. Soppio [ID95](#), F. Sopkova [ID28b](#), V. Sothilingam [ID63a](#), S. Sottocornola [ID72a,72b](#),
 R. Soualah [ID115b](#), Z. Soumami [ID35e](#), D. South [ID48](#), S. Spagnolo [ID69a,69b](#), M. Spalla [ID109](#), F. Spanò [ID94](#),
 D. Sperlich [ID54](#), G. Spigo [ID36](#), M. Spina [ID145](#), S. Spinali [ID90](#), D.P. Spiteri [ID59](#), M. Spousta [ID132](#),
 E.J. Staats [ID34](#), A. Stabile [ID70a,70b](#), R. Stamen [ID63a](#), M. Stamenkovic [ID113](#), A. Stampekis [ID20](#),
 M. Standke [ID24](#), E. Stanecka [ID85](#), B. Stanislaus [ID17a](#), M.M. Stanitzki [ID48](#), M. Stankaityte [ID125](#),
 B. Stapf [ID48](#), E.A. Starchenko [ID37](#), G.H. Stark [ID135](#), J. Stark [ID101,z](#), D.M. Staro [ID155b](#), P. Staroba [ID130](#),
 P. Starovoitov [ID63a](#), S. Stärz [ID103](#), R. Staszewski [ID85](#), G. Stavropoulos [ID46](#), J. Steentoft [ID160](#),
 P. Steinberg [ID29](#), A.L. Steinhebel [ID122](#), B. Stelzer [ID141,155a](#), H.J. Stelzer [ID128](#), O. Stelzer-Chilton [ID155a](#),
 H. Stenzel [ID58](#), T.J. Stevenson [ID145](#), G.A. Stewart [ID36](#), M.C. Stockton [ID36](#), G. Stoicea [ID27b](#),
 M. Stolarski [ID129a](#), S. Stonjek [ID109](#), A. Straessner [ID50](#), J. Strandberg [ID143](#), S. Strandberg [ID47a,47b](#),
 M. Strauss [ID119](#), T. Strebler [ID101](#), P. Strizenec [ID28b](#), R. Ströhmer [ID165](#), D.M. Strom [ID122](#), L.R. Strom [ID48](#),
 R. Stroynowski [ID44](#), A. Strubig [ID47a,47b](#), S.A. Stucci [ID29](#), B. Stugu [ID16](#), J. Stupak [ID119](#), N.A. Styles [ID48](#),
 D. Su [ID142](#), S. Su [ID62a](#), W. Su [ID62d,137,62c](#), X. Su [ID62a,66](#), K. Sugizaki [ID152](#), V.V. Sulin [ID37](#),
 M.J. Sullivan [ID91](#), D.M.S. Sultan [ID77a,77b](#), L. Sultanaliyeva [ID37](#), S. Sultansoy [ID3b](#), T. Sumida [ID86](#),
 S. Sun [ID105](#), S. Sun [ID169](#), O. Sunneborn Gudnadottir [ID160](#), M.R. Sutton [ID145](#), M. Svatos [ID130](#),
 M. Swiatlowski [ID155a](#), T. Swirski [ID165](#), I. Sykora [ID28a](#), M. Sykora [ID132](#), T. Sykora [ID132](#), D. Ta [ID99](#),
 K. Tackmann [ID48,v](#), A. Taffard [ID159](#), R. Tafirout [ID155a](#), J.S. Tafoya Vargas [ID66](#), R.H.M. Taibah [ID126](#),
 R. Takashima [ID87](#), K. Takeda [ID83](#), E.P. Takeva [ID52](#), Y. Takubo [ID82](#), M. Talby [ID101](#), A.A. Talyshv [ID37](#),
 K.C. Tam [ID64b](#), N.M. Tamir [ID150](#), A. Tanaka [ID152](#), J. Tanaka [ID152](#), R. Tanaka [ID66](#), M. Tanasini [ID57b,57a](#),
 J. Tang [ID62c](#), Z. Tao [ID163](#), S. Tapia Araya [ID80](#), S. Tapprogge [ID99](#), A. Tarek Abouelfadl Mohamed [ID106](#),
 S. Tarem [ID149](#), K. Tariq [ID62b](#), G. Tarna [ID27b](#), G.F. Tartarelli [ID70a](#), P. Tas [ID132](#), M. Tasevsky [ID130](#),
 E. Tassi [ID43b,43a](#), A.C. Tate [ID161](#), G. Tateno [ID152](#), Y. Tayalati [ID35e](#), G.N. Taylor [ID104](#), W. Taylor [ID155b](#),
 H. Teagle [ID91](#), A.S. Tee [ID169](#), R. Teixeira De Lima [ID142](#), P. Teixeira-Dias [ID94](#), J.J. Teoh [ID154](#),

K. Terashi ¹⁵², J. Terron ⁹⁸, S. Terzo ¹³, M. Testa ⁵³, R.J. Teuscher ^{154,w}, N. Themistokleous ⁵²,
 T. Thevenaux-Pelzer ¹⁸, O. Thielmann ¹⁷⁰, D.W. Thomas ⁹⁴, J.P. Thomas ²⁰, E.A. Thompson ⁴⁸,
 P.D. Thompson ²⁰, E. Thomson ¹²⁷, E.J. Thorpe ⁹³, Y. Tian ⁵⁵, V. Tikhomirov ^{37,a},
 Yu.A. Tikhonov ³⁷, S. Timoshenko ³⁷, E.X.L. Ting ¹, P. Tipton ¹⁷¹, S. Tisserant ¹⁰¹, S.H. Tlou ^{33g},
 A. Tnourji ⁴⁰, K. Todome ^{23b,23a}, S. Todorova-Nova ¹³², S. Todt ⁵⁰, M. Togawa ⁸², J. Tojo ⁸⁸,
 S. Tokár ^{28a}, K. Tokushuku ⁸², R. Tombs ³², M. Tomoto ^{82,110}, L. Tompkins ^{142,p},
 P. Tornambe ¹⁰², E. Torrence ¹²², H. Torres ⁵⁰, E. Torró Pastor ¹⁶², M. Toscani ³⁰, C. Tosciri ³⁹,
 D.R. Tovey ¹³⁸, A. Traeet ¹⁶, I.S. Trandafir ^{27b}, T. Trefzger ¹⁶⁵, A. Tricoli ²⁹, I.M. Trigger ^{155a},
 S. Trincaz-Duvoid ¹²⁶, D.A. Trischuk ¹⁶³, B. Trocmé ⁶⁰, A. Trofymov ⁶⁶, C. Troncon ^{70a},
 L. Truong ^{33c}, M. Trzebinski ⁸⁵, A. Trzupiek ⁸⁵, F. Tsai ¹⁴⁴, M. Tsai ¹⁰⁵, A. Tsiamis ¹⁵¹,
 P.V. Tsiarehka ³⁷, S. Tsigaridas ^{155a}, A. Tsirigotis ^{151,t}, V. Tsiskaridze ¹⁴⁴, E.G. Tskhadadze ^{148a},
 M. Tsopoulou ¹⁵¹, Y. Tsujikawa ⁸⁶, I.I. Tsukerman ³⁷, V. Tsulaia ^{17a}, S. Tsuno ⁸², O. Tsur ¹⁴⁹,
 D. Tsybychev ¹⁴⁴, Y. Tu ^{64b}, A. Tudorache ^{27b}, V. Tudorache ^{27b}, A.N. Tuna ³⁶, S. Turchikhin ³⁸,
 I. Turk Cakir ^{3a}, R. Turra ^{70a}, T. Turtuvshin ³⁸, P.M. Tuts ⁴¹, S. Tzamarias ¹⁵¹, P. Tzanis ¹⁰,
 E. Tzovara ⁹⁹, K. Uchida ¹⁵², F. Ukegawa ¹⁵⁶, P.A. Ulloa Poblete ^{136c}, G. Unal ³⁶, M. Unal ¹¹,
 A. Undrus ²⁹, G. Unel ¹⁵⁹, K. Uno ¹⁵², J. Urban ^{28b}, P. Urquijo ¹⁰⁴, G. Usai ⁸, R. Ushioda ¹⁵³,
 M. Usman ¹⁰⁷, Z. Uysal ^{21b}, V. Vacek ¹³¹, B. Vachon ¹⁰³, K.O.H. Vadla ¹²⁴, T. Vafeiadis ³⁶,
 C. Valderanis ¹⁰⁸, E. Valdes Santurio ^{47a,47b}, M. Valente ^{155a}, S. Valentinetti ^{23b,23a}, A. Valero ¹⁶²,
 A. Vallier ^{101,z}, J.A. Valls Ferrer ¹⁶², T.R. Van Daalen ¹³⁷, P. Van Gemmeren ⁶, S. Van Stroud ⁹⁵,
 I. Van Vulpen ¹¹³, M. Vanadia ^{75a,75b}, W. Vandelli ³⁶, M. Vandenbroucke ¹³⁴, E.R. Vandewall ¹²⁰,
 D. Vannicola ¹⁵⁰, L. Vannoli ^{57b,57a}, R. Vari ^{74a}, E.W. Varnes ⁷, C. Varni ^{17a}, T. Varol ¹⁴⁷,
 D. Varouchas ⁶⁶, L. Varriale ¹⁶², K.E. Varvell ¹⁴⁶, M.E. Vasile ^{27b}, L. Vaslin ⁴⁰, G.A. Vasquez ¹⁶⁴,
 F. Vazeille ⁴⁰, T. Vazquez Schroeder ³⁶, J. Veatch ³¹, V. Vecchio ¹⁰⁰, M.J. Veen ¹¹³,
 I. Veliscek ¹²⁵, L.M. Veloce ¹⁵⁴, F. Veloso ^{129a,129c}, S. Veneziano ^{74a}, A. Ventura ^{69a,69b},
 A. Verbitskiy ¹⁰⁹, M. Verducci ^{73a,73b}, C. Vergis ²⁴, M. Verissimo De Araujo ^{81b},
 W. Verkerke ¹¹³, J.C. Vermeulen ¹¹³, C. Vernieri ¹⁴², P.J. Verschuuren ⁹⁴, M. Vessella ¹⁰²,
 M.L. Vesterbacka ¹¹⁶, M.C. Vetterli ^{141,af}, A. Vgenopoulos ¹⁵¹, N. Viaux Maira ^{136f},
 T. Vickey ¹³⁸, O.E. Vickey Boeriu ¹³⁸, G.H.A. Viehhauser ¹²⁵, L. Vigani ^{63b}, M. Villa ^{23b,23a},
 M. Villaplana Perez ¹⁶², E.M. Villhauer ⁵², E. Vilucchi ⁵³, M.G. Vincter ³⁴, G.S. Virdee ²⁰,
 A. Vishwakarma ⁵², C. Vittori ^{23b,23a}, I. Vivarelli ¹⁴⁵, V. Vladimirov ¹⁶⁶, E. Voevodina ¹⁰⁹,
 F. Vogel ¹⁰⁸, P. Vokac ¹³¹, J. Von Ahnen ⁴⁸, E. Von Toerne ²⁴, B. Vormwald ³⁶, V. Vorobel ¹³²,
 K. Vorobev ³⁷, M. Vos ¹⁶², J.H. Vosseveld ⁹¹, M. Vozak ¹¹³, L. Vozdecky ⁹³, N. Vranjes ¹⁵,
 M. Vranjes Milosavljevic ¹⁵, M. Vreeswijk ¹¹³, R. Vuillermet ³⁶, O. Vujanovic ⁹⁹, I. Vukotic ³⁹,
 S. Wada ¹⁵⁶, C. Wagner ¹⁰², W. Wagner ¹⁷⁰, S. Wahdan ¹⁷⁰, H. Wahlberg ⁸⁹, R. Wakasa ¹⁵⁶,
 M. Wakida ¹¹⁰, V.M. Walbrecht ¹⁰⁹, J. Walder ¹³³, R. Walker ¹⁰⁸, W. Walkowiak ¹⁴⁰,
 A.M. Wang ⁶¹, A.Z. Wang ¹⁶⁹, C. Wang ^{62a}, C. Wang ^{62c}, H. Wang ^{17a}, J. Wang ^{64a},
 P. Wang ⁴⁴, R.-J. Wang ⁹⁹, R. Wang ⁶¹, R. Wang ⁶, S.M. Wang ¹⁴⁷, S. Wang ^{62b}, T. Wang ^{62a},
 W.T. Wang ⁷⁹, W.X. Wang ^{62a}, X. Wang ^{14c}, X. Wang ¹⁶¹, X. Wang ^{62c}, Y. Wang ^{62d},
 Y. Wang ^{14c}, Z. Wang ¹⁰⁵, Z. Wang ^{62d,51,62c}, Z. Wang ¹⁰⁵, A. Warburton ¹⁰³, R.J. Ward ²⁰,
 N. Warrack ⁵⁹, A.T. Watson ²⁰, M.F. Watson ²⁰, G. Watts ¹³⁷, B.M. Waugh ⁹⁵, A.F. Webb ¹¹,
 C. Weber ²⁹, M.S. Weber ¹⁹, S.A. Weber ³⁴, S.M. Weber ^{63a}, C. Wei ^{62a}, Y. Wei ¹²⁵,
 A.R. Weidberg ¹²⁵, J. Weingarten ⁴⁹, M. Weirich ⁹⁹, C. Weiser ⁵⁴, C.J. Wells ⁴⁸, T. Wenaus ²⁹,
 B. Wendland ⁴⁹, T. Wengler ³⁶, N.S. Wenke ¹⁰⁹, N. Wermes ²⁴, M. Wessels ^{63a}, K. Whalen ¹²²,
 A.M. Wharton ⁹⁰, A.S. White ⁶¹, A. White ⁸, M.J. White ¹, D. Whiteson ¹⁵⁹,
 L. Wickremasinghe ¹²³, W. Wiedenmann ¹⁶⁹, C. Wiel ⁵⁰, M. Wielers ¹³³, N. Wieseotte ⁹⁹,
 C. Wiglesworth ⁴², L.A.M. Wiik-Fuchs ⁵⁴, D.J. Wilbern ¹¹⁹, H.G. Wilkens ³⁶, D.M. Williams ⁴¹,
 H.H. Williams ¹²⁷, S. Williams ³², S. Willocq ¹⁰², P.J. Windischhofer ¹²⁵, F. Winklmeier ¹²²,

B.T. Winter ⁵⁴, M. Wittgen ¹⁴², M. Wobisch ⁹⁶, A. Wolf ⁹⁹, R. Wölker ¹²⁵, J. Wollrath ¹⁵⁹, M.W. Wolter ⁸⁵, H. Wolters ^{129a,129c}, V.W.S. Wong ¹⁶³, A.F. Wongel ⁴⁸, S.D. Worm ⁴⁸, B.K. Wosiek ⁸⁵, K.W. Woźniak ⁸⁵, K. Wraight ⁵⁹, J. Wu ^{14a,14d}, M. Wu ^{64a}, S.L. Wu ¹⁶⁹, X. Wu ⁵⁶, Y. Wu ^{62a}, Z. Wu ^{134,62a}, J. Wuerzinger ¹²⁵, T.R. Wyatt ¹⁰⁰, B.M. Wynne ⁵², S. Xella ⁴², L. Xia ^{14c}, M. Xia ^{14b}, J. Xiang ^{64c}, X. Xiao ¹⁰⁵, M. Xie ^{62a}, X. Xie ^{62a}, J. Xiong ^{17a}, I. Xiotidis ¹⁴⁵, D. Xu ^{14a}, H. Xu ^{62a}, H. Xu ^{62a}, L. Xu ^{62a}, R. Xu ¹²⁷, T. Xu ¹⁰⁵, W. Xu ¹⁰⁵, Y. Xu ^{14b}, Z. Xu ^{62b}, Z. Xu ¹⁴², B. Yabsley ¹⁴⁶, S. Yacoob ^{33a}, N. Yamaguchi ⁸⁸, Y. Yamaguchi ¹⁵³, H. Yamauchi ¹⁵⁶, T. Yamazaki ^{17a}, Y. Yamazaki ⁸³, J. Yan ^{62c}, S. Yan ¹²⁵, Z. Yan ²⁵, H.J. Yang ^{62c,62d}, H.T. Yang ^{17a}, S. Yang ^{62a}, T. Yang ^{64c}, X. Yang ^{62a}, X. Yang ^{14a}, Y. Yang ⁴⁴, Z. Yang ^{62a,105}, W-M. Yao ^{17a}, Y.C. Yap ⁴⁸, H. Ye ^{14c}, J. Ye ⁴⁴, S. Ye ²⁹, X. Ye ^{62a}, I. Yeletsikh ³⁸, M.R. Yexley ⁹⁰, P. Yin ⁴¹, K. Yorita ¹⁶⁷, C.J.S. Young ⁵⁴, C. Young ¹⁴², M. Yuan ¹⁰⁵, R. Yuan ^{62bj}, L. Yue ⁹⁵, X. Yue ^{63a}, M. Zaazoua ^{35e}, B. Zabinski ⁸⁵, E. Zaid ⁵², T. Zakareishvili ^{148b}, N. Zakharchuk ³⁴, S. Zambito ⁵⁶, J. Zang ¹⁵², D. Zanzi ⁵⁴, O. Zaplatilek ¹³¹, S.V. Zeiβner ⁴⁹, C. Zeitnitz ¹⁷⁰, J.C. Zeng ¹⁶¹, D.T. Zenger Jr ²⁶, O. Zenin ³⁷, T. Ženiš ^{28a}, S. Zenz ⁹³, S. Zerradi ^{35a}, D. Zerwas ⁶⁶, B. Zhang ^{14c}, D.F. Zhang ¹³⁸, G. Zhang ^{14b}, J. Zhang ⁶, K. Zhang ^{14a,14d}, L. Zhang ^{14c}, R. Zhang ¹⁶⁹, S. Zhang ¹⁰⁵, T. Zhang ¹⁵², X. Zhang ^{62c}, X. Zhang ^{62b}, Z. Zhang ^{17a}, Z. Zhang ⁶⁶, H. Zhao ¹³⁷, P. Zhao ⁵¹, T. Zhao ^{62b}, Y. Zhao ¹³⁵, Z. Zhao ^{62a}, A. Zhemchugov ³⁸, Z. Zheng ¹⁴², D. Zhong ¹⁶¹, B. Zhou ¹⁰⁵, C. Zhou ¹⁶⁹, H. Zhou ⁷, N. Zhou ^{62c}, Y. Zhou ⁷, C.G. Zhu ^{62b}, C. Zhu ^{14a,14d}, H.L. Zhu ^{62a}, H. Zhu ^{14a}, J. Zhu ¹⁰⁵, Y. Zhu ^{62a}, X. Zhuang ^{14a}, K. Zhukov ³⁷, V. Zhulanov ³⁷, N.I. Zimine ³⁸, J. Zinsser ^{63b}, M. Ziolkowski ¹⁴⁰, L. Živković ¹⁵, A. Zoccoli ^{23b,23a}, K. Zoch ⁵⁶, T.G. Zorbas ¹³⁸, O. Zormpa ⁴⁶, W. Zou ⁴¹, L. Zwalinski ³⁶.

¹Department of Physics, University of Adelaide, Adelaide; Australia.

²Department of Physics, University of Alberta, Edmonton AB; Canada.

³(^a)Department of Physics, Ankara University, Ankara; (^b)Division of Physics, TOBB University of Economics and Technology, Ankara; Türkiye.

⁴LAPP, Université Savoie Mont Blanc, CNRS/IN2P3, Annecy; France.

⁵APC, Université Paris Cité, CNRS/IN2P3, Paris; France.

⁶High Energy Physics Division, Argonne National Laboratory, Argonne IL; United States of America.

⁷Department of Physics, University of Arizona, Tucson AZ; United States of America.

⁸Department of Physics, University of Texas at Arlington, Arlington TX; United States of America.

⁹Physics Department, National and Kapodistrian University of Athens, Athens; Greece.

¹⁰Physics Department, National Technical University of Athens, Zografou; Greece.

¹¹Department of Physics, University of Texas at Austin, Austin TX; United States of America.

¹²Institute of Physics, Azerbaijan Academy of Sciences, Baku; Azerbaijan.

¹³Institut de Física d'Altes Energies (IFAE), Barcelona Institute of Science and Technology, Barcelona; Spain.

¹⁴(^a)Institute of High Energy Physics, Chinese Academy of Sciences, Beijing; (^b)Physics Department, Tsinghua University, Beijing; (^c)Department of Physics, Nanjing University, Nanjing; (^d)University of Chinese Academy of Science (UCAS), Beijing; China.

¹⁵Institute of Physics, University of Belgrade, Belgrade; Serbia.

¹⁶Department for Physics and Technology, University of Bergen, Bergen; Norway.

¹⁷(^a)Physics Division, Lawrence Berkeley National Laboratory, Berkeley CA; (^b)University of California, Berkeley CA; United States of America.

¹⁸Institut für Physik, Humboldt Universität zu Berlin, Berlin; Germany.

¹⁹Albert Einstein Center for Fundamental Physics and Laboratory for High Energy Physics, University of

Bern, Bern; Switzerland.

²⁰School of Physics and Astronomy, University of Birmingham, Birmingham; United Kingdom.

²¹(^a)Department of Physics, Bogazici University, Istanbul; (^b)Department of Physics Engineering, Gaziantep University, Gaziantep; (^c)Department of Physics, Istanbul University, Istanbul; (^d)Istinye University, Sariyer, Istanbul; Türkiye.

²²(^a)Facultad de Ciencias y Centro de Investigaciones, Universidad Antonio Nariño, Bogotá; (^b)Departamento de Física, Universidad Nacional de Colombia, Bogotá; Colombia.

²³(^a)Dipartimento di Fisica e Astronomia A. Righi, Università di Bologna, Bologna; (^b)INFN Sezione di Bologna; Italy.

²⁴Physikalisches Institut, Universität Bonn, Bonn; Germany.

²⁵Department of Physics, Boston University, Boston MA; United States of America.

²⁶Department of Physics, Brandeis University, Waltham MA; United States of America.

²⁷(^a)Transilvania University of Brasov, Brasov; (^b)Horia Hulubei National Institute of Physics and Nuclear Engineering, Bucharest; (^c)Department of Physics, Alexandru Ioan Cuza University of Iasi, Iasi; (^d)National Institute for Research and Development of Isotopic and Molecular Technologies, Physics Department, Cluj-Napoca; (^e)University Politehnica Bucharest, Bucharest; (^f)West University in Timisoara, Timisoara; Romania.

²⁸(^a)Faculty of Mathematics, Physics and Informatics, Comenius University, Bratislava; (^b)Department of Subnuclear Physics, Institute of Experimental Physics of the Slovak Academy of Sciences, Kosice; Slovak Republic.

²⁹Physics Department, Brookhaven National Laboratory, Upton NY; United States of America.

³⁰Universidad de Buenos Aires, Facultad de Ciencias Exactas y Naturales, Departamento de Física, y CONICET, Instituto de Física de Buenos Aires (IFIBA), Buenos Aires; Argentina.

³¹California State University, CA; United States of America.

³²Cavendish Laboratory, University of Cambridge, Cambridge; United Kingdom.

³³(^a)Department of Physics, University of Cape Town, Cape Town; (^b)iThemba Labs, Western Cape; (^c)Department of Mechanical Engineering Science, University of Johannesburg, Johannesburg; (^d)National Institute of Physics, University of the Philippines Diliman (Philippines); (^e)University of South Africa, Department of Physics, Pretoria; (^f)University of Zululand, KwaDlangezwa; (^g)School of Physics, University of the Witwatersrand, Johannesburg; South Africa.

³⁴Department of Physics, Carleton University, Ottawa ON; Canada.

³⁵(^a)Faculté des Sciences Ain Chock, Réseau Universitaire de Physique des Hautes Energies - Université Hassan II, Casablanca; (^b)Faculté des Sciences, Université Ibn-Tofail, Kénitra; (^c)Faculté des Sciences Semlalia, Université Cadi Ayyad, LPHEA-Marrakech; (^d)LPMR, Faculté des Sciences, Université Mohamed Premier, Oujda; (^e)Faculté des sciences, Université Mohammed V, Rabat; (^f)Institute of Applied Physics, Mohammed VI Polytechnic University, Ben Guerir; Morocco.

³⁶CERN, Geneva; Switzerland.

³⁷Affiliated with an institute covered by a cooperation agreement with CERN.

³⁸Affiliated with an international laboratory covered by a cooperation agreement with CERN.

³⁹Enrico Fermi Institute, University of Chicago, Chicago IL; United States of America.

⁴⁰LPC, Université Clermont Auvergne, CNRS/IN2P3, Clermont-Ferrand; France.

⁴¹Nevis Laboratory, Columbia University, Irvington NY; United States of America.

⁴²Niels Bohr Institute, University of Copenhagen, Copenhagen; Denmark.

⁴³(^a)Dipartimento di Fisica, Università della Calabria, Rende; (^b)INFN Gruppo Collegato di Cosenza, Laboratori Nazionali di Frascati; Italy.

⁴⁴Physics Department, Southern Methodist University, Dallas TX; United States of America.

⁴⁵Physics Department, University of Texas at Dallas, Richardson TX; United States of America.

- ⁴⁶National Centre for Scientific Research "Demokritos", Agia Paraskevi; Greece.
- ⁴⁷(^a) Department of Physics, Stockholm University; (^b) Oskar Klein Centre, Stockholm; Sweden.
- ⁴⁸Deutsches Elektronen-Synchrotron DESY, Hamburg and Zeuthen; Germany.
- ⁴⁹Fakultät Physik, Technische Universität Dortmund, Dortmund; Germany.
- ⁵⁰Institut für Kern- und Teilchenphysik, Technische Universität Dresden, Dresden; Germany.
- ⁵¹Department of Physics, Duke University, Durham NC; United States of America.
- ⁵²SUPA - School of Physics and Astronomy, University of Edinburgh, Edinburgh; United Kingdom.
- ⁵³INFN e Laboratori Nazionali di Frascati, Frascati; Italy.
- ⁵⁴Physikalisches Institut, Albert-Ludwigs-Universität Freiburg, Freiburg; Germany.
- ⁵⁵II. Physikalisches Institut, Georg-August-Universität Göttingen, Göttingen; Germany.
- ⁵⁶Département de Physique Nucléaire et Corpusculaire, Université de Genève, Genève; Switzerland.
- ⁵⁷(^a) Dipartimento di Fisica, Università di Genova, Genova; (^b) INFN Sezione di Genova; Italy.
- ⁵⁸II. Physikalisches Institut, Justus-Liebig-Universität Giessen, Giessen; Germany.
- ⁵⁹SUPA - School of Physics and Astronomy, University of Glasgow, Glasgow; United Kingdom.
- ⁶⁰LPSC, Université Grenoble Alpes, CNRS/IN2P3, Grenoble INP, Grenoble; France.
- ⁶¹Laboratory for Particle Physics and Cosmology, Harvard University, Cambridge MA; United States of America.
- ⁶²(^a) Department of Modern Physics and State Key Laboratory of Particle Detection and Electronics, University of Science and Technology of China, Hefei; (^b) Institute of Frontier and Interdisciplinary Science and Key Laboratory of Particle Physics and Particle Irradiation (MOE), Shandong University, Qingdao; (^c) School of Physics and Astronomy, Shanghai Jiao Tong University, Key Laboratory for Particle Astrophysics and Cosmology (MOE), SKLPPC, Shanghai; (^d) Tsung-Dao Lee Institute, Shanghai; China.
- ⁶³(^a) Kirchhoff-Institut für Physik, Ruprecht-Karls-Universität Heidelberg, Heidelberg; (^b) Physikalisches Institut, Ruprecht-Karls-Universität Heidelberg, Heidelberg; Germany.
- ⁶⁴(^a) Department of Physics, Chinese University of Hong Kong, Shatin, N.T., Hong Kong; (^b) Department of Physics, University of Hong Kong, Hong Kong; (^c) Department of Physics and Institute for Advanced Study, Hong Kong University of Science and Technology, Clear Water Bay, Kowloon, Hong Kong; China.
- ⁶⁵Department of Physics, National Tsing Hua University, Hsinchu; Taiwan.
- ⁶⁶IJCLab, Université Paris-Saclay, CNRS/IN2P3, 91405, Orsay; France.
- ⁶⁷Department of Physics, Indiana University, Bloomington IN; United States of America.
- ⁶⁸(^a) INFN Gruppo Collegato di Udine, Sezione di Trieste, Udine; (^b) ICTP, Trieste; (^c) Dipartimento Politecnico di Ingegneria e Architettura, Università di Udine, Udine; Italy.
- ⁶⁹(^a) INFN Sezione di Lecce; (^b) Dipartimento di Matematica e Fisica, Università del Salento, Lecce; Italy.
- ⁷⁰(^a) INFN Sezione di Milano; (^b) Dipartimento di Fisica, Università di Milano, Milano; Italy.
- ⁷¹(^a) INFN Sezione di Napoli; (^b) Dipartimento di Fisica, Università di Napoli, Napoli; Italy.
- ⁷²(^a) INFN Sezione di Pavia; (^b) Dipartimento di Fisica, Università di Pavia, Pavia; Italy.
- ⁷³(^a) INFN Sezione di Pisa; (^b) Dipartimento di Fisica E. Fermi, Università di Pisa, Pisa; Italy.
- ⁷⁴(^a) INFN Sezione di Roma; (^b) Dipartimento di Fisica, Sapienza Università di Roma, Roma; Italy.
- ⁷⁵(^a) INFN Sezione di Roma Tor Vergata; (^b) Dipartimento di Fisica, Università di Roma Tor Vergata, Roma; Italy.
- ⁷⁶(^a) INFN Sezione di Roma Tre; (^b) Dipartimento di Matematica e Fisica, Università Roma Tre, Roma; Italy.
- ⁷⁷(^a) INFN-TIFPA; (^b) Università degli Studi di Trento, Trento; Italy.
- ⁷⁸Universität Innsbruck, Department of Astro and Particle Physics, Innsbruck; Austria.
- ⁷⁹University of Iowa, Iowa City IA; United States of America.
- ⁸⁰Department of Physics and Astronomy, Iowa State University, Ames IA; United States of America.
- ⁸¹(^a) Departamento de Engenharia Elétrica, Universidade Federal de Juiz de Fora (UFJF), Juiz de

- Fora;^(b) Universidade Federal do Rio De Janeiro COPPE/EE/IF, Rio de Janeiro;^(c) Instituto de Física, Universidade de São Paulo, São Paulo;^(d) Rio de Janeiro State University, Rio de Janeiro; Brazil.
- ⁸² KEK, High Energy Accelerator Research Organization, Tsukuba; Japan.
- ⁸³ Graduate School of Science, Kobe University, Kobe; Japan.
- ⁸⁴ ^(a) AGH University of Science and Technology, Faculty of Physics and Applied Computer Science, Krakow; ^(b) Marian Smoluchowski Institute of Physics, Jagiellonian University, Krakow; Poland.
- ⁸⁵ Institute of Nuclear Physics Polish Academy of Sciences, Krakow; Poland.
- ⁸⁶ Faculty of Science, Kyoto University, Kyoto; Japan.
- ⁸⁷ Kyoto University of Education, Kyoto; Japan.
- ⁸⁸ Research Center for Advanced Particle Physics and Department of Physics, Kyushu University, Fukuoka ; Japan.
- ⁸⁹ Instituto de Física La Plata, Universidad Nacional de La Plata and CONICET, La Plata; Argentina.
- ⁹⁰ Physics Department, Lancaster University, Lancaster; United Kingdom.
- ⁹¹ Oliver Lodge Laboratory, University of Liverpool, Liverpool; United Kingdom.
- ⁹² Department of Experimental Particle Physics, Jožef Stefan Institute and Department of Physics, University of Ljubljana, Ljubljana; Slovenia.
- ⁹³ School of Physics and Astronomy, Queen Mary University of London, London; United Kingdom.
- ⁹⁴ Department of Physics, Royal Holloway University of London, Egham; United Kingdom.
- ⁹⁵ Department of Physics and Astronomy, University College London, London; United Kingdom.
- ⁹⁶ Louisiana Tech University, Ruston LA; United States of America.
- ⁹⁷ Fysiska institutionen, Lunds universitet, Lund; Sweden.
- ⁹⁸ Departamento de Física Teórica C-15 and CIAFF, Universidad Autónoma de Madrid, Madrid; Spain.
- ⁹⁹ Institut für Physik, Universität Mainz, Mainz; Germany.
- ¹⁰⁰ School of Physics and Astronomy, University of Manchester, Manchester; United Kingdom.
- ¹⁰¹ CPPM, Aix-Marseille Université, CNRS/IN2P3, Marseille; France.
- ¹⁰² Department of Physics, University of Massachusetts, Amherst MA; United States of America.
- ¹⁰³ Department of Physics, McGill University, Montreal QC; Canada.
- ¹⁰⁴ School of Physics, University of Melbourne, Victoria; Australia.
- ¹⁰⁵ Department of Physics, University of Michigan, Ann Arbor MI; United States of America.
- ¹⁰⁶ Department of Physics and Astronomy, Michigan State University, East Lansing MI; United States of America.
- ¹⁰⁷ Group of Particle Physics, University of Montreal, Montreal QC; Canada.
- ¹⁰⁸ Fakultät für Physik, Ludwig-Maximilians-Universität München, München; Germany.
- ¹⁰⁹ Max-Planck-Institut für Physik (Werner-Heisenberg-Institut), München; Germany.
- ¹¹⁰ Graduate School of Science and Kobayashi-Maskawa Institute, Nagoya University, Nagoya; Japan.
- ¹¹¹ Department of Physics and Astronomy, University of New Mexico, Albuquerque NM; United States of America.
- ¹¹² Institute for Mathematics, Astrophysics and Particle Physics, Radboud University/Nikhef, Nijmegen; Netherlands.
- ¹¹³ Nikhef National Institute for Subatomic Physics and University of Amsterdam, Amsterdam; Netherlands.
- ¹¹⁴ Department of Physics, Northern Illinois University, DeKalb IL; United States of America.
- ¹¹⁵ ^(a) New York University Abu Dhabi, Abu Dhabi; ^(b) University of Sharjah, Sharjah; United Arab Emirates.
- ¹¹⁶ Department of Physics, New York University, New York NY; United States of America.
- ¹¹⁷ Ochanomizu University, Otsuka, Bunkyo-ku, Tokyo; Japan.
- ¹¹⁸ Ohio State University, Columbus OH; United States of America.

- ¹¹⁹Homer L. Dodge Department of Physics and Astronomy, University of Oklahoma, Norman OK; United States of America.
- ¹²⁰Department of Physics, Oklahoma State University, Stillwater OK; United States of America.
- ¹²¹Palacký University, Joint Laboratory of Optics, Olomouc; Czech Republic.
- ¹²²Institute for Fundamental Science, University of Oregon, Eugene, OR; United States of America.
- ¹²³Graduate School of Science, Osaka University, Osaka; Japan.
- ¹²⁴Department of Physics, University of Oslo, Oslo; Norway.
- ¹²⁵Department of Physics, Oxford University, Oxford; United Kingdom.
- ¹²⁶LPNHE, Sorbonne Université, Université Paris Cité, CNRS/IN2P3, Paris; France.
- ¹²⁷Department of Physics, University of Pennsylvania, Philadelphia PA; United States of America.
- ¹²⁸Department of Physics and Astronomy, University of Pittsburgh, Pittsburgh PA; United States of America.
- ¹²⁹^(a)Laboratório de Instrumentação e Física Experimental de Partículas - LIP, Lisboa; ^(b)Departamento de Física, Faculdade de Ciências, Universidade de Lisboa, Lisboa; ^(c)Departamento de Física, Universidade de Coimbra, Coimbra; ^(d)Centro de Física Nuclear da Universidade de Lisboa, Lisboa; ^(e)Departamento de Física, Universidade do Minho, Braga; ^(f)Departamento de Física Teórica y del Cosmos, Universidad de Granada, Granada (Spain); ^(g)Departamento de Física, Instituto Superior Técnico, Universidade de Lisboa, Lisboa; Portugal.
- ¹³⁰Institute of Physics of the Czech Academy of Sciences, Prague; Czech Republic.
- ¹³¹Czech Technical University in Prague, Prague; Czech Republic.
- ¹³²Charles University, Faculty of Mathematics and Physics, Prague; Czech Republic.
- ¹³³Particle Physics Department, Rutherford Appleton Laboratory, Didcot; United Kingdom.
- ¹³⁴IRFU, CEA, Université Paris-Saclay, Gif-sur-Yvette; France.
- ¹³⁵Santa Cruz Institute for Particle Physics, University of California Santa Cruz, Santa Cruz CA; United States of America.
- ¹³⁶^(a)Departamento de Física, Pontificia Universidad Católica de Chile, Santiago; ^(b)Millennium Institute for Subatomic physics at high energy frontier (SAPHIR), Santiago; ^(c)Instituto de Investigación Multidisciplinario en Ciencia y Tecnología, y Departamento de Física, Universidad de La Serena; ^(d)Universidad Andres Bello, Department of Physics, Santiago; ^(e)Instituto de Alta Investigación, Universidad de Tarapacá, Arica; ^(f)Departamento de Física, Universidad Técnica Federico Santa María, Valparaíso; Chile.
- ¹³⁷Department of Physics, University of Washington, Seattle WA; United States of America.
- ¹³⁸Department of Physics and Astronomy, University of Sheffield, Sheffield; United Kingdom.
- ¹³⁹Department of Physics, Shinshu University, Nagano; Japan.
- ¹⁴⁰Department Physik, Universität Siegen, Siegen; Germany.
- ¹⁴¹Department of Physics, Simon Fraser University, Burnaby BC; Canada.
- ¹⁴²SLAC National Accelerator Laboratory, Stanford CA; United States of America.
- ¹⁴³Department of Physics, Royal Institute of Technology, Stockholm; Sweden.
- ¹⁴⁴Departments of Physics and Astronomy, Stony Brook University, Stony Brook NY; United States of America.
- ¹⁴⁵Department of Physics and Astronomy, University of Sussex, Brighton; United Kingdom.
- ¹⁴⁶School of Physics, University of Sydney, Sydney; Australia.
- ¹⁴⁷Institute of Physics, Academia Sinica, Taipei; Taiwan.
- ¹⁴⁸^(a)E. Andronikashvili Institute of Physics, Iv. Javakhishvili Tbilisi State University, Tbilisi; ^(b)High Energy Physics Institute, Tbilisi State University, Tbilisi; ^(c)University of Georgia, Tbilisi; Georgia.
- ¹⁴⁹Department of Physics, Technion, Israel Institute of Technology, Haifa; Israel.
- ¹⁵⁰Raymond and Beverly Sackler School of Physics and Astronomy, Tel Aviv University, Tel Aviv; Israel.

- ¹⁵¹Department of Physics, Aristotle University of Thessaloniki, Thessaloniki; Greece.
- ¹⁵²International Center for Elementary Particle Physics and Department of Physics, University of Tokyo, Tokyo; Japan.
- ¹⁵³Department of Physics, Tokyo Institute of Technology, Tokyo; Japan.
- ¹⁵⁴Department of Physics, University of Toronto, Toronto ON; Canada.
- ¹⁵⁵^(a) TRIUMF, Vancouver BC; ^(b) Department of Physics and Astronomy, York University, Toronto ON; Canada.
- ¹⁵⁶Division of Physics and Tomonaga Center for the History of the Universe, Faculty of Pure and Applied Sciences, University of Tsukuba, Tsukuba; Japan.
- ¹⁵⁷Department of Physics and Astronomy, Tufts University, Medford MA; United States of America.
- ¹⁵⁸United Arab Emirates University, Al Ain; United Arab Emirates.
- ¹⁵⁹Department of Physics and Astronomy, University of California Irvine, Irvine CA; United States of America.
- ¹⁶⁰Department of Physics and Astronomy, University of Uppsala, Uppsala; Sweden.
- ¹⁶¹Department of Physics, University of Illinois, Urbana IL; United States of America.
- ¹⁶²Instituto de Física Corpuscular (IFIC), Centro Mixto Universidad de Valencia - CSIC, Valencia; Spain.
- ¹⁶³Department of Physics, University of British Columbia, Vancouver BC; Canada.
- ¹⁶⁴Department of Physics and Astronomy, University of Victoria, Victoria BC; Canada.
- ¹⁶⁵Fakultät für Physik und Astronomie, Julius-Maximilians-Universität Würzburg, Würzburg; Germany.
- ¹⁶⁶Department of Physics, University of Warwick, Coventry; United Kingdom.
- ¹⁶⁷Waseda University, Tokyo; Japan.
- ¹⁶⁸Department of Particle Physics and Astrophysics, Weizmann Institute of Science, Rehovot; Israel.
- ¹⁶⁹Department of Physics, University of Wisconsin, Madison WI; United States of America.
- ¹⁷⁰Fakultät für Mathematik und Naturwissenschaften, Fachgruppe Physik, Bergische Universität Wuppertal, Wuppertal; Germany.
- ¹⁷¹Department of Physics, Yale University, New Haven CT; United States of America.
- ^a Also Affiliated with an institute covered by a cooperation agreement with CERN.
- ^b Also at Borough of Manhattan Community College, City University of New York, New York NY; United States of America.
- ^c Also at Bruno Kessler Foundation, Trento; Italy.
- ^d Also at Center for High Energy Physics, Peking University; China.
- ^e Also at Centro Studi e Ricerche Enrico Fermi; Italy.
- ^f Also at CERN, Geneva; Switzerland.
- ^g Also at Département de Physique Nucléaire et Corpusculaire, Université de Genève, Genève; Switzerland.
- ^h Also at Departament de Física de la Universitat Autònoma de Barcelona, Barcelona; Spain.
- ⁱ Also at Department of Financial and Management Engineering, University of the Aegean, Chios; Greece.
- ^j Also at Department of Physics and Astronomy, Michigan State University, East Lansing MI; United States of America.
- ^k Also at Department of Physics and Astronomy, University of Louisville, Louisville, KY; United States of America.
- ^l Also at Department of Physics, Ben Gurion University of the Negev, Beer Sheva; Israel.
- ^m Also at Department of Physics, California State University, East Bay; United States of America.
- ⁿ Also at Department of Physics, California State University, Sacramento; United States of America.
- ^o Also at Department of Physics, King's College London, London; United Kingdom.
- ^p Also at Department of Physics, Stanford University, Stanford CA; United States of America.
- ^q Also at Department of Physics, University of Fribourg, Fribourg; Switzerland.

- r* Also at Department of Physics, University of Thessaly; Greece.
- s* Also at Department of Physics, Westmont College, Santa Barbara; United States of America.
- t* Also at Hellenic Open University, Patras; Greece.
- u* Also at Institutio Catalana de Recerca i Estudis Avancats, ICREA, Barcelona; Spain.
- v* Also at Institut für Experimentalphysik, Universität Hamburg, Hamburg; Germany.
- w* Also at Institute of Particle Physics (IPP); Canada.
- x* Also at Institute of Physics, Azerbaijan Academy of Sciences, Baku; Azerbaijan.
- y* Also at Institute of Theoretical Physics, Ilia State University, Tbilisi; Georgia.
- z* Also at L2IT, Université de Toulouse, CNRS/IN2P3, UPS, Toulouse; France.
- aa* Also at Lawrence Livermore National Laboratory, Livermore; United States of America.
- ab* Also at National Institute of Physics, University of the Philippines Diliman (Philippines); Philippines.
- ac* Also at Physics Department, An-Najah National University, Nablus; Palestine.
- ad* Also at The City College of New York, New York NY; United States of America.
- ae* Also at The Collaborative Innovation Center of Quantum Matter (CICQM), Beijing; China.
- af* Also at TRIUMF, Vancouver BC; Canada.
- ag* Also at Università di Napoli Parthenope, Napoli; Italy.
- ah* Also at University of Chinese Academy of Sciences (UCAS), Beijing; China.
- ai* Also at University of Colorado Boulder, Department of Physics, Colorado; United States of America.
- aj* Also at Yeditepe University, Physics Department, Istanbul; Türkiye.
- * Deceased